Technical, Economic and Environmental Feasibility of an Innovative Small-Scale Pumped Storage Hydropower Plant in the Urban Built Environment

Stuart Daniel James

Faculty of Industrial Engineering, Mechanical Engineering and Computer Science
University of Iceland
2019

Technical, Economic and Environmental Feasibility of an Innovative Small-Scale Pumped Storage Hydropower Plant in the Urban Built Environment

Stuart Daniel James

60 ECTS thesis submitted in partial fulfillment of a
Magister Scientiarum degree in Environment and Natural Resources

MS Committee
Halldór Pálsson
Daði Sverrisson
Hafþór Ægir Sigurjónsson
Bjarni Bessason

Master's Examiner
Einar Jón Ásbjörnsson

Faculty of Industrial Engineering, Mechanical Engineering and Computer Science
School of Engineering and Natural Sciences
University of Iceland
Reykjavik, October 2019

Technical, Economic and Environmental Feasibility of an Innovative Small-Scale Pumped Hydro Energy Storage Plant in the Urban Built Environment
Feasibility of a PHES Plant in a Building System
60 ECTS thesis submitted in partial fulfillment of a *Magister Scientiarum* degree in Environment and Natural Resources

Faculty of Industrial Engineering, Mechanical Engineering and Computer Science
School of Engineering and Natural Sciences
University of Iceland
Hjarðarhagi 2-6
107 Reykjavik
Iceland

Telephone: 525 4000

Bibliographic information:
Stuart Daniel James, 2019, *Technical, Economic and Environmental Feasibility of an Innovative Small-Scale Pumped Storage Hydropower Plant in the Urban Built Environment*, Master's thesis, Faculty of Industrial Engineering, Mechanical Engineering and Computer Science, University of Iceland, pp. 159.

Printing: Háskólaprent
Reykjavik, Iceland, October 2019

Abstract

The energy transition in Germany requires new ways to integrate renewable power generation technologies into the energy system. Due to the intermittent nature of wind and solar power, new measures are needed to balance demand and supply. Power system flexibility can be provided by energy storage systems that store energy when supply exceeds the demand, and feed power back into the grid when demand exceeds the supply. Many different energy storage technologies are available. The oldest, most mature, and only large-scale technology that has been operational for decades, is pumped hydro energy storage. While the potential for large-scale systems has become scarce in Germany, due to space restrictions and lack of public acceptance, there has been an increasing interest in small-scale systems.

The current study lays a focus on the development of a new innovative approach to store energy in a small-scale pumped hydro energy storage plant that can be integrated into the urban built environment, namely in a building. Therefore, a product development approach was conducted, followed by an analysis of the economic and environmental viability of the plant. In a final step, the proposed system was compared to lithium-ion battery systems and power-to-gas-to-power systems in terms of economic and environmental feasibility.

The study finds that the proposed small-scale pumped hydro energy storage system has considerable potential, whereas serious competition comes from the lithium-ion battery system with its predicted future developments. However, the implementation of the proposed system comprises major technical challenges due to its considerable size.

Útdráttur

Orkuskiptin í Þýskalandi krefjast nýrra leiða til að samþætta endurnýjanlega orkuframleiðslutækni í raforkukerfinu. Vegna eðlis vind- og sólarorku þarf nýjar ráðstafanir til að koma á jafnvægi milli eftirspurnar og framboðs. Hægt er að veita sveigjanleika í raforkukerfinu með geymslukerfum sem geyma orku þegar framboð er meira en eftirspurnin, og skilar afli aftur í kerfið þegar eftirspurn er meiri en framboðið. Margar mismunandi tæknilausnir til að geyma orku eru til. Elsta, þróaðasta og ein stærsta tæknin sem hefur verið starfrækt í áratugi, er vatnsorkudælimiðlun. Þrátt fyrir að möguleikar á stórfelldum kerfum hafi verið af skornum skammti í Þýskalandi, vegna takmarkana á rými og skorts á samþykki almennings, hefur vaxandi áhugi verið fyrir smáskalakerfi.

Þessi rannsókn leggur áherslu á þróun nýrrar nýstárlegrar aðferðar til að geyma orku í smáskala vatnsorkudælimiðlun sem hægt er að samþætta í þéttbýlu umhverfi, aðallega í byggingu. Þess vegna var völ á viðeigandi aðferð, í kjölfar greiningar á hagkvæmni og umhverfisvænni stöðvarinnar. Að lokum var fyrirhugaða kerfið borið saman við liþínrafgeyma og afl í gas í raforkukerfi hvað varðar hagkvæmni í efnahags- og umhverfismálum.

Rannsóknin leiðir í ljós að smáskala vatnsorkudælimiðlun hefur talsverða möguleika en mikil samkeppni kemur frá liþínrafgeymum miðað við framtíðarþróun þeirra. Hins vegar felur útfærsla fyrirhugaðs kerfis í sér miklar tæknilegar áskoranir vegna talsverðrar stærðar.

Dedication

To the mothers.

Table of Contents

List of Figures

List of Tables

Abbreviations

AbLaV	Verordnung zu Abschaltbaren Lasten
AfA	Absetzung für Abnutzung
API	American Petroleum Institute
APOS	Allocation at the Point of Substitution
BDEW	Bundesverband der Energie- und Wasserwirtschaft e.V.
CO_2	Carbon Dioxide
DC	Direct Current
DE	Deutschland
EEG	Erneuerbare-Energien-Gesetz
EN	European Norm
EPEX	European Power Exchange
IEA	International Energy Agency
ILCD	International Reference Life Cycle Data System
IRENA	International Renewable Energy Agency
ISO	International Standards Organization
KWKG	Kraft-Wärme-Kopplungs-Gesetz
LCA	Life Cycle Assessment
LCIA	Life Cycle Inventory Analysis
LMO	Lithium Manganese Oxide
MACRS	Modified Accelerated Cost Recovery System
NGO	Non-Governmental Organization
NMC	Nickel Manganese Cobalt
O_2	Oxygen
OECD	Organization for Economic Co-operation and Development
P2G2P	Power to Gas to Power
PaT	Pump as Turbine
PEM	Proton Exchange Membrane
PEMEC	Proton Exchange Membrane Electrolysis Cells
PHES	Pumped Hydro Energy Storage

PV	Photo-Voltaic
QFD	Quality Function Deployment
RoW	Rest of World
SCCT	Simple-Cycle Combustion Turbine
StromNEV	Stromnetzentgeltverordnung
VAT	Value Added Tax
VFD	Variable Frequency Driver
VRE	Variable Renewable Energy
WACC	Weighted Average Cost of Capital

List of Variables

γ	Unit Weight of Stored Liquid
γ_F	Partial Factor
$\Delta\sigma_p$	Stress Variation in Prestressing Tendons
ΔP_e	Long-term Inflation Forecast
η_{charge}	Efficiency of the Charging Process
$\eta_{discharge}$	Efficiency of the Discharging Process
η_{gen}	Generator Efficiency
η_{motor}	Motor Efficiency
η_p	Pumping Efficiency
η_{pipe}	Pipe Efficiency
η_t	Turbine Efficiency
η_{total}	Total System Efficiency
η_{trans}	Transformer Efficiency
ξ	Ratio of Bond Strength
ξ_1	Adjusted Ratio of Bond Strength
ρ_{ct}	Density of Concrete
ρ_{st}	Density of Steel
ρ_w	Water Density
σ_t	Tensile Stress
a	Distance between End of Footing and Tank Wall
A	Required Area of Footing in Contact with Soil
A_{ct}	Cross-sectional Area of Concrete for Floor Slabs

$A_{ct,h}$	Horizontal Area of Concrete within the Tensile Zone
$A_{ct,v}$	Vertical Cross-sectional Area of Concrete within the Tensile Zone
A_n	Annual Costs
$A_p{}'$	Cross-sectional Area of Tendons
$A_p{}'_{total}$	Cross-sectional Area of all Tendons over Entire Tank Wall
A_s	Cross-sectional Area of Reinforcement for Floor Slabs
$A_{s,v}$	Cross-sectional Area of Vertical Reinforcement
b_F	Width of the Footing
c_0	Corrosion Allowance
c_1	Value of Tolerance
c_2	Thinning Allowance
$CAPEX$	Capital Expenditure
$CExD$	Cumulative Exergy Demand
CF	Capacity Factor
d	Thickness of the Footing Slice
d_i	Required Inner Pipe Diameter
D_o	Outer Pipe Diameter
e	Minimum Required Wall Thickness for Pipe
EC_{charge}	Electricity Costs to Charge
$EC_{discharge}$	Electricity Costs to Discharge
EC_{total}	Total Electricity Costs
e_{ord}	Ordered Pipe Thickness
E_{pot}	Potential Energy
f	Design Stress
$f_{ct,eff}$	Mean Value of Tensile Strength of Concrete
f_{ctm}	Mean Tensile Strength

F_p	Compressive Force
F_t	Tensile Force
$f_{y,d}$	Design Yield Strength of Steel
g	Gravitational Acceleration
GWP_{100}	Global Warming Potential for 100-year Period
h_{eff}	Effective Hydrostatic Load
h_F	Depth of the Footing
i	Nominal WACC
IQR	Interquartile Range
k	Coefficient for the Effect of Non-uniform Self-equilibrating Stresses
k_c	Stress Distribution Coefficient
$L\&C$	Levies and Concessions
$LCOE_{Storage}$	Levelized Cost of Stored Energy
$LCOE$	Levelized Cost of Electricity
M	System Lifetime / Year of Decommissioning
n	Year Index
NP	Nameplate Power Capacity
NRG_n	Annual Energy Production
$OPEX_{fixed,n}$	Fixed Annual Operational Expenditure
$OPEX_n$	Operational Expenditure
$OPEX_{variable,n}$	Variable Annual Operational Expenditure
p	Pressure
$p(z)$	Characteristic Value of Pressure
$p(z_{max})$	Maximum Hydrostatic Pressure at Bottom of the Upper Reservoir
p_c	Calculation Pressure
P_s	Specific Load Acting on the Footing

Q	Flow Rate
$Q1$	25th Percentile
$Q3$	75th Percentile
q_a	Allowable Bearing Value
r	Tank Radius
R	Discount Rate / Real WACC
R_e	Economic Rating
$R_{eH\ t}$	Minimum Upper Yield Strength at the Calculation Temperature
R_m	Tensile Strength of Steel
$R_{p0.2\ t}$	Yield Strength at the Calculation Temperature
R_t	Technical Rating
RV_M	Residual Value at the End of the System Lifetime
t	Tank Wall Thickness
t_a	Minimum Nominal Thickness of the Base Ring
t_b	Minimum Nominal Thickness of the Bottom Plate
TR	Corporate Tax Rate
t_s	Steel Plate Thickness
$TS_{DEP,n}$	Tax Shield for Depreciation
v	Flow Velocity
V	Required Volume of the Upper Reservoir
w_a	Limiting Value for Width of Base Ring
x	Observed Tank Height
z	Tank Height
z_{jc}	Joint Coefficient
z_{max}	Maximum Tank Height

Acknowledgements

I would like to offer my very great appreciation to Halldór Pálsson for his valuable and constructive suggestions during the planning and development of the current study. His willingness to supervise this very comprehensive and interdisciplinary research work is highly appreciated. I would like to offer my special thanks to Bjarni Bessason for introducing me to the world of civil engineering. His willingness to give his time so generously has been very much appreciated. Advice given by Daði Sverrisson has been a great help in understanding the relevant principles of finance and controlling. I would furthermore like to thank Hafþór Ægir Sigurjónsson for his highly appreciated advice on the environmental side of this research work. Assistance provided by Wolfgang Schick from BBV-Systems GmbH regarding the prestressing steel technology was also greatly appreciated. I would also like to offer very special thanks to Bjarki Axelsson who translated the abstract of the current study to Icelandic.

I would like to extend my thanks to Brynhildur Davíðsdóttir for her sparkish enthusiasm in teaching, and to Bjargey Anna Guðbrandsdóttir for her great organizational work in the ENR programme. Their support and advice have always been of great help. I would also like to express my very great appreciation to my dear friends from all over the world who made my stay in Iceland such a joyful experience. I am now more certain than ever that this world can be transformed into a place that values the principle of sustainability.

Finally, I would like to express my deep gratitude to my dearest friend Tabea for her appreciation and patience during the past two years.

1 Introduction

In January 2019, another milestone for the world-famous German Energiewende has been set. The government-appointed coal commission came to an agreement and announced that Germany will phase out coal- and lignite-fired power plants by no later than 2038 (Deutsche Welle, 2019). While a range of NGO's state that this goal still is not sufficient to achieve the reduction target of the Paris agreement, as described by Sadik (2019), there is no doubt that the energy transition in Germany is now entering an important phase. So far, the transition has already taken a rapid pathway. As of 2018, the share of power from renewable sources was 40.3% of the total German electricity mix (Fraunhofer-Gesellschaft, 2019b). Thereof, a large proportion came from the variable renewable energy (VRE) sources wind and solar PV. The increasing share of intermittent power sources demands a new level of power system flexibility to balance supply and demand but also for the sake of energy security.

Energy storage systems have been used for over one century to shift energy supply, as described by Giesecke, Heimerl, and Mosonyi (2014). The technology is traditionally used to store energy from baseload power plants, such as nuclear or coal-fired power plants, in times of low demand to supply the energy later when the demand peaks. Modern applications of energy storage focus on the load balancing properties of such systems in a power grid with high shares of VRE.

Analyzing the different energy storage technologies reveals that the most important technology in regards of installed capacity is Pumped Hydro Energy Storage (PHES), representing around 96% of the worldwide installed energy storage capacity (IRENA, 2017). Pumped hydro is the oldest and most mature energy storage technology. However, in areas where large PHES-plants have been operational for decades there also is a lack of suitable sites for new facilities (Ardizzon, Cavazzini, & Pavesi, 2014). This, as well as environmental and public concerns, has limited the further development of PHES systems in Europe.

While the public acceptance for large-scale energy projects in Germany is very low, there has been a new interest in decentralized storage solutions that are rather on a community or even a household scale. Downscaling pumped hydro systems could potentially decrease the technology's environmental impact and increase public acceptance. Moreover, small systems that are integrated into the urban built environment, namely in buildings, could significantly reduce the land-use impact. However, at this small-scale new battery technologies, such as lithium-ion systems, potentially perform better than PHES solutions, and have taken the lead in the growing small-scale energy storage market (Abdon et al., 2017).

Despite the odds, small-scale PHES systems have still been subject to research interest in recent years. de Oliveira E Silva and Hendrick (2016), for instance, describe a real-life PHES system that is located in a building. The researchers, however, find that at this small scale the pumped hydro system is far from economically viable. Better results have been found in the case studies of PHES systems in existing buildings by Fonseca and Schlueter (2013) and Schulze (2017). But also in these cases, an economical operation is highly questionable. On the other hand, Manolakos, Papadakis, Papantonis, and Kyritsis (2004) find that small scale

PHES have proven to be a cost-efficient option for island grids when combined with intermittent renewables, such as solar power. These observations show that the economies of scale, but also the market conditions, play an important role for the feasibility of PHES systems. It appears that the viability of PHES facilities strongly depends on the system capacity. Fitting PHES plants into *existing* buildings does not deliver the desired economic viability that is gained from conventional, large-scale PHES (de Oliveira E Silva & Hendrick, 2016).

The current case study aims on finding a technical solution that allows the economic and environmentally-benign operation of a PHES plant at a small scale, namely in the urban built-environment. The focus thereby lies on the implementation of an entirely new building that is specifically designed to accommodate a pumped hydro system, and not on the retrospective equipping of an existing building. This approach marks a gap in the literature.

From the previous observations, three research questions arise:

1. How small can a pumped hydro system be while remaining economically feasible?

2. How can an economically feasible pumped hydro energy storage system be implemented in the urban built environment?

3. How does the proposed PHES plant in the urban built environment compare to other PHES systems, lithium-ion battery systems and power to gas to power (P2G2P) systems in terms of economic and environmental feasibility?

Following this introduction in chapter one, a background chapter provides detailed insight into the basic concepts that are discussed in the current study. Chapter three introduces the methodologies that are applied. The economic pre-study in chapter four has the aim to find the smallest economically feasible capacity of a PHES plant, answering the first research question. The following engineering design study represents the backbone of the current study. It examines the technical possibilities for implementing a PHES system in the urban built environment. At the end of chapter five, the most promising concept is selected from the engineering design study. Based on this proposed solution, an economic comparison study is performed in chapter 6, followed by an environmental comparison study in chapter 7. In these chapters, the performance of the proposed innovative PHES system is compared to other energy storage technologies and small-scale PHES case-studies. The combined results are then presented and discussed in chapter eight. Finally, a conclusion is drawn in chapter nine. The feasibility of the proposed solution is evaluated, and a conclusive recommendation is stated

2 Background

The current study builds on the recent developments of power systems in Germany and worldwide. The main challenge, namely power system flexibility, is addressed and put into context. The following subchapters describe the relevance of energy storage systems and their place among other technical solutions for the integration of variable renewable energy plants into the changing power system. The basic working principle of energy storage as well as the individual technologies, namely pumped hydro energy storage systems, lithium-ion battery systems and P2G2P systems, are described, and particular case studies for PHES in buildings are introduced. Furthermore, the working principle of simple-cycle combustion gas turbines is introduced, as this technology is considered as the baseline scenario in the further assessment. Finally, the different applications and timescales of energy storage systems are discussed and the according application for the current study is defined.

2.1 Implications of the Energy Transition

Over the past years, the German electricity system has gone through a rapid and substantial transition. According to the Fraunhofer-Gesellschaft (2019b), the share of power from renewable sources has more than doubled in the past decade: from 16.2% in the year 2008 to 40.3% in 2018. In 2018, almost 30% of the grid power originated from the volatile renewable energy sources wind and solar. This high share of intermittent power has created the need for a more flexible power system. While the German electricity mix traditionally relies on nuclear and coal-fired power plants that provide continuous baseload power, the phaseout from nuclear power by 2022 (Wecker, 2019), and the coal phaseout by 2038 (Deutsche Welle, 2019) call for solutions that enable the integration of intermittent renewable energy into a modern and reliable power grid. This endeavor can be accomplished by applying a set of technical solutions and economic incentives (IEA, 2018).

The main challenge is to balance the supply and demand of electrical power. According to Ter-Gazarian (2011), the demand side can be categorized into three main consumers: industrial, domestic and commercial. The electricity demand of these consumers can be predicted easily. Domestic consumption, for instance, peaks in the morning and evening hours or on weekends when people are at home and use their electrical devices. The maximum of commercial consumption is usually reached at lunch hours and industrial consumption is usually more evenly distributed over the day due to the possibility of nighttime production. Depending on the portions of electricity used by the three consumers, the demand curve in countries with high living standards tends to have visible morning and evening peaks caused by the domestic consumption patterns, while the minimum demand is usually expected in the early morning hours when people are sleeping.

Figure 1 depicts an exemplary week in September 2018. The energy demand is represented by the red line. While the lowest demand occurs at nighttime – between 2:00 and 4:00 AM, a slight morning peak can be identified at around 8:00 AM. The peak demand is usually reached around noon and the evening peak occurs at 20:00 PM. At this time, many Germans

watch the news on television. The diagram also reveals that the overall energy demand is much lower on weekends. This is due to the fact that many commercial and industrial consumers do not operate on weekends. The lowest demand occurs on Sundays as most businesses are closed.

The behavior of the supply side depends strongly on the power source. As described above, thermal power plants usually provide baseload power and are ideally operated permanently. Volatile renewable energy sources, on the other hand, are not entirely predictable. While solar power generation can only be expected during daytime, with its peak production at noon, the actual power generation from solar sources still strongly depends on the weather and the time of year. The characteristic solar PV power peaks are depicted in Figure 1. The maximum usually occurs around 1:00 PM. Wind can occur at day- and nighttime. Therefore, on- and offshore wind power varies more strongly and does not necessarily show patterns as shown in Figure 1.

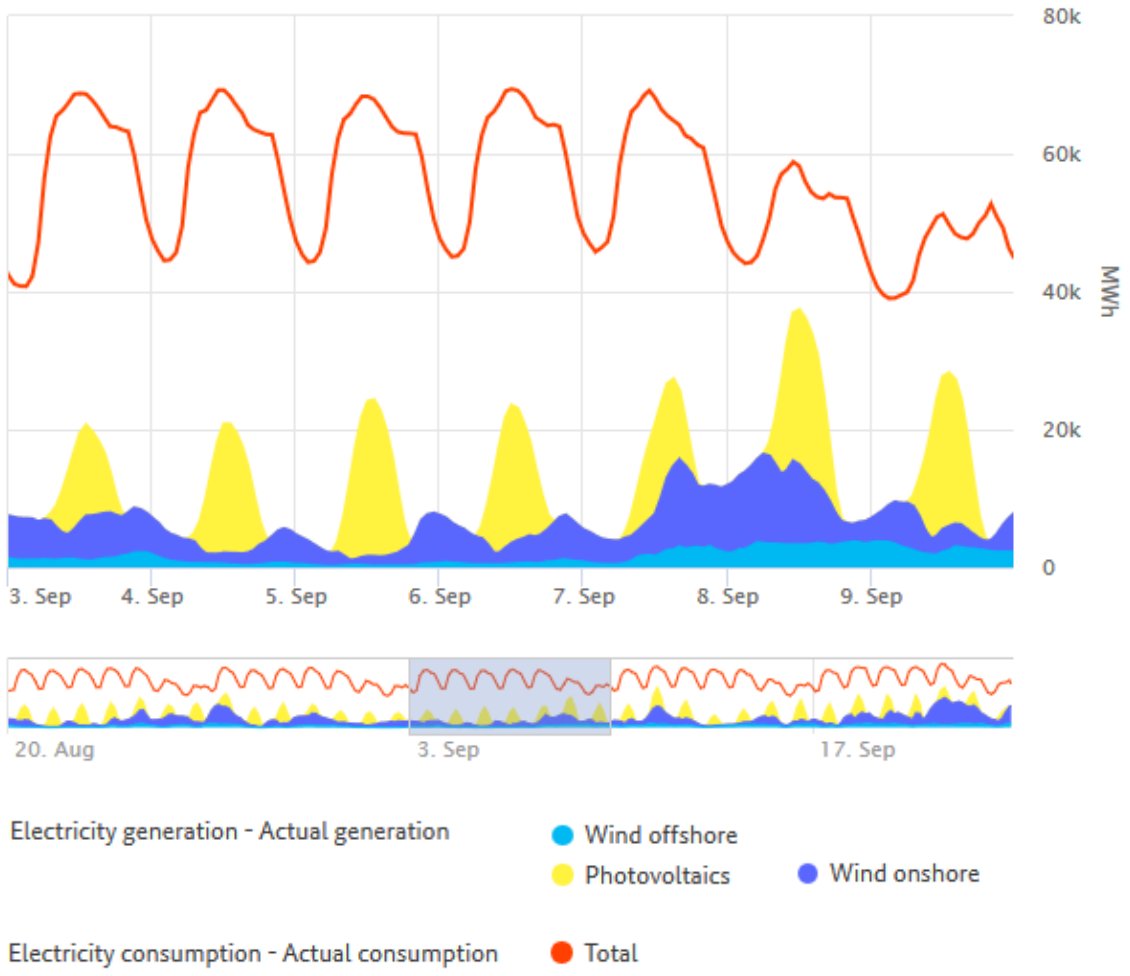

Figure 1 Power supply from intermittent renewables and power demand from 03rd September 2018 to 09th September 2018. Reprinted from Bundesnetzagentur (2019).

The IEA (2018) defines six phases of required system flexibility for variable renewable energy integration. These phases are characterized by their share of VRE generation. While first phase systems only deploy very few VRE plants that are insignificant on the systems scale, phase 2 systems show noticeable changes between load and net load. However, even

phase 2 systems can be easily operated by using the existing system resources effectively. In phase 3 systems, the fluctuation of the demand-supply balance exceeds the possibilities of the existing infrastructure and a systematic increase in power system flexibility becomes necessary. In 2016, Germany was considered a phase 3 country with a VRE share slightly below 20% (IEA, 2018).

Phase 4 is characterized by periods in which VRE generation can supply a large proportion of electricity demand. Large gaps between supply and demand can be expected, concerning the power system stability. Thus, operational and regulatory approaches need to be adapted to secure the power system. In phase 5, additional measures are required. Demand shifting and interchange with neighboring power systems can be applied in order to balance supply and demand. In this phase, VRE systems regularly generate more electricity than is demanded, making conventional baseload plants temporarily redundant. The sixth and last phase is characterized by even higher shares of VRE deployment. The greatest challenge in this phase is to meet the demand in longer periods of low availability of power from wind and solar – thus when the sun does not shine, and the wind does not blow. In this phase seasonal energy storage is required (IEA, 2018).

The IEA (2018) furthermore proposes three different aspects that have an influence on the power system flexibility. These three layers include technical, economic and institutional policies as depicted in Figure 2. In order to enhance the flexibility of power systems, all layers need to be considered consistently.

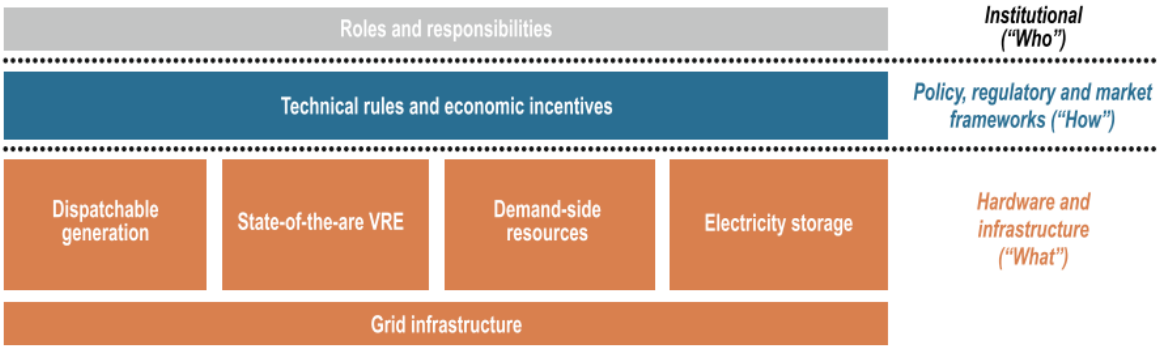

Figure 2 Three layers of system flexibility. Reprinted from IEA (2018, p. 23).

The technical solutions for integrating large shares of VRE sources are: the grid infrastructure, dispatchable generation, state-of-the-art VRE, demand-side resources and electricity storage (IEA, 2018). Currently, dispatchable generation is the main technical solution for ensuring power system flexibility. Flexible coal- or gas-fired power plants adjust their power output depending on the share of VRE in the grid. Moreover, peak power plants are used to cover demand peaks that occur throughout the day (IEA, 2018). Simple-cycle combustion gas turbines are commonly used for this task. This technical solution can solve the problem of too small VRE shares but does not provide solutions for when VRE generation exceeds the demand.

State-of -the-art VRE deployment refers to the idea of making VRE plants more "system-friendly" by equipping them with software-controlled power electronics that provide important services such as fast frequency response. Another option is to choose the optimal locations for wind and solar PV plants so that the systems complement each other, reducing

strong fluctuations in the local power supply. Demand-side resources have the aim to shift electricity demand to times of the day when the supply is abundant. Furthermore, upgrading the grid infrastructure is an important task for increasing the power system flexibility. This can be achieved by providing larger and meshed networks and applying grid digitalization (IEA, 2018).

Finally, electricity storage can be considered another important technical solution for a changing power system. Storage systems fill the gap that dispatchable generation leaves open. They do not only supply electricity to the grid when demand exceeds supply, but they also store excess electricity when VRE generation exceeds the demand. This characteristic makes them very valuable for power system flexibility services. Depending on the energy storage technology applied, many different services can be provided, ranging from fast frequency response at ultra-short timescales to long-term bulk energy storage (IEA, 2018).

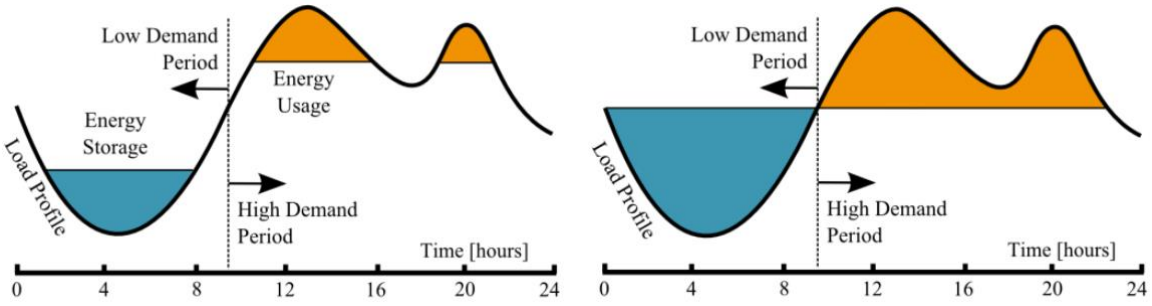

Figure 3a) (left) Schematic operation principle of energy storage systems for peak shaving. Reprinted from Sabihuddin, Kiprakis, and Mueller (2015, p. 174). b) (right) Schematic operation principle of energy storage systems for load leveling. Reprinted from Sabihuddin et al. (2015, p. 174).

Figure 3a shows a typical load profile of an energy storage system for peak shaving. In times of low demand, the storage system is charged and when the energy demand is high, the electricity is discharged. Figure 3b shows the same load profile but a larger energy storage system that completely levels the load. To which extent a storage system is used, depends on the availability of VRE.

2.2 Simple-Cycle Combustion Turbine

Due to their rapid start-up capabilities, gas turbines have been used as standby and peak power units as early as the 1970s (Breeze, 2005). In recent years, such facilities have become more and more important as the share of volatile renewable energy generators in the power grid have increased significantly. Sterner and Stadler (2017) stress the importance of gas turbines to regulate and balance the intermittent generation through volatile renewable energy sources.

Modern gas turbines are based on an invention by the German engineer F. Stolze in 1872. In his design a compressor is used to pressurize air and force it through a combustor in which it is mixed with fuel and ignited. The occurring hot flow of gas is then directed into a turbine where it generates rotary motion. The design by the Norwegian A. Elling in 1903 includes “a rotary compressor on the same axis as the turbine” (Breeze, 2005, pp. 47-48). The block

diagram of a simple-cycle gas turbine for power generation is shown in Figure 4. In modern applications the rotary motion is utilized by a generator to harness electricity.

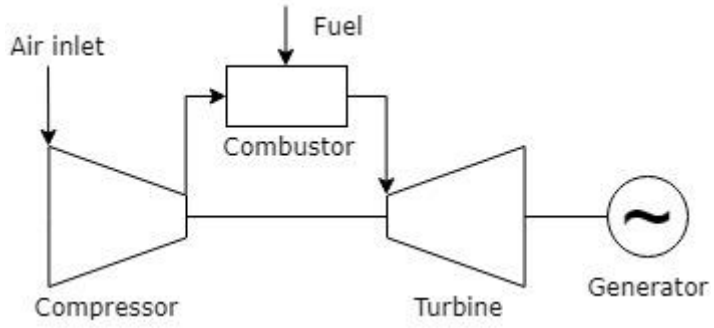

Figure 4 Block diagram of a simple-cycle gas turbine for power generation. Reprinted from Breeze (2005, p. 47).

The efficiency of gas turbines is crucial for their economical operation as they require natural gas. The higher the efficiency of the plant is, the higher the power output is for a given quantity of natural gas input. Furthermore, the process of natural gas combustion also emits greenhouse gases and other pollutants, making a higher efficiency important, also from an environmental viewpoint. The efficiency of modern simple-cycle combustion turbines can reach up to 41% as described by Krein (2011) for the gas turbine power plant in Darmstadt, Germany.

According to Boyce (2012) the simple-cycle combustion turbine currently is the most commonly used gas turbine. However, despite their importance for a rapidly changing energy system, they usually cannot be operated economically in Germany as described by Entega AG (2019). The plant-operator states that this is due to the low price for CO_2 certificates and the fact that coal-fired power plants can therefore operate more economically than the less polluting gas turbine power plants. Still, gas turbine plants are often classified as system-relevant and therefore need to be available at any time to balance the grid.

2.3 Energy Storage Technologies

Several technologies are available for storing energy. The variation of working principles between them is substantial. They range from physical systems, including mechanical and thermal, to electrical, electrochemical and chemical systems (Sterner & Stadler, 2017). In the current study a selection of promising technologies is discussed. The following subchapters provide an insight into these energy storage technologies, namely pumped hydro energy storage, power to gas to power systems and lithium-ion battery systems.

2.3.1 Pumped Hydro Energy Storage Systems

According to IRENA (2017), pumped hydro energy storage plants dominate the worldwide installed capacity of electricity storage plants, with 96% of the total installed capacity of 176 GW in mid-2017. The first facilities have been realized as early as 1890 in Switzerland and Germany, making PHES systems a proven and mature technology. Thus, the technology has

been used for decades to balance supply and demand in power systems (Giesecke et al., 2014).

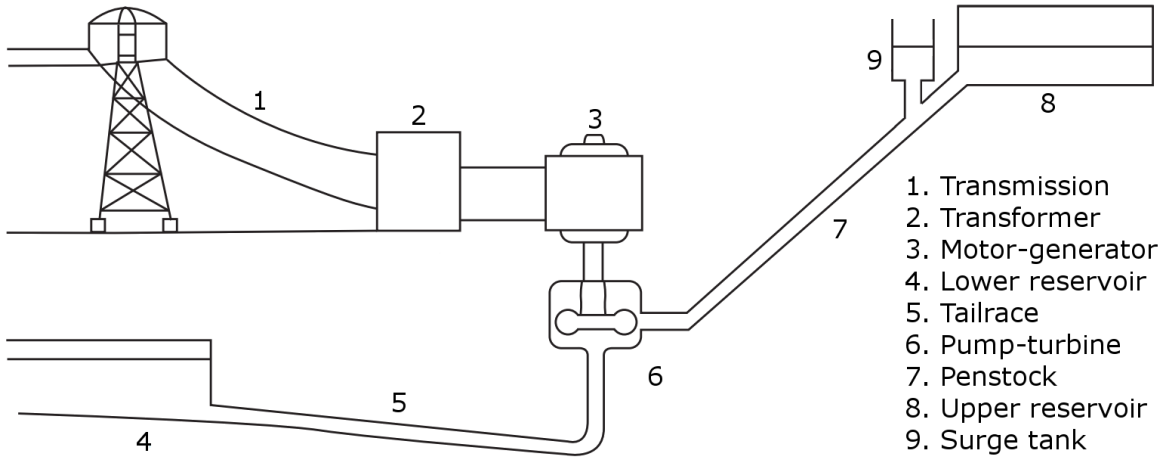

Figure 5 Pumped hydro energy storage scheme. Adapted from Ter-Gazarian (2011, p. 86).

Ter-Gazarian (2011) states that pumped hydro systems utilize the potential energy of water when stored at a high elevation. When the electricity supply is higher than the demand, the PHES system balances this disparity by pumping water from a lower reservoir to an upper reservoir. The water is then stored at a higher elevation, so that its potential energy can be released as soon as the power demand exceeds the supply again. In that case, the water flows back from the upper reservoir to the lower reservoir and thereby passes through the pump-turbine, generating electricity in the motor-generator which is transformed and sent back into the electricity transmission system. The components of a typical PHES system can be viewed in Figure 5. The piping system between the lower reservoir and the pump-turbine is also referred to as the tailrace. The piping connection between the upper reservoir and the pump-turbine is called penstock. Depending on the size of the system and the specific layout, a surge tank might be required to balance the sudden start or stop of the plant, avoiding water hammers through the initiated pressure change (Sterner & Stadler, 2017).

PHES plants are historically implemented at very large scales. Small-scale systems are usually not feasible because of the concept of *economy of scales* that strongly applies to pumped hydro systems. This is due to the low energy density of PHES systems. According to IRENA (2017), pumped hydro energy storage is the technology with the lowest energy and power density. Therefore, large reservoirs for pumped hydro plants are usually deployed in mountainous regions.

Nevertheless, there has been an increased interest in small-scale PHES systems in recent years. Partially due to the implementation of hybrid plants that combine wind or solar plants with the storage abilities of pumped hydro, as described by Katsaprakakis et al. (2012) and Max Bögl Wind AG (2019b), but also due to the growing trend of decentralization of power systems, as pointed out by de Oliveira E Silva and Hendrick (2016). However, only few researchers have analyzed the feasibility of pumped hydro systems in buildings, and only one real-life system has actually been implemented. Still, three case studies of PHES systems in buildings are introduced in the subchapters below. They are important reference studies for the current thesis.

Case Study 1 – The Goudemand Residence

de Oliveira E Silva and Hendrick (2016) describe and analyze the only known real-life PHES system in a building. The Goudemand residence is an apartment building complex in Arras, France. As part of a building renovation, the building owner decided to implement new energy saving measures and ventured an innovative approach: a small-scale PHES system was implemented in the 10-storey building. The according building can be viewed in Figure 6a before the renovation. The pumped hydro system complements two 500W wind turbines and nine 230W photovoltaic panels on the roof of the building and is supported by a lead-acid gel battery bank that acts as a buffer for the renewable energy sources and the PHES system. The upper reservoir of the PHES system is also situated on the roof of the building, as shown in Figure 6b, storing around 3.5 kWh of useful energy at a height of 30m. It is implemented by sealing off a part of the roof with a waterproof cover. The weight of the reservoir is stated at 60 tons which is supported by the building structure.

Figure 6a) (left) View of the Goudemand residence from above. Reprinted from de Oliveira E Silva and Hendrick (2016, p. 1244). b) (right) View of the upper reservoir of the PHES system on the building roof. Reprinted from de Oliveira E Silva and Hendrick (2016, p. 1244).

The lower reservoir is situated in the basement of the building. Five rectangular plastic water storage tanks with a total capacity of 50 m^3 retain the water. The system uses a separate pump and turbine layout. A Pelton turbine is used to generate electricity while pumping is performed using a multi-stage pump. The system has a rated power capacity of 1.5 kW and an estimated total efficiency of 35% (de Oliveira E Silva & Hendrick, 2016). The low efficiency is due to the small scale of the system. Efficiency losses accrue because small-scale systems – especially their turbines and pumps, or pumps as turbines – have never been optimized to a utilization in small-scale PHES plants because such small-scales are simply not considered economically viable. A specifically designed turbine and pump – as used in large-scale systems – would increase the efficiency but also massively increase the capital costs and render the system unfeasible. This is why small-scale systems use "off-the-shelf" solutions; at cost of the system efficiency. Large-scale systems, on the other hand, take advantage of economies of scale and can be optimized to high efficiencies (Giesecke et al., 2014).

Case Study 2 – The Torre Confinanzas Complex

The Torre Confinanzas Complex consists of five unfinished and formerly abandoned buildings in Caracas, Venezuela, of which the tallest is 190m high. According to Fonseca and Schlueter (2013) the building complex has been informally settled by 3000 inhabitants

and an improvised electricity and water infrastructure has been implemented by the settlers. The improvised infrastructure is failure-prone, which is why the authors of the study propose an innovative renewable energy supply and storage system for the building complex that will, both, provide electricity and water to the 750 families of the vertical community. As the building mainly provides vertical surfaces, and the height of the building offers good exposure to constant winds, the deployment of a pico-scale wind power system is proposed. In order to store energy at high electricity supply through the wind power plant, but also to secure a more constant water supply to the building, an additional PHES system is suggested. Therefore, a sophisticated system is proposed with an array of water tanks on different floors. Two separate circuits are planned, operating 17 pumps and 23 turbines in total. The proposed system has an electric rated turbine power of 30.1 kW and the efficiency is estimated to be around 30-35% (Fonseca & Schlueter, 2013).

Case Study 3 – The Wesermühlen

In his dissertation, Schulze (2017) systematically examines existing building structures in Germany by their potential suitability for energy storage projects. Four different energy storage technologies are considered in his study: flywheel energy storage systems, gravitational energy storage – using an array of masses that are raised and lowered during the process, compressed air energy storage and finally pumped hydro energy storage. Different industrial building complexes, such as military bunkers, power plant cooling towers or silos for dry bulk, are analyzed and evaluated by their suitability.

Schulze (2017) finds that abandoned silos are the most promising structures for energy storage purposes and performs an analysis for the existing silo complex "The Wesermühlen" which has closed operation in previous years. In his study he examines both, the integration of a gravitational energy storage system that uses cranes to lift and lower masses, and a pumped hydro system that uses the silo as an upper reservoir. He concludes that the pumped hydro system is the preferential system as it has a seven times higher storage capacity than the mass-lifting system with a similar capital expenditure.

Figure 7 The Wesermühlen industry complex with silo. Adapted from Schulze (2017, p. 112).

The industry complex is depicted in Figure 7. For his study, Schulze (2017) only examines the silo shown in the front. He finds that the walls of the silo need to be reinforced and sealed in order to withstand the forces of the stored water and to prevent leaks. A nearby river serves

as the lower reservoir. The structure is 40m high and has a storage capacity of 20,000 m^3 of water or 1027 kWh of energy. While no specific turbine or pump type is specified, the turbine is assumed to have a rated power capacity of 230 kW. The efficiency of the system is assumed to be 80% (Schulze, 2017).

2.3.2 Lithium Ion Battery Systems

Lithium-ion batteries currently represent the strongest growing energy storage system in terms of installed capacity. They represent the third largest installed energy storage capacity with over 1 GW worldwide in mid-2017, only outnumbered by PHES systems (96% of the worldwide operational capacity) and molten salt thermal storage. In mid-2017 their operational capacity made up for 59% of all electrochemical – or battery – systems. They are well-suited for mobile applications, due to their high energy density, which is why they are the prime choice in electric vehicles. However, there has also been an increasing trend to apply them in stationary systems to provide services to the electricity grid. Since Elon Musk promoted his Gigafactory, for the production of over 50 GWh of battery packs annually, this technology has been the most discussed energy storage option in recent years. The technology was originally introduced by Sony Corporation in the early 1990s. Mainly for the application in consumer electronics (IRENA, 2017).

Currently, the technology achieves outstanding efficiencies of around 95%, but is still very costly compared to bulk energy storage technologies. The worldwide largest operational lithium-ion battery system is a 100 MW facility that was erected by Tesla in South Australia in 2017 (Wahlquist, 2018).

It must be noted, that despite their good performance, lithium-ion battery systems are also criticized due to their resource demands. Especially cobalt is considered a rare and expensive ingredient. Furthermore, it has been repeatedly reported that the material is mined under poor working conditions in the Democratic Republic of the Congo where 60% of all cobalt originates from (Frankel, 2016). Battery manufacturers have already announced to cut out cobalt in their production. However, this goal remains difficult to achieve due to the importance of cobalt for the good performance of lithium-ion batteries, as described by Chen (2018).

2.3.3 Power to Gas to Power Systems

Hydrogen has been discussed as one of the most promising energy storage options. It does not only enable the integration of volatile renewable energy but also allows for sector coupling between the three energy sectors: electricity, heating and transport – as defined by (Sterner & Stadler, 2017). Power-to-X technologies have emerged that potentially allow storing energy over very long periods in form of gaseous or liquid fuels. These fuels can then be used in mobile applications, in the industry as a feedstock for processes or can be re-electrified as a backup fuel for the electricity grid (IEA, 2015).

In the current study such a power to power system will be assessed, maintaining the comparability with the other examined systems. There are several ways to implement power to power systems. They all start with the transformation of electricity into hydrogen by means of electrolysis. The hydrogen can then be stored, or it can be further processed into methane or even into liquid fuels. It must, however, be considered that each transformation

step decreases the overall efficiency of the process. According to Dörr et al. (2016), the natural gas grid can be used to store hydrogen as long as the total share of hydrogen in the grid remains below 10%. Alternatively, hydrogen can be stored in underground caverns or in pressurized tanks. This process requires a compressor. The next step is the re-electrification of the stored fuel. This can be performed by using fuel cells or a hydrogen gas turbine. If methane is to be re-electrified, a reformer needs to be applied that converts methane into hydrogen (IEA, 2015).

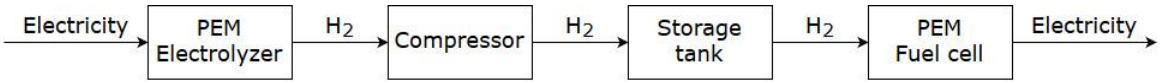

Figure 8 Power to gas to power process examined in the current study.

For reasons of simplicity, the higher total efficiency and lower costs, the current analysis focuses on a power to gas to power system that stores hydrogen in a pressurized tank before it is converted back into electricity. The methanization and methane reforming process therefore become obsolete.

The total efficiency of the P2G2P system described in the current study can be estimated at around 30% considering the current state of the art. This value is considered very low compared to other energy storage options. The chosen system, however, achieves the highest electrical efficiency among the hydrogen-based power to power options described by IEA (2015). Power capacities in the megawatt range are imaginable due to the modularity of electrolyzers and fuel cells.

2.4 Energy Storage Applications

As mentioned in subchapter 2.1, energy storage systems provide many different services to the power system. These services strongly depend on the timescale and the size of the system. Abdon et al. (2017) proposes three different timescales for energy storage systems: the short, medium and long timescale. The short timescale is commonly used for frequency control within a range of seconds to minutes. Such systems can complete around 20 cycles per hour. The medium timescale systems store energy on a daily basis in a range around 4.5 hours, shifting the supply from off-peak to peak hours, while the long timescale systems represent large seasonal storage systems that can store energy over months.

The IEA (2018) on the other hand defines six different timescales that play a role for power system flexibility: ultra-short-term, very short-term, short-term, medium-term, long-term and very long-term. The definition of these different timescales can be found in Table 1.

Supercapacitors and flywheels are used for ultra-short-term frequency control. PHES ternary units can also be applied in this timescale due to the fact that the “changeover from turbine mode to pump mode is possible without changing the direction of rotation” (Rufer, 2018, p. 200), thus instantly.

While battery storage systems are mainly used in the short-term for maintaining the power system frequency – from subseconds to hours – standard PHES systems are rather used in medium and long-term applications for intermittent balancing and bulk energy storage (Aneke & Wang, 2016). Compressed air energy storage (CAES) systems are usually applied

for short-term flexibility. Power-to-gas/liquid systems are expected to play a significant role in very long-term energy storage due to the easy storability and high energy density of gaseous and liquid fuels.

Table 1 Different timescales of power system flexibility. Adapted from IEA (2018, p. 24).

	Ultra-short-term	**Very short-term**	**Short-term**	**Medium-term**	**Long-term**	**Very long-term**
Timescale	Subseconds to seconds	Seconds to minutes	Minutes to hours	Hours to days	Days to months	Months to years
Suitable storage systems	Superca-pacitors; flywheels; battery storage; PHES ternary units	Battery storage	Battery storage; CAES; PHES	PHES	PHES	PHES; hydrogen pro-duction; other power-to-gas/liquid

Another common application and positive side-effect of medium-term energy storage is arbitrage. Price arbitrage describes the process of storing energy at low prices during periods of low demand and selling it when the price is high. The typical timescale of systems that utilize the price-difference between, for instance, night and day is within a range of hours to days (Aneke & Wang, 2016). A high round trip efficiency is beneficial for such systems.

The current study focuses on short/medium-term systems with a cycle duration of four hours. The assessment compares PHES systems, lithium-ion systems and power-to-gas-to-power systems.

3 Methodologies

The following subchapters describe the applied methodologies of the current feasibility study. For the economic assessment, the levelized cost of electricity (LCOE) method is applied and adapted to energy storage applications. The technical feasibility is assessed by applying the engineering design methodology, and finally the environmental feasibility study is performed using parts of the life cycle assessment methodology as described in the ISO 14040 and 14044 standards.

3.1 Levelized Cost of Electricity Storage Methodology

According to Jülch (2016) most studies evaluate the economic viability of energy storage options by comparing the LCOE or levelized cost of stored energy ($LCOE_{Storage}$) in $€/MWh$. It is very important to note that comparing the LCOE or $LCOE_{Storage}$ results between different studies is not recommendable, as the methods they are based on usually vary strongly and back on completely different assumptions (Obi, Jensen, Ferris, & Bass, 2017). Some researchers have therefore developed methods that allow the comparison between very different kinds of energy storage technologies. The studies by Jülch (2016) and Obi et al. (2017) aim on generalizing the LCOE/ $LCOE_{Storage}$ method to make it applicable for any energy storage system, located anywhere in the world.

The $LCOE_{Storage}$ framework model used in the current case study combines features from both models. The detailed algorithm provided by Obi et al. (2017) is used as the foundation for the following adjusted model. In their method, Obi et al. (2017) consider price arbitrage between an off-peak price for charging the storage system and an on-peak price for discharging the storage system. For the current study, the framework model is adjusted to reflect the German market conditions in 2018. The adjusted $LCOE_{Storage}$ framework model for German market conditions in 2018 is shown in equation 1 below.

$$LCOE_{Storage} = \frac{CAPEX - \sum_{n=1}^{M} \frac{TS_{DEP,n}}{(1+R)^n} + \sum_{n=1}^{M} \frac{A_n}{(1+R)^n} - \frac{RV_M}{(1+R)^M}}{\sum_{n=1}^{M} \frac{NRG_n}{(1+R)^n}} \quad (1)$$

The first term in equation 1 reflects the capital expenditure $CAPEX$ as described by Jülch (2016). It represents the investment costs at the beginning of the storage systems' lifetime. The second term represents the tax shield for depreciation $TS_{DEP,n}$ discounted over the system lifetime M with the discount rate R, as described by Obi et al. (2017). The third term represents the annual costs A_n, again, discounted over the system lifetime M with the discount rate R. The annual costs of energy storage systems – as shown in equation 2 – comprise the annual operation and maintenance costs $OPEX_n$ and the total electricity costs EC_{total} – both as calculated in Obi et al. (2017).

$$A_n = OPEX_n + EC_{total} \quad (2)$$

The residual value at the end of the system lifetime RV_M reflects the scrap value of the equipment at its end of life and is subtracted from the other terms after being discounted over the system lifetime M with the discount rate R. Finally, all terms are divided by the annual energy production NRG_n discounted over the system lifetime M with the discount rate R (Obi et al., 2017).

Because a real discount rate is used, as described in subchapter 3.1.8, all costs and benefits of the current study are in real terms. The inflation effect is realized by using a real discount rate. Moles, Parrino, and Kidwell (2011) describe the real value of money as "the actual purchasing power of money [..] regardless of when the money is received" (p. 424).

The following subchapters take a closer look at the variables of equation 1 and equation 2 and assumptions for the economic evaluations of the current study are established. These assumptions are valid for the economic pre-study in chapter 4 and the main comparative economic study in chapter 6.

3.1.1 System Lifetime

The system lifetime M of energy storage technologies refers to the duration of their estimated lifetime, from the commissioning until their end of life. In Germany, the system lifetime of any fixed asset is defined in the tables for the depreciation of fixed assets (AfA-table) by the German Federal Ministry of Finance. These values are to be used for depreciation but also deliver a good estimation of an assets system lifetime. The system lifetime of energy storage systems can alternatively be sourced from the literature for the individual technologies.

3.1.2 Capital Expenditure

The overnight capital expenditure $CAPEX$ includes civil and structural costs, mechanical equipment supplies and installation, electrical instrumentation and control, project indirect costs and owner's costs of a project (U.S. Energy Information Administration, 2013). Overnight costs explicitly exclude interest costs over the construction period. They imply that the plant was built "overnight". The capital expenditure is thus a site-specific information and is sourced from the literature for the individual projects described in the economic pre-study in chapter 4 and the main comparative economic study in chapter 6.

As for all cost-related data, the $CAPEX$ values for sites that were constructed in the years before 2018 need to be price adjusted to the year 2018 (Jülch, 2016). This is accomplished by using the producer price index published by Statistisches Bundesamt (2019a) for the Euro market and the producer price index by the OECD (2019b) for the U.S. dollar market. The U.S. dollar values are then transferred to Euros using the average exchange rate in 2018 according to the European Central Bank (2019).

3.1.3 Tax Shield for Depreciation

Obi et al. (2017) models the tax shield for depreciation $TS_{DEP,n}$ assuming the depreciation method used in the United States – the so-called MACRS (Modified Accelerated Cost Recovery System) depreciation. In Germany, this depreciation method does not apply. The most commonly used depreciation method in Germany is the straight-line method

(Dennerlein, 2018). The tax shield for depreciation is thus calculated as shown in equation 3 (Atrill & McLaney, 2017, p. 92).

$$TS_{DEP,n} = \frac{CAPEX - RV_M}{M} \cdot TR \quad (3)$$

According to Atrill and McLaney (2014) the residual value RV_M is subtracted from the $CAPEX$ and divided by the system lifetime M to receive the depreciation expense for each year. The depreciation expense is then multiplied by the corporate tax rate TR. The average German corporate tax rate in the year 2018 was 30% (KPMG, 2019).

3.1.4 Operational Expenditure

The annual operation and maintenance costs $OPEX_n$ can be provided as a single value that remains constant over the system lifetime M. However, in some cases these costs are divided into fixed annual operational expenditures $OPEX_{fixed,n}$ and variable annual operational expenditures $OPEX_{variable,n}$. In these cases, the annual operational expenditure is calculated as shown in equation 4 (Obi et al., 2017, p. 918).

$$OPEX_n = OPEX_{fixed,n} \cdot NP + OPEX_{variable,n} \cdot NRG_n \quad (4)$$

The fixed operation and maintenance costs $OPEX_{fixed,n}$ are power capacity NP related, whereas the variable operation and maintenance costs $OPEX_{variable,n}$ are energy capacity NRG_n related. Just as the capital expenditure, the operational expenditure is a site-specific information and is sourced from the literature for the individual projects described in the economic pre-study in chapter 4 and the main comparative economic study in chapter 6. As for all cost-related input data, the $OPEX_n$ values for sites that were constructed in the years before 2018 need to be inflation adapted to the year 2018 (Jülch, 2016).

3.1.5 Electricity Costs

As described previously, the total electricity cost is calculated according to Obi et al. (2017). Equation 5 shows the total electricity costs (Obi et al., 2017, p. 918). Therein, the annual energy production NRG_n is multiplied by the price difference between the electricity costs to charge EC_{charge} and the electricity costs to discharge $EC_{discharge}$ while incorporating the total storage system round-trip efficiency η_{total}. German levies and concessions $L\&C$ also need to be considered for the electricity charging process. These additional costs are further discussed in subchapter 3.1.10.

$$EC_{total} = NRG_n \cdot \left(\frac{EC_{charge} + L\&C}{\eta_{total}} - EC_{discharge}\right) \quad (5)$$

The electricity costs are derived from the EPEX (European Power Exchange) SPOT SE trading market. Therefore, German market data is gathered from the EPEX SPOT online database for the day-ahead markets for the year 2018. The block prices are used for the current study. Block prices represent average prices for certain time-periods of every day (EPEXSPOT, 2018).

Table 2 shows the annual average of the daily average block prices for the day ahead auction at the EPEX spot market in 2018. Each predefined block represents a certain time of the day

and is named accordingly. By calculating the average price for each block, the best buy- and sell-prices for electricity are determined on an annual average for a predefined daytime. This price arbitrage can be utilized in energy storage systems. Thereby, the lowest price represents a buy-price. When the price is low, the storage system should charge electricity – resulting in electricity costs to charge EC_{charge}.

Table 2 Average 4h block prices for the day ahead auction in 2018 (EPEXSPOT, 2018)

Time of day	Average Block Price 2018 [€/MWh]
Middle Night (01-04)	34.98
Early Morning (05-08)	40.61
Late Morning (09-12)	49.76
Early Afternoon (13-16)	42.81
Rush Hour (17-20)	51.94
Off-Peak 2 (21-24)	46.71

The highest price represents a sell-price. When the price is high, the storage system should discharge the stored electricity – resulting in negative electricity costs to discharge $EC_{discharge}$. The choice of an ideal daytime to charge and discharge also depends on the duration of one charging / discharging cycle. This timespan marks a physical limit.

3.1.6 Residual Value

According to Franco Podio, Gilfredo Cavagnolo, and Cipriano (2012), the residual value RV_M of most hydropower plant components can be estimated at 5 to 10% of the capital expenditure $CAPEX$. For the adjusted $LCOE_{Storage}$ model the residual value is assumed to be 5% of the $CAPEX$ as shown in equation 6. It is furthermore assumed that the same value applies to other energy storage technologies and the simple-cycle combustion turbine (SCCT) baseline scenario.

$$RV_M = CAPEX \cdot 0.05 \tag{6}$$

The residual value RV_M emerges at the systems end of life, thus is to be discounted over the year of decommissioning M with the discount rate R. It is then subtracted from the other terms in the numerator of equation 1.

3.1.7 Annual Energy Production

According to Obi et al. (2017), the annual energy production NRG_n is calculated based on equation 7 for the individual projects described in the economic pre-study in chapter 4 and the main comparative economic study in chapter 6 (Obi et al., 2017, p. 918).

$$NRG_n = NP \cdot (8760\ hr/yr) \cdot CF \tag{7}$$

The capacity factor CF thereby is a ratio that represents the actual operational hours of a system in contrast to the theoretical full-capacity hours of the same time period. The ratio accounts for the duration of the charging and discharging cycles and is deducted by outages due to maintenance or local weather patterns. It is multiplied by the number of hours per

year and the nameplate power capacity NP of the individual energy storage plant. Both values are required as input data from the individual projects (Obi et al., 2017).

3.1.8 Discount Rate

In subchapter 3.1.3, the tax shield is modelled without considering the tax shield for interest. Furthermore, there is no distinction between equity costs and loan costs in the adjusted $LCOE_{Storage}$ model – as opposed to the model presented by Obi et al. (2017). Instead, the adjusted model consolidates equity and debt in the $CAPEX$ – while excluding the interest costs. This is because the adjusted $LCOE_{Storage}$ model assumes the discount rate R to equal the weighted average cost of capital (WACC) after tax. This method is also applied by Jülch (2016).

According to Moles et al. (2011) the WACC is a financial value that accounts for the capital costs from the different sources that have been used to finance a firm or a project. It depends highly on the shares of equity and debt. The WACC considers these shares and their cost of capital in one rate. In compliance with Berk and DeMarzo (2011), the WACC after tax additionally takes into account the tax-deductibility of interest payments and thus replaces the tax shield for interest as modelled in Obi et al. (2017). This simplifies the model considerably.

The WACC is an entity that is usually calculated according to a company's or a projects individual share of equity and debt and their cost of capital. In the current case study, the model needs to be kept rather general which is why assumptions need to be made for the WACC. The consulting firm KPMG (2018) analyzed the cost of capital of over 250 companies from Germany, Austria, and Switzerland in the year 2018. The study delivers an overview of the average WACC after corporate taxes by industry. For the energy and natural resources sector, an average nominal WACC of 5.5% is determined for 2018 (p. 20). As real data is used for this study, the nominal WACC needs to be converted to a real WACC by incorporating the long-term inflation forecast. This is accomplished by using the Fisher Equation for inflation as shown in equation 8 (Moles et al., 2011, p. 59).

$$R = \frac{1+i}{1+\Delta P_e} - 1 \tag{8}$$

In equation 8, R is the real WACC, i represents the nominal WACC, and ΔP_e is the long-term inflation forecast or the expected annualized price-level change. According to the OECD (2019a), the current long-term inflation forecast for Germany is 2.2%. Thus, the real WACC, and consequently the discount rate R for the adjusted $LCOE_{Storage}$ model, is calculated as $R = 3.23\%$.

3.1.9 Storage System Round Trip Efficiency

The site-specific round-trip storage system efficiency η_{total} is sourced from the literature for the individual projects described in the economic pre-study in chapter 4 and the main comparative economic study in chapter 6. It includes the efficiency of the charging process η_{charge} and the efficiency of the discharging process $\eta_{discharge}$. If the total efficiency is divided into subprocesses, the total efficiency can be easily calculated by multiplying the subprocess efficiencies by another.

3.1.10 Levies and Concessions

As shown in subchapter 3.1.5, certain levies and concessions need to be considered as additional costs for each distributed MWh of electricity. According to Sterner and Stadler (2017) these additional costs can potentially determine the feasibility of an energy storage system. Despite the increasing importance of storage systems, the operation of such facilities has become increasingly unfeasible in Germany due to a jurisdiction by the German Federal Supreme Court. The court classified energy storage systems as final consumers, obliging the operators to pay all regular levies and concessions. According to BDEW (2016), this development has slowed down the further expansion of large-scale energy storage facilities in Germany and creates unequal competition conditions between Germany and its neighboring countries. However, the German legislature has meanwhile introduced exceptions for energy storage systems. Under certain conditions facilities can be exempt from the system usage charge, the electricity tax, and the EEG reallocation charge for renewable energies. Other levies and concessions are still charged (Sterner & Stadler, 2017).

Table 3 Levies and concessions for energy storage facilities in 2018 (BDEW, 2019)

Levy	Amount of charge 2018 [€/MWh]
Concession levy	1.1
KWKG levy	2.6
§19 StromNEV levy	2.5
Offshore-grid levy	0.4
AbLaV levy	0.11
	Σ 6.71

The different levies can be found in Table 3. The sum of all levies and concessions is therefore $L\&C = 6.71\ €/MWh$, assuming that all energy storage facilities analyzed in the current study are eligible for the exemptions described above.

3.1.11 Other Taxes

For simplification reasons the income tax and the property tax, which are considered as annual costs in Obi et al. (2017), are not regarded in the adjusted model. If the income and property tax were considered in the current study, the income from the energy storage system and the size of the property would need to be estimated. Real-life data on these entities is hardly made public by energy storage system operators. Income and property taxes are therefore neglected in the current case study.

3.2 Engineering Design Methodology

The current study aims on systematically finding a suitable design for a feasible PHES system in a building. An engineering design methodology is applied to find an innovative solution. Product innovation is not necessarily based on good luck or a single good idea. According to Pahl et al. (2007) it can also be achieved by utilizing a systematic engineering design approach. Performing a step-by-step analysis and synthesis can even result in better solutions, because the systematic approach opens a very wide range of possible solutions to

a defined problem. A thorough comparison and analysis of this field of solutions can then result in the optimal design – including the certainty that the whole range of possible solutions has proven inferior towards the selected solution.

Pahl et al. (2007) describe four main phases of the planning and engineering design process: planning and task clarification, the conceptual design, the embodiment design and the detail design phase. However, Pahl et al. (2007) also state that a clear distinction between these phases is not always possible and desired as the engineering design technique is a very fluent process. The main steps and tasks of the planning and engineering design process can be viewed in Figure 9.

The first phase is characterized by the clarification of the task. It is important that the task is defined very well before the next steps are undertaken. It makes sense to define technical requirements but also to consider the customers or users requirements as these can play an important role for the success of a product. The task clarification always results in a requirements list that documents the optimal and minimum requirements that the product must fulfill in order to be accepted as a solution. This requirements list needs to be adapted and updated during the entire engineering design process due to unforeseen, new or changed requirements that evolve during the process. The requirements list can be considered the central document of the engineering design (Pahl et al., 2007).

The goal of the conceptual design phase is to specify the principle solution or concept. Therefore, the essential problem behind the task is defined. Abstraction is the key element to formulating and finding the crux of the problem. The aim should be to find a very broad problem formulation that opens the field of conventional solutions and allows for new and innovative ideas. The essential problems are determined by analyzing the requirements list. Once found, a function structure is defined that describes the layout or function of the task. The overall function can be described in a block diagram by considering energy and material flows, as well as signals. In a next step, this overall function is broken down into subfunctions. In many cases – also in the current study – the general solution is already well known and only certain subfunctions need to be reimagined. These cases are referred to as *adaptive designs* (Pahl et al., 2007).

For each subfunction working principles need to be found, followed by the combination of these working principles into a principle solution – or concept. This procedure often leads to a set of solution variants that all have pros and cons. In the final step, these variants need to be evaluated. If the variants do not fulfill the requirements list, they are eliminated. The other solution variants are compared systematically “by the methodical application of specific criteria” (Pahl et al., 2007, p. 132). These criteria are mainly of technical nature, but economic criteria also play a role during this phase. The assessment may require a further development of the concept.

Very often, elements of embodiment design, for instance the establishment of the preliminary form design, material selection and basic calculations can be required during this stage. This also is the case in the current study. In the further assessment, embodiment design has the aim to improve the conceptual layout. An iterative approach is applied to improve the design, eliminate weak spots and minimize costs. This process results in the definitive layout. The detail design then includes the preparation of detailed technical drawings and part lists. These documents then serve as an important tool for the production preparation. At the end of this phase stands the final product or solution.

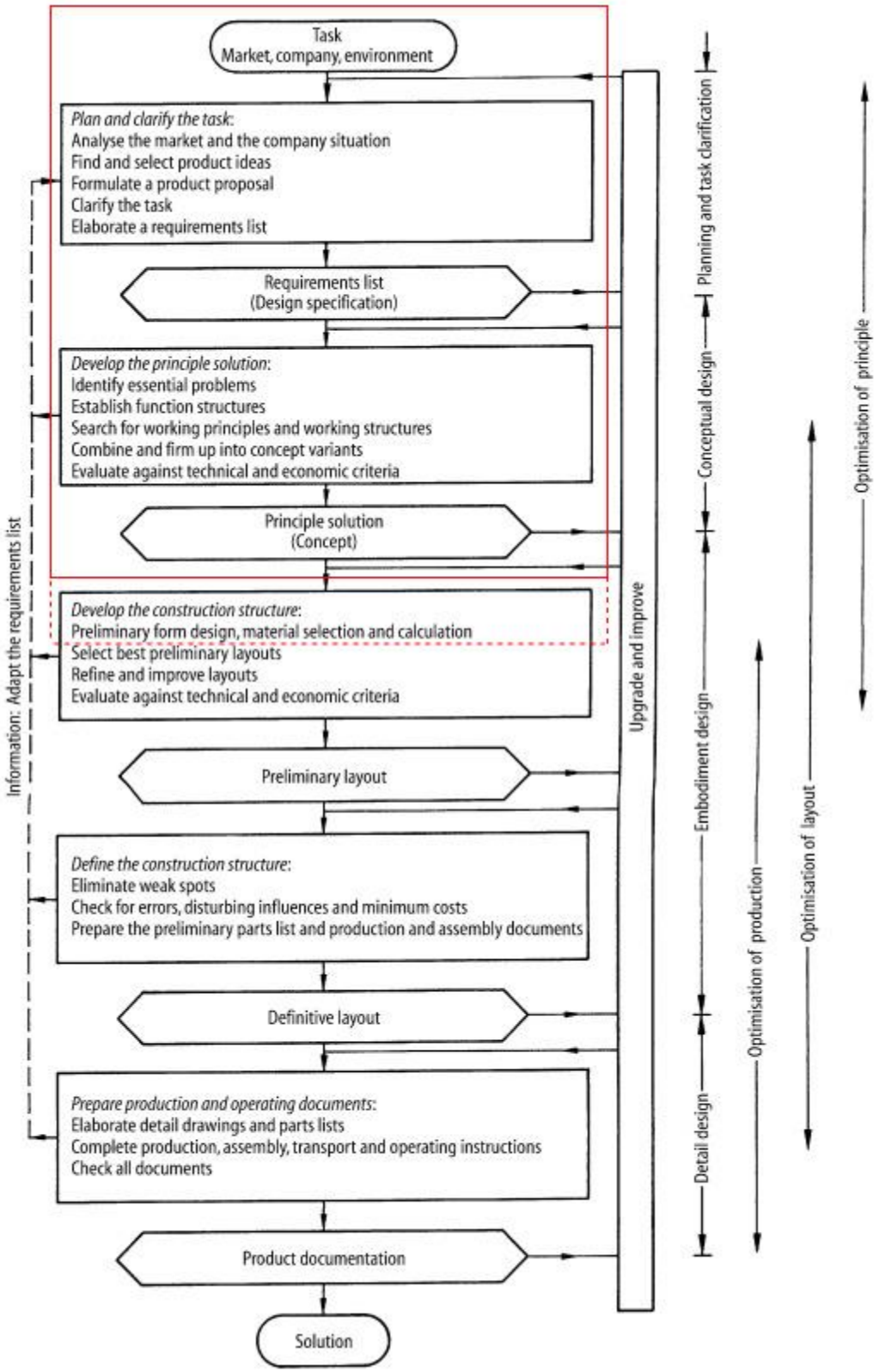

Figure 9 Steps in the planning and engineering design process. Adapted from Pahl et al. (2007, p. 130).

The current study includes the planning and task clarification as well as the conceptual design phase of the engineering design process. The basic goal is to develop a concept for a PHES in the urban built environment. Elements from the embodiment design phase are also applied, as described above. The red box in Figure 9 depicts the steps that are applied in the current study.

3.3 Life Cycle Assessment Methodology

Life cycle assessment (LCA) is a methodology that finds the environmental impact of a product, process, or service. A full LCA thereby takes every single phase of the products lifetime into account, starting with the extraction of raw materials, the material and energy consumption during the planning, design and manufacturing of the product, as well as the packaging and transport. Furthermore, the use-phase of the product is considered as well as the end-of-life, including all related pollution or waste (Agarwal et al., 2012). The entire product life-cycle is depicted in Figure 10.

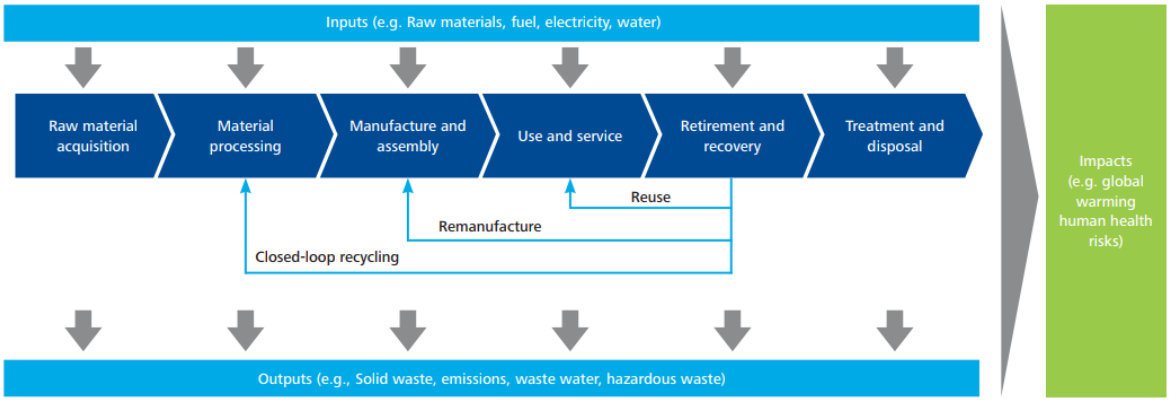

Figure 10 The product life cycle as decribed in ISO 14040:2006. Reprinted from Agarwal et al. (2012, p. 2)

A full LCA also considers every aspect of the environmental impact, defined by a set of different impact categories; for example, the climate change impact, the resource depletion impact, the ozone depletion potential or the human health impact. LCA can be considered a holistic approach that enables organizations and businesses to examine the entire lifecycle of a product, process or service from a complete set of environmental viewpoints. The four phases of an LCA study are: defining the goal and scope of the study; gathering information on the product system also referred to as the life cycle inventory; performing the actual life cycle impact assessment; and discussing the results of the study. This approach is determined by the International Standards Organization (ISO) in the ISO 14040 and 14044 standards for performing life cycle assessment studies (Agarwal et al., 2012).

In some cases – as also in the current study – a full standardized ISO life cycle impact assessment is not necessary or desired. This can be due to time restrictions or because only certain focus areas for sustainability need to be assessed. If only a rough estimate is required, and no primary data is available, a high-level “desktop” study is sufficient. According to Agarwal et al. (2012), such a desktop spreadsheet uses readily available data from industry sources and is easily performed without gathering company-specific primary data.

In the current study this type of assessment is referred to as an *environmental study*. The ecoinvent 3.5 database is used for background data and most life-cycle inventories. Any lacking information is gathered from open industry sources. The open source software for sustainability assessment openLCA – version 1.8.0 is used for the simulations. The life cycle inventory analysis (LCIA) methods used in this study are the climate change impact and the resource depletion impact as described below.

3.3.1 Climate Change Impact

The climate change impact is examined by using the LCIA method "ILCD 2011 Midpoint". According to the European Commission Joint Research Centre Institute for Environment and Sustainability (2012), the indicator for the climate change impact is the global warming potential for a 100 year period – GWP_{100}. The unit for the GWP_{100} is in kilograms of CO_2-equivalents, meaning that other greenhouse gases are "converted" to CO_2-equivalents depending on their potency as a greenhouse gas.

3.3.2 Resource Depletion Impact

For the current assessment, the resource depletion impact shall only consider the depletion of non-renewable resources so that the resource depletion of wind is not considered. A resource depletion impact category that includes renewable and non-renewable resources in one value does not deliver the desired results. Therefore, the LCIA method "Cumulative exergy demand" with the three impact categories "non-renewable exergy resources, fossil", "non-renewable exergy resources, metals" and "non-renewable exergy resources, minerals" is used (Hischier et al., 2010). Bösch, Hellweg, Huijbregts, and Frischknecht (2006) define the indicator Cumulative Exergy Demand (CExD) "as the sum of exergy of all resources required to provide a process or product" (p. 182). They also state that chemical exergy is applied on all material resources and fossil fuels. The unit of the CExD is given in MJ-equivalents.

4 Economic Pre-Study

The aim of the economic pre-study is to find the threshold that marks the smallest capacity of a PHES plant that still is economically feasible. In the current study, a PHES plant is considered feasible as soon as it has a lower $LCOE$ than the baseline SCCT peaking plant. Therefore, the minimum power capacity of the smallest competitive PHES plant is to be defined. Information on numerous PHES plants is selected and analyzed in the following subchapters in order to find that threshold.

4.1 Assumptions

The following subchapter outlines further assumptions that are made for the economic pre-study. SCCT plants and PHES systems need to be distinguished when calculating their $LCOE$.

4.1.1 Simple-Cycle Combustion Turbine Baseline Scenario

For the SCCT plant the same basic LCOE-model is applied as for the energy storage systems. However, the energy costs need to be adapted. The differences are described below.

System Lifetime

The German energy agency – dena (2010) – estimates the system lifetime of gas turbines at 50 years, based on average values from real-life simple-cycle combustion turbine plants.

Natural Gas Costs

Unlike the PHES systems, the energy-related costs of SCCT plants are based on the natural gas price. Therefore, the total electricity costs EC_{total} in equation 2 are replaced by the costs for natural gas. The average natural gas price for Europe in 2018 is sourced from The World Bank (2019b). It is 7.7 $/MMBtu which is converted to 24.81 €/MWh by applying the average exchange rate in 2018, as sourced from the European Central Bank (2019). Unlike the LCOE-model for SCCT plants in Obi et al. (2017), no additional taxes or fees are paid for the natural gas and its transport. This is due to the system relevancy of German SCCT plants. Any fees or taxes are reimbursed by the legislator as confirmed by the energy utility company Entega AG (personal communication, March 06, 2019).

4.1.2 PHES Systems

The following assumptions for PHES systems apply to all pumped hydro plants in the current study. A distinction is made for large-scale and small-scale plants. Large-scale plants are assumed to have a power capacity of over 10 MW, while small-scale plants have a power capacity of equal and below 10 MW as defined by Rehman, Al-Hadhrami, and Alam (2015).

System Lifetime

The AfA-table for the energy industry by the Bundesministerium der Finanzen (1995) contains system lifetime values for hydropower plants which can also be used for PHES plants. As the system lifetime is given for each component of the plant, it is still necessary to estimate an average system lifetime. Most of the system components of hydropower plants have a very long system lifetime (buildings and structures), thus the system lifetime for the $LCOE_{Storage}$ model is estimated to be 50 years. Compared with other $LCOE_{Storage}$ studies this is a conservative estimate. Jülch (2016), for instance, uses a system lifetime of 80 years.

Electricity Costs

The electricity costs of energy storage systems are calculated as described in 3.1.5. Thereby, two different prices for electricity are considered: a buy price and a sell price. This allows for the utilization of price arbitrage. For the current economic pre-study, it is assumed that the energy storage systems are run on a daily basis to utilize the price arbitrage of everyday power fluctuations between highest demand (also highest price) and lowest demand (also lowest price). The duration of the charging and discharging cycle of an energy storage system is the main variable that determines the average electricity buy and sell prices. This cycle depends on the system size. Systems with large power and energy capacities tend to have a long charging and discharging cycle, while small-scale systems have short cycles.

Following assumptions are made in the current pre-study to represent these differences in size and according differences in electricity pricing: for small-scale systems with power capacities below and equal to 10 MW the cycle duration is assumed to be four hours which is exactly the timespan covered by the EPEXSPOT (2018) price blocks shown in Table 2. For these small-scale systems, it is therefore assumed that the energy storage plant always charges electricity from 01-04 am, because the Middle Night (01-04) block price in the day-ahead market is the cheapest price on an annual average – at only 34.98 €/MWh, as shown in Table 2. The energy storage plant discharges at Rush Hour from 17-20 pm with the highest electricity price on average in the day-ahead market. At this time the average electricity price is 51.94 €/MWh – as shown in Table 2. In conclusion, the electricity costs to charge EC_{charge} are assumed to be 34.98 €/MWh and the electricity costs to discharge $EC_{discharge}$ are assumed to be 51.94 €/MWh for small-scale systems. This assumption has the aim to simplify the current calculation model. However, this also limits the possibilities of an energy storage system, as arbitrage opportunities also occur outside these predetermined price blocks, e.g. when excess wind power is available during the day, bringing down the price for electricity. In real storage systems the operation of the plant is controlled by automated systems.

For large-scale systems a different assumption is made which represents the longer charging and discharging duration. An analysis of all examined PHES plants of the economic pre-study suggests an average cycle duration of around 12 hours. This large timespan limits the flexibility of such systems and limits arbitrage opportunities. For the current analysis, the three cheapest average block prices – representing 12 hours – are selected and averaged to represent the buy price for large-scale PHES systems. The three highest average block prices are selected and averaged to represent the sell price for large-scale PHES systems. The cheapest average prices are available at Middle Night (01-04), Early Morning (05-08) and Early Afternoon (13-16), resulting in averaged electricity costs to charge EC_{charge} of 39.47 €/MWh for the large-scale systems. Furthermore, the highest average electricity prices are

available at Late Morning (09-12), Rush Hour (17-20) and Off Peak 2 (21-24), resulting in averaged electricity costs to discharge $EC_{discharge}$ of 49.47 €/MWh for large-scale systems. The levies and concessions described in chapter 3.1.10 are added to the electricity costs to charge EC_{charge} for both, small- and large-scale systems.

4.2 Input Data and $LCOE_{Storage}$

In the current study, data is collected for the SCCT baseline scenario and for 45 PHES plants of different scales. Thereof, only the plants that were built after the year 2000 were selected for the final analysis, due to large uncertainties regarding the cost data of very old plants which skewed the final results of the economic pre-study. Input-data for the 30 remaining PHES plants and the baseline scenario, as well as the final $LCOE$ can be viewed in Table 5.

Table 4 Reference list for technology cases in Table 5

	References
#1	Krein (2011), HSE (2010), Obi et al. (2017), NREL (2018)
#2	de Oliveira E Silva and Hendrick (2016)
#3	Fonseca and Schlueter (2013)
#4	Schulze (2017)
#5	Godina, Rodrigues, Matias, and Catalão (2015)
#6	Sandia National Laboratories (2019)
#7	Sandia National Laboratories (2019)
#8	Sandia National Laboratories (2019)
#9	Sandia National Laboratories (2019), POWER Engineering (2011)
#10	The European Commission (2016b)
#11	Sandia National Laboratories (2019), Barry (2018)
#12	Sandia National Laboratories (2019)
#13	Sandia National Laboratories (2019), The European Commission (2016a)
#14	Sandia National Laboratories (2019), TPF (2019)
#15	Sandia National Laboratories (2019), illwerke vkw (2019)
#16	Sandia National Laboratories (2019)
#17	Sandia National Laboratories (2019)
#18	Sandia National Laboratories (2019), Organic power International SL (2013)
#19	Sandia National Laboratories (2019), Nevada Hydro (2019)
#20	Sandia National Laboratories (2019), The World Bank (2019a)
#21	Sandia National Laboratories (2019), Gridflex Energy (2019)
#22	Sandia National Laboratories (2019)
#23	Sandia National Laboratories (2019), Patel (2013)
#24	Steinwender (2016)
#25	IUB Engineering Ltd. (2013), Vattenfall (2019)
#26	Max Bögl Wind AG (2019b), Färber (2016), Max Bögl Wind AG (2019a)
#27	Heimerl and Kohler (2017), Janjanin and Schumann (2016)
#28	Heimerl and Kohler (2017), AllgäuStrom (2019)
#29	Heimerl and Kohler (2017), GFA (2013)
#30	Katsaprakakis et al. (2012)
#31	Kusakana (2015)

Table 5 Input data and LCOE for all examined technology cases after 2000

	Technology Case	CAPEX [€]	OPEX [€]	CF	η_{total} [%]	LCOE [€/MWh]
#1	SCCT baseline – 94 MW	59,130,000	1,140,000	0.08	37	115.31
#2	Goudemand residence – 1.5 kW	45,820	1,604	0.0761	35	3250.14
#3	Torre Confinanzas (hypoth.) – 30.1 kW	142,000	4,971	0.31*	32.5	197.03
#4	Wesermühlen (hypothetical) – 0.23 MW	3,347,000	117,100	0.31*	80*	372.37
#5	El Hierro Hydro-Wind Plant – 10 MW	63,120,000	2,209,000	0.07	69	693.19
#6	Gilboa – 300 MW	138,100,000	4,835,000	0.31*	80*	20.03
#7	Olivenhain-Hodges – 40 MW	207,200,000	7,251,000	0.31*	80*	140.73
#8	Afourer – 465 MW	248,900,000	8,711,000	0.31*	80*	21.94
#9	Salamonde II – 211 MW	235,700,000	8,248,000	0.21	80*	50.67
#10	Amari Hybrid Project – 50 MW	161,100,000	5,638,000	0.52	80*	57.54
#11	Kidston – 250 MW	239,000,000	8,365,000	0.31*	80*	32.71
#12	Venda Nova III – 736 MW	413,700,000	14,480,000	0.31*	80*	22.63
#13	Amfilochia – 680 MW	515,100,000	17,930,000	0.14	80*	52.20
#14	Foz Tua – 259 MW	447,100,000	15,650,000	0.12	80*	121.21
#15	Obervermuntwerk II – 360 MW	589,700,000	20,640,000	0.31*	80*	50.15
#16	Pushihe – 1200 MW	732,700,000	25,650,000	0.18	77	37.39
#17	Aguayo II – 1014 MW	673,900,000	23,590,000	0.17	80*	39.45
#18	MAREX PHES Glinsk – 1500 MW	678,000,000	23,730,000	0.23	75	27.80
#19	Lake Elsinore Advanced – 500 MW	678,000,000	23,730,000	0.31*	83	40.85
#20	Upper Cisokan – 1040 MW	705,700,000	24,700,000	0.31*	80*	25.61
#21	White Pine Pumped Storage – 750 MW	847,500,000	29,660,000	0.31*	80*	37.16
#22	Jixi Pumped Storage – 1800 MW	1,133,000,000	39,670,000	0.31*	80*	24.36
#23	La Muela – 2000 MW	1,410,000,000	49,350,000	0.29	80*	27.84
#24	Rellswerk – 12 MW	38,680,000	1,354,000	0.19	80*	142.58
#25	Niederwartha – 40 MW	131,900,000	4,616,000	0.31*	80*	92.59
#26	Naturstromspeicher Gaildorf – 16 MW	57,000,000	1,995,000	0.31*	80*	99.38
#27	Blautal (discontinued) – 60 MW	84,240,000	2,948,000	0.31*	80*	44.16

Table 5 (continued) Input data and LCOE for all examined technology cases after 2000

	Technology Case	CAPEX [€]	OPEX [€]	CF	η_{total} [%]	LCOE [€/MWh]
#28	Breitenstein (deferred) – 60 MW	80,640,000	2,822,000	0.31*	80*	42.63
#29	Lägerdorf (deferred) – 70 MW	100,800,000	3,528,000	0.31*	80*	45.09
#30	Karpathos-Kasos – 4.15 MW	17,960,000	628,600	0.46	62	89.10
#31	Rural South Africa (hypothetical) – 1 kW	3,593	126	0.31*	50	122.46

* average value for large-scale systems chosen based on Obi et al. (2017)

Table 4 shows the according references for every single technology case that is examined in the economic pre-study. The main source for the current research is the global energy storage database provided by the Sandia National Laboratories (2019). Further details are gathered from the plant operators and contractors, local newspaper articles or technical magazines.

The $CAPEX$ and $OPEX$ values in Table 5 are rounded to four significant digits. All monetary values are inflation-adjusted to €$_{2018}$.

Although very big effort and research was undertaken to gather data for 45 different PHES plants, not every piece of information is openly available. Therefore, some assumptions are made to fill any lack of information. These assumptions are made for the operational expenditures $OPEX$, the capacity factor CF and the total efficiency η_{total}. If no information on the operational expenditure is provided for the particular PHES site, it is assumed to be within the range of 3 to 5% of the capital expenditure $CAPEX$, as recommended by Giesecke et al. (2014, p. 81). For the current study, it is assumed to be 3.5% of the $CAPEX$. The assumptions for the capacity factor and the total efficiency are based on the average values for PHES systems gathered from Obi et al. (2017, p. 912). Thus, the capacity factor CF is assumed to be 31% if this information is not available from online sources, and the average total efficiency of 80% is used if the efficiency of the particular technology case is not available.

The input data for technology cases #1 to #4 – as displayed in Table 5 – is discussed in detail in the economic study in subchapter 6.2. This includes the SCCT baseline plant.

4.3 Outcome

Table 5 shows the $LCOE$ results for each technology case analyzed for the current pre-study. These results are depicted in the order of their nameplate power capacity NP in Figure 11.

The figure uses a logarithmic scale for the x- and y-axis to offset the large scale-variation in $LCOE$ and NP. Although the figure reveals that the levelized costs of PHES systems of similar capacity are highly site-specific, as shown for Foz Tua (259 MW) at 121.21 €$_{2018}$/MWh and Kidston (250 MW) at 32.71 €$_{2018}$/MWh, it also demonstrates that the $LCOE$ of PHES plants generally depends strongly on the scale of the system.

While large systems are much cheaper than the simple-cycle combustion turbine (SCCT) baseline scenario, that has a calculated $LCOE$ of 115.31 €$_{2018}$/MWh, the smaller systems move within the same range as the SCCT plant. Micro-scale PHES plants with a nameplate power capacity of less than 0.1 MW, as defined by Rehman et al. (2015), have an extremely high $LCOE$ compared to the SCCT plants. These observations suggest that the feasibility limit must lie within the range of small-scale systems. To prove this, Figure 12 shows an excerpt from Figure 11 for the power capacity range of 0 to 100 MW, with a logarithmic scale for the x-axis. The figure shows a steady increase in levelized costs for the PHES systems depending on their capacity. The blue-dotted power trendline depicts this correlation.

For the SCCT baseline scenario, a Monte Carlo simulation is performed in order to reflect the model uncertainty. The most susceptible variables are determined in a sensitivity analysis

beforehand. The variables that have the highest impact on the $LCOE$ for the SCCT baseline scenario are the total efficiency, the natural gas price, the capacity factor, and the capital expenditure. For the Monte Carlo simulation a standard deviation of 10% is assumed for all variables. The natural gas price standard deviation is based on forecasts for the natural gas price by The World Bank (2019b). A detailed presentation of the results of the sensitivity analysis and Monte Carlo simulation for the $LCOE_{Storage}$ model are performed in chapter 8.1.

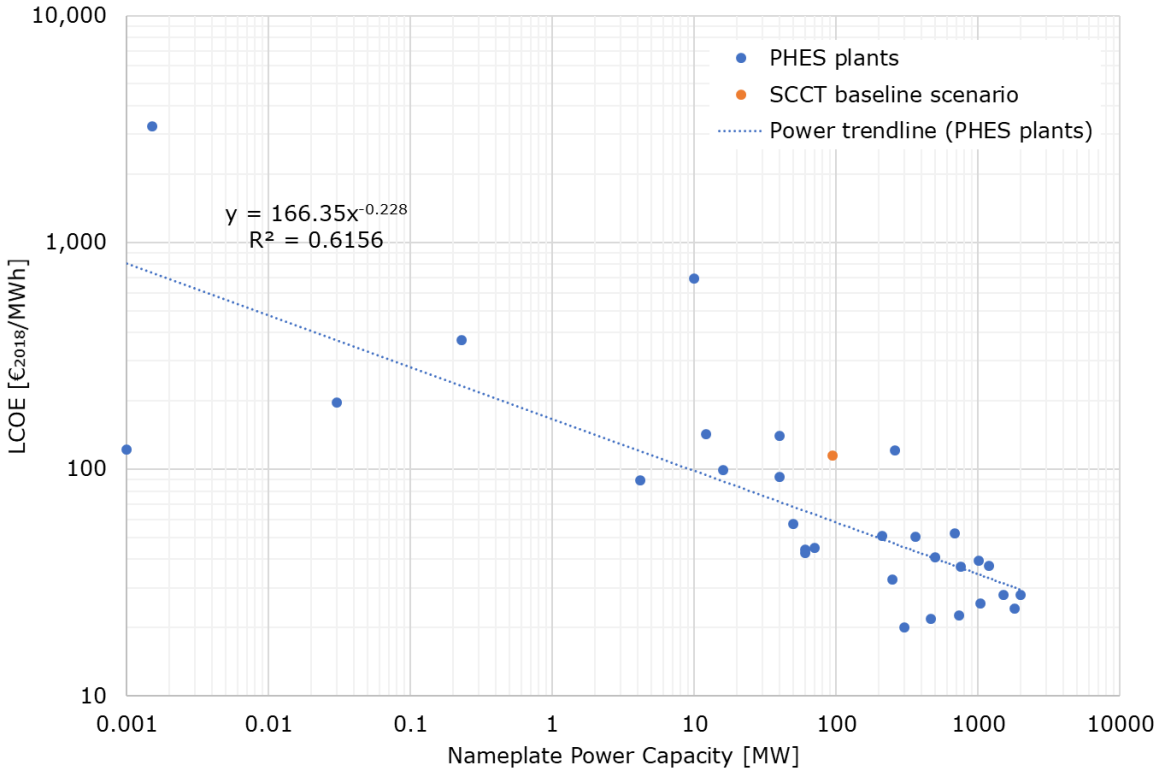

Figure 11 LCOE of PHES plants and SCCT baseline over their nameplate power capacity

The Monte Carlo simulation is performed with 10,000 trials. The 20th, 50th and 80th percentiles of all observations are depicted in Figure 12. 20% of all observations are found below 111.60 €$_{2018}$/MWh, 50% are found below 121.26 €$_{2018}$/MWh, and 80% are found below 131.27 €$_{2018}$/MWh for the SCCT baseline scenario.

The logarithmic scale for the nameplate power capacity in Figure 12 enables an easy assessment of the smallest capacity for a feasible PHES plant. The analysis of the power trendline for the PHES plants and the 20th, 50th and 80th percentile $LCOE$ values for the SCCT baseline scenario reveals that PHES plants become a feasible option when their nameplate power capacity is larger than ~ 4 MW. This is for the assumption that PHES plants are considered feasible if their $LCOE$ is lower than that of the SCCT baseline scenario.

However, it must be noted that this result cannot be considered highly accurate due to the low number of available PHES samples, the approximation through the power trendline and the uncertainty of the $LCOE_{Storage}$ model. Especially in the range of small-scale plants (between 0.1 and 10 MW) and micro-scale (between 0.005 and 0.1 MW) there are only very few case studies available.

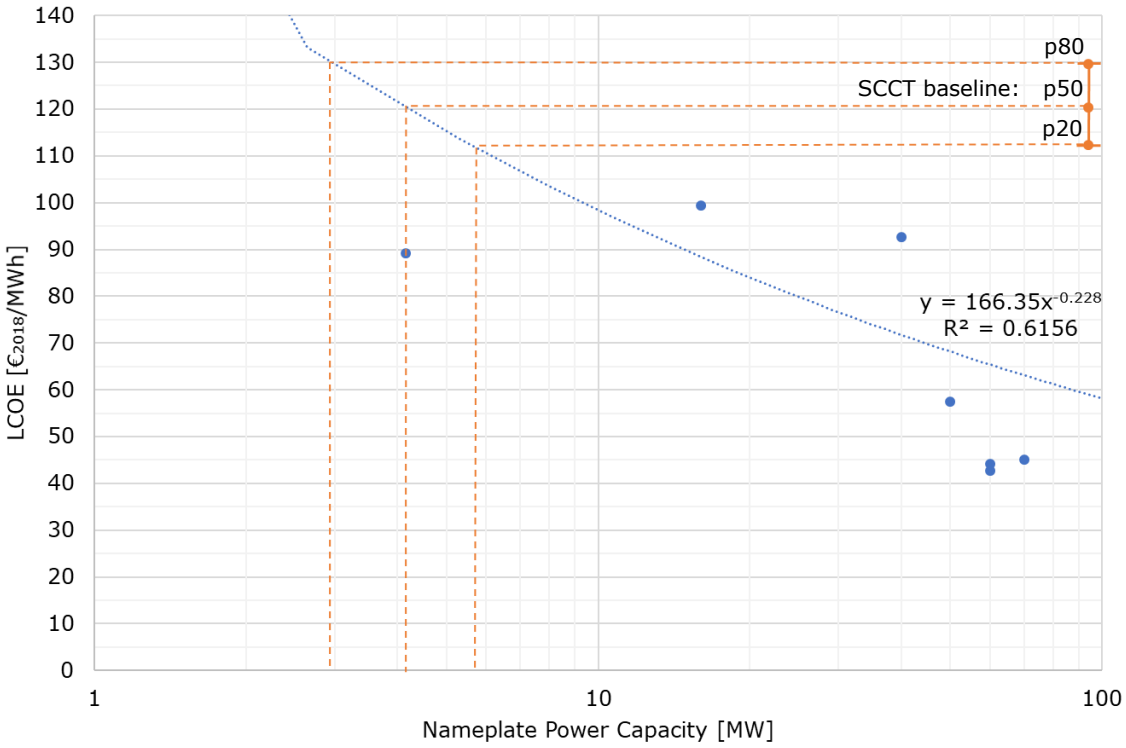

Figure 12 Feasible power capacity of PHES systems compared to SCCT baseline

It does, however, deliver the plausible estimate that PHES plants with a nameplate power capacity above a range of 3 to 5.5 MW can be operated at a lower $LCOE$ than SCCT plants.

5 Engineering Design Study

Based on the findings in the economic pre-study, the following chapter aims on discovering a suitable design for an innovative pumped hydro scheme in the urban built environment. The systematic engineering design approach by Pahl et al. (2007) is thereby used as the basic framework. A task clarification is performed in order to refine a requirements list for the anticipated solution, followed by the conceptual design. After defining the function structure of the PHES system, solutions are sought by researching existing technical systems and analogies. Finally, promising concepts are firmed up into tangible solutions. A final concept is then selected, which is further analyzed in the economic and environmental studies of this thesis.

5.1 Task Clarification

The first step in the engineering design process is to clarify the task. Information needs to be gathered about the requirements that the final system is supposed to meet. It is important that this step is performed thoroughly to make sure that all requirements – explicit and implicit – can be addressed during the development of the innovative pumped hydro scheme. The result of the task clarification phase can then be presented in a requirements list that is also used as a basic working document for the entire engineering design study (Pahl et al., 2007).

Table 6 Basic requirements list for the engineering design study

	Requirement	**Target**	**Minimum**	**Unit**
#1	Power output	4	-	MW
#2	Duration of one cycle	4	-	h
#3	System roundtrip efficiency	80	35	%
#4	Levelized cost of electricity storage	120	-	€$_{2018}$ / MWh
#5	System lifetime	50	-	years
#6	High accessibility			
#7	High availability (wish)			
#8	Corrosion prevention			
#9	Cavitation prevention			
#10	Overpumping protection			
#11	Protection against intake of foreign objects			
#12	Appealing architectural design			
#13	Synergies with other systems (wish)	1	-	#
#14	Low area requirement (wish)			

The task clarification is performed by following the structured checklist by Pahl et al. (2007). To conduct a thorough task clarification, the checklist – with subitems, such as: geometry, energy, material or costs – is used as an aid to assess the requirements for each subsystem of pumped hydro schemes as depicted in Figure 5. The transmission and transformer

subsystems as well as the electronic control system are thereby not included in this assessment. The obtained requirements list can be viewed in Table 6. A more detailed version is found in Appendix III.

The first requirement is that the power output of the proposed pumped hydro system is targeted to be 4 MW. This requirement is derived directly from the results in chapter 4. According to the economic pre-study, a power output of 4 MW is determined as the smallest feasible system output for pumped hydro systems. The second requirement is the duration of one cycle. The target is to provide the maximum power output of the system (4 MW) for four hours. This requirement is based on the assumption that the storage system is charged at night, taking advantage of the EPEXSPOT (2018) "Middle Night" electricity price, and discharged during "Rush Hour" the next day. The first two requirements also determine the system capacity. In total, 16 MWh of energy will be stored by the PHES plant according to the power capacity and duration of one cycle. The third requirement demands that a system roundtrip efficiency of 80% is targeted which is the average efficiency of large-scale PHES systems according to Giesecke et al. (2014, p. 721). As this value is unlikely to be reached by the small-scale system examined in the current study, a minimum demand of 35% is determined. This minimum value is based on the efficiencies achieved by the small-scale systems described by de Oliveira E Silva and Hendrick (2016) and Fonseca and Schlueter (2013).

The fourth requirement is that the $LCOE_{Storage}$ is targeted to be 120 $€_{2018}$ per MWh. This value is based on the 50^{th} percentile of the levelized cost of electricity for gas peaking plants that was calculated in the economic pre-study in chapter 4. It is defined as a reference value for the economic feasibility of energy storage systems. Furthermore, the system lifetime is defined as the fifth requirement. It is aimed to be 50 years which is the standard estimation used by Bundesministerium der Finanzen (1995). The requirements "High accessibility" and "High availability" refer to the basic demand for a simple design and easy maintainability of the system.

Requirements eight to eleven aim to maximize the system lifetime as well as the availability. Corrosion prevention is required for any corrodible components that are in touch with water, whereas cavitation prevention and protection against the intake of foreign objects is mainly required to protect the pump-turbine (Giesecke et al., 2014). The overpumping protection is needed in case the pumping control system fails. Such an overpumping protection allows the upper reservoir to overflow without causing any damage or threat to people (Levine & Barnes, 2011).

As the PHES system is supposed to be located in the urban built environment, an appealing architectural design is an important requirement to be acknowledged. The last two requirements are classified as wishes of major importance, which means that they should be acknowledged if possible. Especially, if they help to achieve important requirements such as the demand for low costs. Requirement 13 "Synergies with other systems" has been pointed out by de Oliveira E Silva and Hendrick (2016) as a possible approach of lowering costs and increasing the overall attractiveness of PHES systems in the urban built environment, while the "Low area requirement" aims to minimize the land-use of the proposed PHES system for economic but also for environmental reasons.

In the next step, the priorities of the engineering design study are determined. Therefore, the Quality Function Deployment (QFD) method is applied, as described by Pahl et al. (2007).

This method supports the refinement and prioritization of system requirements by translating customer requirements into technical requirements. In the current case the customer requirements are assumed by analyzing real-world energy storage projects. The method assists the designer with considering requirements that are not of technical nature, such as the systems visual appearance. Each customer requirement is weighted to represent its relative importance. For example, while a "low price" of the energy storage system is considered highly important for the client, the requirement "simple system design" is rated less important. Finally, the customer requirements are cross-checked with the technical requirements so that the importance of the individual technical requirements can be examined in a client-oriented way. The additional assessment of the technical difficulty of their implementation allows for an evaluation of where to lay the focus of the engineering design study. The results of this assessment are depicted in Figure 13. They are based on the QFD assessment shown in Appendix IV.

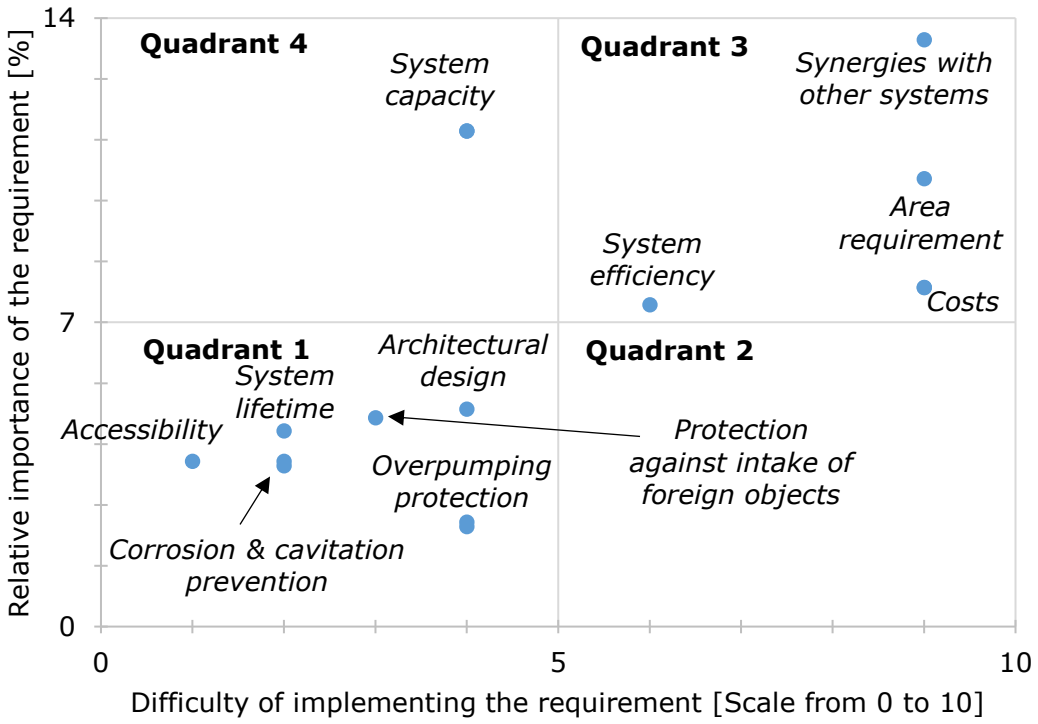

Figure 13 Classification of the relevance of technical requirements

Each dot in Figure 13 represents a requirement. Their location on the graph, in either of the four quadrants, allows a quick analysis of their relevance. Because the requirements located in the first quadrant are considered, both, less important and technically less difficult, they will not be strongly examined in this study (Birkhofer & Kloberdanz, 2017). These requirements, including overpumping protection, an appealing architectural design as well as corrosion and cavitation prevention, can be easily met by applying simple, existing solutions. The requirement "System capacity" describes the storage capacity of the PHES system and is located in the fourth quadrant. The system capacity is a simple but important requirement and will be implemented in the engineering design study. It is considered one of the key requirements for developing a feasible PHES system in the urban built environment.

The technical requirements located in the third quadrant are considered very important and very difficult to implement. They are therefore made the key focus of the current engineering design study as recommended by Birkhofer and Kloberdanz (2017). Many technical requirements aim to decrease the costs of a PHES system in the urban built environment as this has already been examined as the key weakness of such small-scale systems in the underlying studies by de Oliveira E Silva and Hendrick (2016), Schulze (2017) & Fonseca and Schlueter (2013). Thus, it is not surprising to see the requirement for cost minimization in the third quadrant. The requirement for a maximization of the "System efficiency" supports the cost requirement but also plays an important role for other reasons such as the energy density of the energy storage system. As the system is supposed to be situated in the urban built environment, where space is limited, the "Area requirement" is to be minimized and will play an important role in the following engineering design study. Finally, the requirement that is considered most important and most difficult is the demand for synergies with other systems that could potentially increase the feasibility and attractiveness of a small-scale pumped hydro system in an urban setting, as already pointed out by de Oliveira E Silva and Hendrick (2016).

Summed up, the essential crux of the task is to lower the costs of small-scale PHES systems in the urban built environment. The main focus of the current study will therefore be to explore possible synergies with other systems, minimize the area requirements of possible solutions and maximize the systems efficiency. These requirements will be based on the system capacity that was found to be economically feasible based on the economic pre-study in chapter 4. The other requirements described in Table 6 are less difficult to implement and do not require a thorough analysis.

5.2 Conceptual Design

The aim of the conceptual design is to abstract the task, identify the essential function structure and find working principles that satisfy the requirements that have been established in the previous chapter. Tangible overall solutions are developed. In essence, the "conceptual design specifies the principle solution" (Pahl et al., 2007, p. 159).

5.2.1 Establishing Function Structures

After examining the requirements list and identifying the essential challenges for the engineering design study, it is expedient to establish the function structure of the problem. Pahl et al. (2007) recommends to first formulate the overall function and then break down this fundamental function into subfunctions iteratively. The overall function of a pumped hydro scheme is to store energy when the electricity supply exceeds the demand and discharge when the electricity demand exceeds the supply. This overall function can be viewed in the flow diagram in Figure 14.

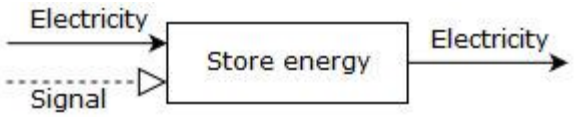

Figure 14 Overall function structure

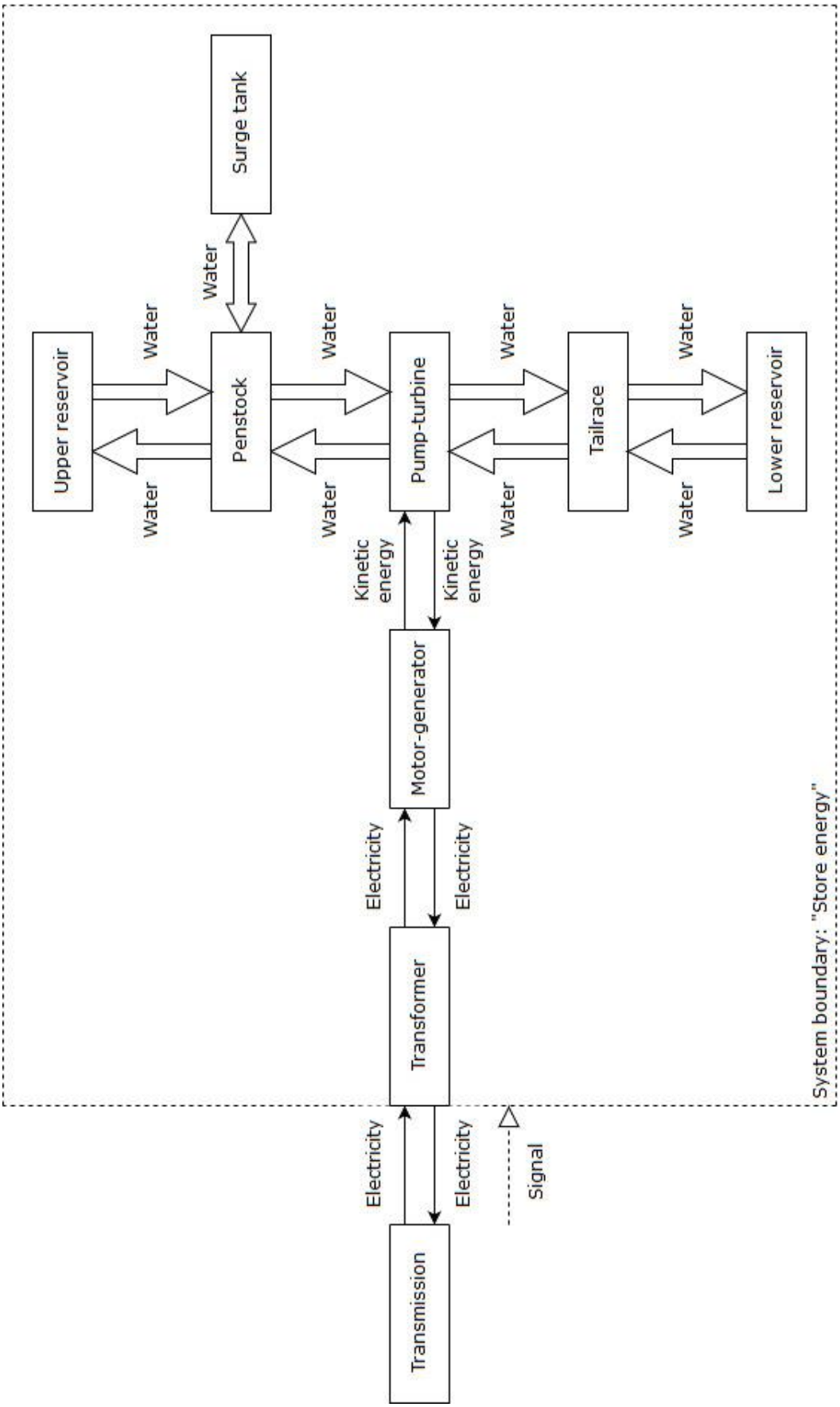

Figure 15 Function structure with subfunctions, based on Ter-Gazarian (2011)

Electricity flows into the energy storage system and flows back to the grid after a certain time. The in- and outflow of electricity is regulated by a signal that may come from the grid operator. However, signals as well as the control subsystems of the PHES scheme will not be further regarded in this study.

In PHES systems, surplus energy from the grid is stored by pumping water into an upper reservoir and discharged into a lower reservoir again to generate electricity when demand exceeds supply. The function structure of pumped hydro systems is well known. The current study can therefore be considered an *adaptive design* study, meaning that the generally established PHES technology is adapted to a new setting (Pahl et al., 2007). Based on Ter-Gazarian (2011), the function structure of a PHES plant can be divided into the subfunctions shown in Figure 15.

Figure 15 depicts how electricity from the transmission system passes through a transformer before it powers the motor-generator where it is converted into rotational kinetic energy. The pump-turbine is coupled to the motor-generator and pumps water from the lower reservoir through the tailrace and the penstock into the upper reservoir where it is now stored at a higher level of potential energy. When the system discharges, the process is reversed: Water is released from the upper reservoir, flows through the penstock, powers the turbine and enters the lower reservoir through the tailrace. The surge tank is connected to the penstock and acts as a dampener in case of sudden pressure changes (Levine & Barnes, 2011).

With the detailed function structure at hand, an analysis of the identified subfunctions can be performed. Not every subfunction requires a thorough analysis and search for new working principles. Especially adaptive design studies that are based on well-known technologies such as PHES systems can easily make use of well-known solutions. Subfunctions for which new and innovative working principles need to be found will, on the other hand, receive more attention in the following design process (Pahl et al., 2007).

In the current study, known solutions can be used for most subfunctions: The transformer and motor-generator can be easily ordered from respective manufacturers, whereas the tailrace and penstock can be easily implemented after calculating the specific requirements. Whether or not a surge tank is required needs to be ascertained. However, the surge tank design is not part of this study. For the lower reservoir an existing water body, such as a river or lake, is to be used. This is due to the fact that the construction of a lower reservoir for small-scale PHES plants has an extensive impact on the systems economic feasibility as shown by de Oliveira E Silva and Hendrick (2016). In their study, the capital costs for the lower reservoir accounts for almost 60% of the total capital costs, resulting in a bad overall economic performance compared to the alternative option that uses a river as the lower reservoir. Standing waters are preferred as a lower reservoir as the risk of taking in foreign objects and suspended matter can be significantly reduced (Schulze, 2017). German water regulations need to be considered in both cases. According to Schulze (2017) the process of acquiring the necessary permits is very time-consuming and it is uncertain whether the permits are granted.

A selection from known solutions needs to be made for the pump-turbine. The current study confines itself to reversible pump-turbine sets as this technology represents the state of the art and leads to capital cost savings of up to 30% compared with separate pump and turbine compositions. However, the overall efficiency of combined pump-turbines is lower than that of two separate units. This is especially observable for PHES plants with low heads and large

head variations and thus needs to be carefully considered in this study (Ter-Gazarian, 2011, p. 89). As the pump-turbine needs to be reversible, Pelton turbines are excluded from the solution field as they technically do not allow a pumping mode. The selection of suitable electromechanical equipment is part of the current study and is assessed in chapter 5.2.4.

The only subfunction that requires the exploration of new working principles is the upper reservoir. The size of the system will require new, innovative solutions for an implementation in the urban built environment. The search for new solutions for the upper reservoir therefore is the core element of the current engineering design study.

5.2.2 Developing Working Structures for the Upper Reservoir

Following the guideline by Pahl et al. (2007), searching for working principles is the next step in the engineering design process. Only one subfunction, namely the upper reservoir, requires to be analyzed and developed in this subchapter. The physical effect of the upper reservoir is already set: Water needs to be stored at a higher elevation than in the lower reservoir. The core challenge is to establish the form design of the upper reservoir – including geometry and material. In order to find suitable solutions, conventional solution finding methods, such as the analysis of existing technical systems and analogies are performed (Pahl et al., 2007). The guiding question for this analysis is: How can a large amount of water be stored in an urban setting so that, in total, 16 MWh of potential energy become available?

Existing Technical Systems

The research question leads directly to classical water storage technologies for urban potable water supply systems. Mutschmann, Stimmelmayr, and Fritsch (2011) classify two different water storage systems that make use of elevation differences to supply water to consumers: Elevated tanks take advantage of naturally occurring elevation and are usually dug into the ground, whereas water towers are built to create an artificial water head that provides the necessary water pressure to supply water to the consumers.

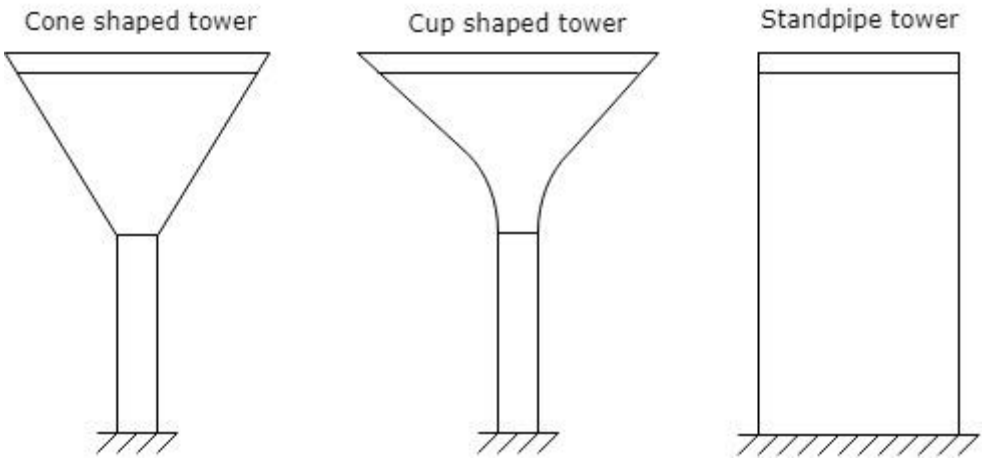

Figure 16 Water tower designs for large capacities. Adapted from Mutschmann et al. (2011, p. 494).

For pumped hydro applications the natural elevation difference is a supporting factor – being the core principle of large-scale PHES plants. However, the idea of creating a PHES system in the urban built environment favors solutions that can be implemented in combination with buildings and without relying on natural elevation. The water tower concept is therefore considered highly relevant for the current study.

Mutschmann et al. (2011) describe rotationally symmetric reservoirs as favorable for handling the occurring load cases of a water tower. Figure 16 displays the different water tower designs for large-scale water storage systems. The most convenient geometry for large amounts of water is the cylinder. The standpipe tower is moreover the cheapest option because the water chamber is directly founded on the ground, meaning that the tower itself does not need to carry the chambers entire weight.

Mutschmann et al. (2011) furthermore note that water towers are usually made of reinforced concrete. While in-situ concrete is always used for the tower's foundation, the tower shaft and water chamber can be pre-cast in factories and joined on site. The optimal founding of the water tower needs to be planned carefully to avoid any uneven distribution of weight. The use of ring foundations or even foundation plates is preferential. Examples for concrete standpipe water towers can be viewed in Figure 17.

Besides being a good example for in-situ concrete standpipe water towers, Reykjavík's landmark "Perlan" can also be considered a great example for integrating an essential utility system into the urban built environment. After being equipped with a huge glass dome on top of the six existing hot-water tanks in 1991, the building currently accommodates the "Wonders of Iceland" exhibition, a planetarium, restaurants and an observation deck. The hot-water tanks each carry 4000 m^3 of geothermal hot water which is supplied to the end consumers in the city of Reykjavík (Perlan, 2019). In contrast, Figure 17b shows the 50 m high water tower of Tübingen that is situated next to an 18-storied building. It contains two separate water chambers and stores a total of 3330 m^3 of water. Although the tower is structurally fully isolated from the residential building, it is designed to appear to be part of it ("Wassersilo Tübingen," n.d.).

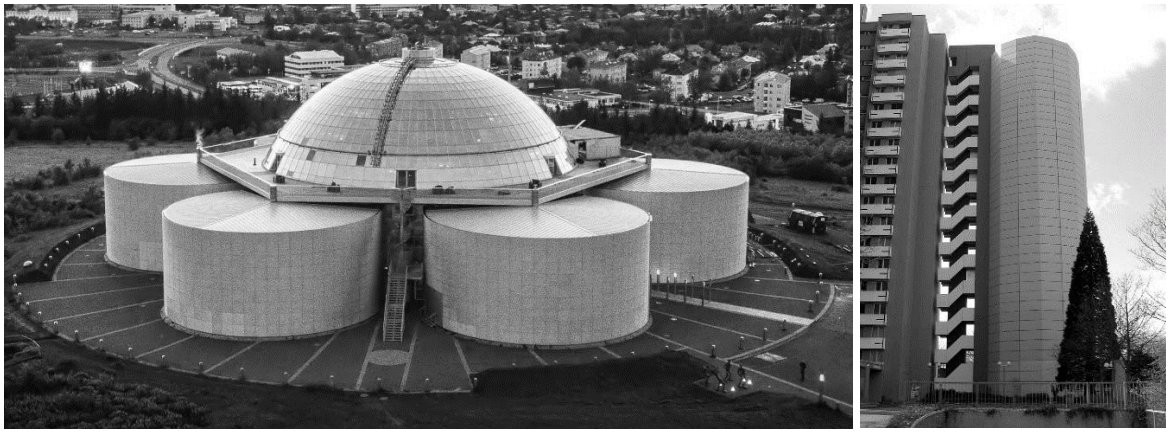

Figure 17a) (left) "Perlan" hot-water tanks and museum in Reykjavík, Iceland. Adapted from What's On (2019). b) (right) Water tower of Tübingen, Germany. Adapted from Karlo (2007).

The concrete water tanks provided by the US company *DN Tanks* are partly prefabricated and partly cast in situ. Furthermore, the company uses prestressing steel wires to place the tank wall into permanent compression. This procedure ensures that the concrete walls do not crack and thus provides greater safety for the reservoir. The wire is placed on the tank wall by using a special wire spacing device, that also puts a defined strain on the strand to compress the tank. In order to create a strong bond between the steel wire and the concrete tank, shotcrete is used to cover the applied layer of strand. This additional layer also prevents the steel from corroding. It is possible to apply several layers of steel prestress wire as described above, depending on the requirements for the tank (DN Tanks, 2019).

Figure 18a) (left) The first layer of shotcrete is applied to the tank wall. Adapted from (DN Tanks, 2019, p. 17). b) (right) Wire being placed on the tank wall. Adapted from (DN Tanks, 2019, p. 17).

The tank construction procedure is partially shown above. Figure 18a shows the process of applying shotcrete to the reservoir wall, and Figure 18b depicts the wire spacing device that applies the steel wire to the tank wall.

Figure 19a) (left) Completed "Naturstromspeicher Gaildorf". Adapted from Max Bögl Wind AG (2019a). b) (right) Upper reservoir under construction. Adapted from Liebherr (2017).

Another highly relevant example in this context is the "Naturstromspeicher Gaildorf" which the company Max Bögl Wind AG (2019a) brought online in 2018. Together with four 3.4 MW wind turbines this innovative PHES pilot plant forms a hybrid system that can generate and store electricity at the same site. Instead of creating the upper reservoir conventionally,

by removing the top of a hill and using the removed soil to create a ring-shaped dam, as described by Giesecke et al. (2014), the water is stored in two different types of water towers at the bottom of each of the four wind turbines. The individual turbine is thereby placed on top of the 40 m high inner water tower that is encircled by the open outer reservoir. The additional height of the inner water tower does not only increase the water head but also allows the wind turbine to reach higher layers of air, maximizing their wind-energy harvest. This also makes them the world's tallest wind turbines at 240 m (Liebherr, 2017).

Figure 19a shows two of the facility's completed upper reservoirs and wind turbines. Figure 19b depicts the construction process of the inner water tower. A crane is used to lift prefabricated tower segments onto the tower. The concrete rings are composed of four single arcs that are precast in a factory and braced together on-site using steel cables. Each prefabricated ring is 1.5 m high and has a diameter of 16 m (Liebherr, 2017). The inner water tower has a storage capacity of around 8000 m^3 and carries the entire weight of the wind turbine.

A final technology approach is proposed by the prestressing steel company BBV Systems GmbH in Germany. The firm accompanied a large-scale project in the year 2013. An almost 60m high sugar silo with a diameter of over 45m was realized by applying the sliding formwork approach for in-situ concrete. The silo was stabilized by BBV Systems GmbH with post-tensioned steel strands as depicted in Figure 20b.

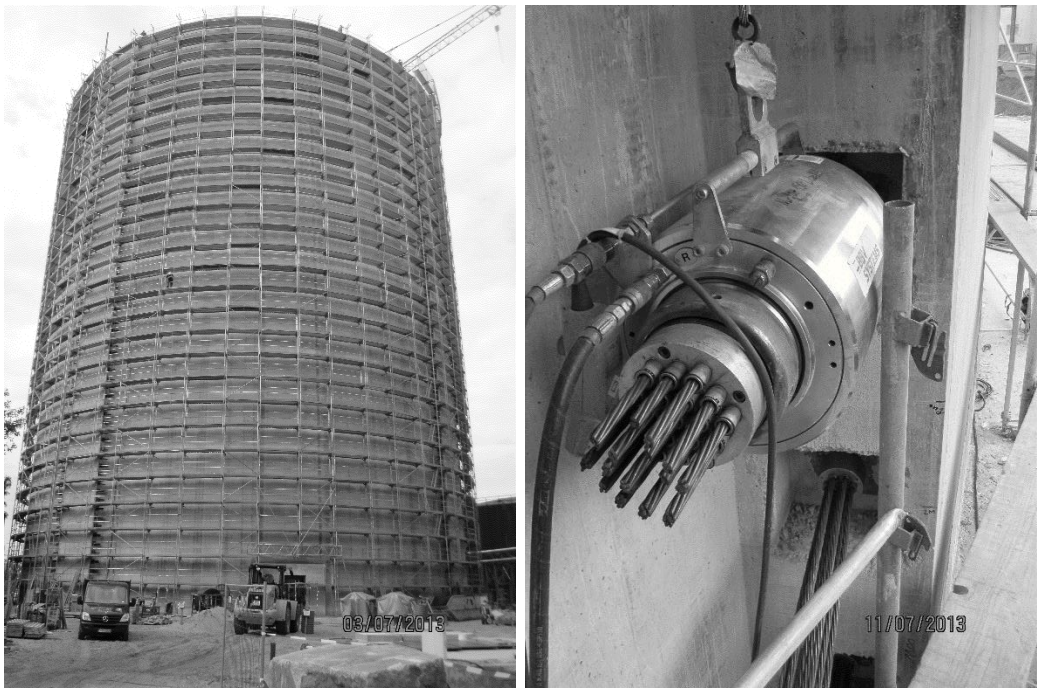

Figure 20a) (left) Sugar silo under construction. Reprinted from W. Schick (personal communication, August 07, 2019). b) (right) Post-tensioning steel strands by BBV Systems GmbH. Reprinted from W. Schick (personal communication, August 07, 2019).

Figure 20a shows the construction site of the sugar silo. BBV Systems GmbH completed the entire works related to the tensioning of the prestressing steel strands.

Analogies

Another technical system that is used to store large quantities of liquid is the steel storage tank – following either the API 650 guideline or Eurocode 3 – Part 4-2. According to the American Petroleum Institute (2012), welded tanks following the API 650 standard were originally established for petroleum products but are also used for storing other liquids. They are generally constructed by welding steel plates together to form a cylindrical reservoir. According to Mutschmann et al. (2011) steel tanks are not usually used to store water in Germany due to the risk of corrosion. Even if a paint coating is applied, storage tanks made of steel are subject to corrosion and require regular maintenance and recoating. The largest potable water storage tank in the U.S. is the Martin Hill Reservoir Water Tank. With its diameter of 79 m and height of 24 m, the steel tank can store around 120.000 m^3 of water. In 2004, the tank required its first repaint after 15 years of service. The cost of the repaint amounted to US$ 1.5 million (WaterWorld, 2004).

The current study's research question encourages the search for analogies in the urban built environment. First rough calculations reveal that the size of the upper reservoir for a 16 MWh gravity storage system needs to be extremely large when natural elevation is not to play a big role. The potential energy stored in a reservoir depends on the volume of stored water and the effective head. The higher the building, the higher the storage capacity. Therefore, different types of high-rise buildings are examined.

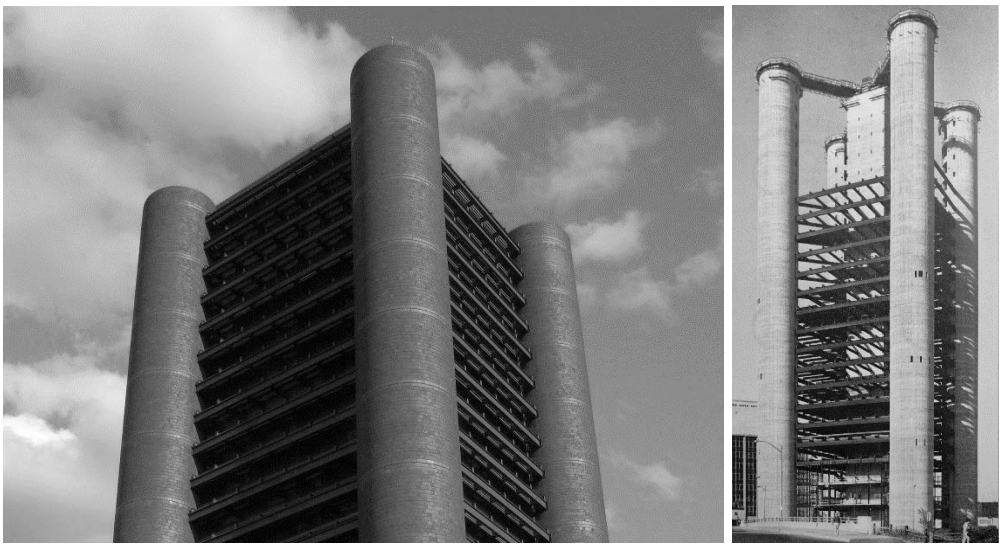

Figure 21a) (left) The "Knights of Columbus Headquarters Building". Adapted from Tisue (2008). b) (right) The building under contruction. Reprinted from Guise (1991).

Two buildings were discovered during this research that feature interesting analogies with water towers: The "Knights of Columbus Headquarters Building" in New Haven, Connecticut (U.S.), as shown in Figure 21a, and the former "Westcoast Transmission Company Building" in Vancouver, British Columbia (Canada), as shown in Figure 22a.

Guise (1991) describes the "Knights of Columbus Headquarters Building" as *"[...] somber, staid, and almost monumental."* (p. 101). The buildings core is divided into five separate towers, as can be seen in Figure 21b. The four windowless towers on the outside remain visible and mark the buildings corners whereas the inner square core contains the elevators and is not visible for the external viewer. The corner towers incorporate the stairs, toilet

facilities and mechanical shafts. The concrete towers are cast in situ and thus monolithic. This makes the structure extremely solid. However, Guise (1991) also describes the main disadvantage of the building: Due to the architectural design with five separate cores, the usable tenant space is very low compared to conventional buildings with similar dimensions. Each corner tower has a theoretical volume of 6200 m^3. The building is 97.5 m tall (Guise, 1991).

The former "Westcoast Transmission Company Building", which has been renamed to "The Qube", is a 15-storey building in Vancouver, Canada (Mitanis, 2017). Guise (1991) considers the building "*unusual"* because the office tower is supported by steel cables at twelve locations which are attached to the top of the monolithic concrete core. The core itself is 18-storeys high and the only structural connection to the ground, meaning that the entire weight of the floors, the wind bracing, and the mechanical shafts are contained by the core. The entire load placed on the floors travels through the cables that are attached to the corners and the frame and are directed into the top of the central core – putting an additional compressive force on the center. The structural design can be viewed in Figure 22b where the building is shown during construction. Besides improving the earthquake resistance of the building, the unique structure allows the office floors to seemingly hover over the ground (Guise, 1991). Freeing the ground level provides the opportunity of using the space underneath for other purposes.

Figure 22a) (left) The former "Westcoast Transmission Company Building". Reprinted from Guise (1991). b) (right) The building under construction. Reprinted from Matthews (1969).

While the core of "The Qube" is square, the same structural principle can be easily imagined as a cylinder. According to Guise (1991) the building has a height of 71 m and the core is 11 x 11 m. The theoretical volume of the tower is therefore over 8000 m^3.

Synergies with Building Systems

In the task clarification, finding synergies with other building systems or communal services has been identified as an important option to lower the costs and increase the attractiveness

of implementing a PHES system in the urban built environment. While some possible synergies have already been discovered in the examples presented in chapter 5.2.2, namely synergies with the structural system of buildings, a systematic analysis of potential synergies with all common building systems will be performed in this subchapter. Merritt and Ambrose (1990) define the main parts of a building to be the building structure, the vertical and horizontal circulation, the environmental control, the plumbing and the electrical systems. Most buildings comprise these basic elements.

Many of the formerly examined examples feature synergies with the buildings structural design. Especially the existing technical systems show that concrete water towers can be well integrated into a buildings architecture. Perlan's hot-water tanks are arranged in a way that allows them to carry the glass dome, as shown in Figure 17a. The museum thereby uses sections of the concrete standpipe towers as exterior walls. Although technically detached, the water tower of Tübingen is at least optically integrated into the architectural environment. Furthermore, the "Naturstromspeicher Gaildorf" utilizes the water tower as a fundamental part of the system. It does not only contain the upper reservoir for the PHES system but also carries the entire weight of the wind turbine. This synergy spares the necessity of building a second foundation for the wind turbine, thus significantly lowers the area requirements and moreover increases its wind-energy harvest. The building cores of the two office buildings introduced above – the "Knights of Columbus Headquarters Building" and "The Qube" – both feature similarities with water towers. It is imaginable to utilize these buildings structural concepts as upper reservoirs of an integrated PHES concept in the urban built environment.

While synergies with the building structure have been proven feasible, synergies with the vertical and horizontal circulation in buildings seem rather limited. Circulation describes the openings in a buildings walls that allow access to different rooms and floors. Openings in the upper reservoir of a PHES system can be considered counter-productive. Environmental control systems include windows to allow daylight to access the building and protect the interior from weather impacts as well as temperature regulation. While synergies with windows cannot be found, heating, ventilating and air conditioning systems are also very unlikely to provide opportunities for synergies with PHES systems. Although rivers have proven to reduce urban temperatures during summer, as shown by Sugawara, Narita, and Sik Kim (2019), this small effect is unlikely to be applied to a building that stores water from a river.

Plumbing systems of a building could be considered the natural ally of a PHES system. But as de Oliveira E Silva and Hendrick (2016) already conclude in their study, the potable water norms do not allow such a synergy – especially not if river water is used in the process. Even if river water was used for wastewater disposal and the buildings fire protection system only, the different dimensions of the PHES system and the water supply system would most likely render the arrangement unfeasible. Moreover, Mutschmann et al. (2011) points out that the installation of two different water supply systems in a building, one with potable and one with non-potable water, is not approved in Germany. The last building system to examine is the electrical system. No useful synergies can be determined for this system.

Synergies with Communal Services

Four possible synergies have been discovered that go beyond the scope of an individual buildings system and are rather on a communal scale. This is a natural consequence of the

large dimension of a 4 MW pumped hydro project in the urban built environment. The options are: Providing water for firefighting, irrigation of urban green areas, flood control services and the formation of a hybrid PHES system that directly stores generated electricity from a local wind- or solar farm. The latter will not be further discussed in the current study because it describes a fundamentally different economical approach. Nonetheless, a hybrid system or the integration of the PHES plant into a smart-grid system could be an attractive option that should be assessed in a different study.

According to Mutschmann et al. (2011), providing water for firefighting is a common task of water towers. They are therefore usually equipped with a water buffer for the case of an emergency. Water for firefighting does not need to fulfill high quality standards so that using river water from a PHES system is an acceptable option. Kaczynski (1994) furthermore points out that, for technical reasons, a certain amount of water always needs to remain in the upper reservoir of a PHES system. Whether or not this amount is sufficient to meet the demand of water for firefighting needs to be assessed in each particular case. Hülsmann, Harby, and Taylor (2015) emphasize that hydro-projects often provide water for irrigation purposes. This usually refers to crop production. In cities the irrigation of public green areas could be accomplished by using the water that is stored in the upper reservoir of the pumped hydro system. However, the use of water from natural water bodies is limited and regulated by the German water law as pointed out by Schulze (2017).

Flood control services might have the largest potential to serve as a useful and valuable synergy of an urban pumped hydro system. Hülsmann et al. (2015) discuss the importance of the multiple uses of pumped storage systems. Flood control and drought management are among those uses. Especially cities located along the waterfront of rivers are regularly threatened by floods that can cause immense damage to buildings and infrastructure. Extreme weather events that lead to the surging of rivers are furthermore expected to increase in the future as an effect of climate change (Wang et al., 2017). The considerable size of the upper reservoir in this study potentially allows the integration into a flood control system. This option is strongly considered. It is imaginable that the upper reservoir could be used as a flood control reservoir to dampen out flood peaks. However, the feasibility of this approach is still to be proven and highly depends on the water storage capacity of the system.

Selection of Suitable Working Structures

Two working principles have been discovered for the upper reservoir of the PHES plant. While the geometry of the reservoir is limited to cylindrical standpipe towers for technical reasons, different materials have been assessed and are now to be compared. Most examined solutions make use of reinforced concrete for the containment of large quantities of water. The foundation is thereby always made with in-situ concrete. The concrete water chamber itself can either be prefabricated in factories and joined on site or be poured-in-place along with the foundation. Another material that is used to store large amounts of water, especially in the USA, is steel. Welded steel tanks following the Eurocode guideline will be further examined along with concrete water towers.

5.2.3 Developing Concepts for the Upper Reservoir

In order to choose a suitable concept for the upper reservoir, the two preselected options from 5.2.2 need to be firmed up. Therefore, the concrete and steel tank will be assessed further in this chapter. Pahl et al. (2007) recommend rough calculations and sketches, but

also a market research, to provide more detailed information on the preselected working structures. With this information it will then be possible to calculate and compare the costs of both options to finally select the most feasible principle solution for the upper reservoir.

As defined in 5.2.2, the cylinder is the most convenient geometry for storing large quantities of water. For both options four different setups are analyzed. The first setup regards one single tank storing the entire energy, the second setup assumes the energy to be stored in two separate tanks, the third setup splits the stored energy into four tanks and the fourth setup splits the stored energy into eight tanks. Smaller tanks are considered to be easier to implement into building structures which is why these different setups are examined. The height of the analyzed tanks ranges from 10 meters to 130 meters. The tank radius is calculated based on the required volume and the given tank height. Whereas the required volume depends on the amount of potential energy E_{pot} that is to be stored – as defined in the requirements list in chapter 5.1 – as well as the effective hydrostatic head h_{eff}, the system efficiency η_{total}, the water density ρ_w and the gravitational acceleration g. The correlation is shown in equation 9 (Sterner & Stadler, 2017, p. 521).

$$V = \frac{E_{pot}}{\eta_{total} \cdot \rho_w \cdot g \cdot h_{eff}} \tag{9}$$

According to Schulze (2017) the effective hydrostatic head h_{eff} is measured from the water level of the lower reservoir up to half of the water level *z* of the upper reservoir. This relation can be viewed in Figure 23 below.

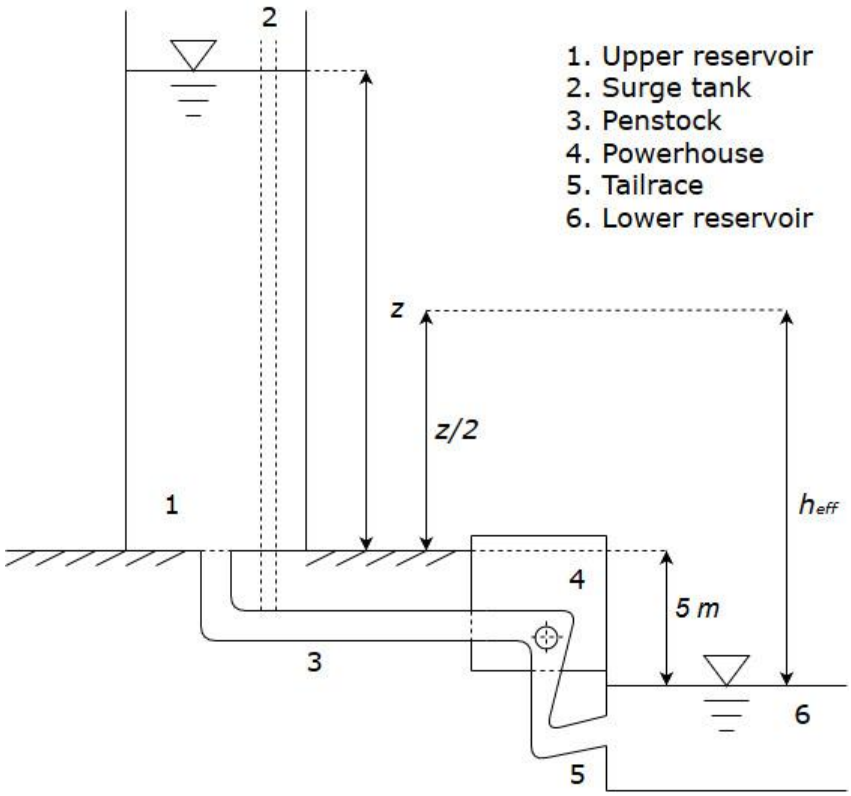

Figure 23 Effective hydrostatic head of the proposed PHES system. Adapted from Schulze (2017, p. 62).

The image furthermore shows the general schematic layout of the proposed PHES system with the upper and lower reservoir, the piping system and the powerhouse. The surge tank – although not part of the following assessment – is also depicted. For the current case study, it is assumed that the water level of the natural water body that serves as a lower reservoir lies 5 meters beneath the ground level on which the upper reservoir stands. The values of the required volume V for the different tank heights z can be viewed in Appendix V, Appendix VI, and Appendix VIII – along with the tank radius r and the effective hydrostatic head h_{eff}.

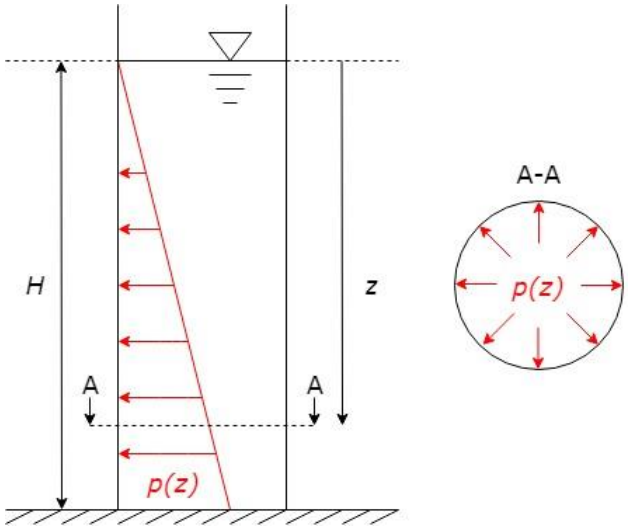

Figure 24 Distribution of the hydrostatic load in a cylindrical tank

The design of liquid retaining structures can be accomplished by following the Eurocode standards. The European Committee for Standardization (2006a) defines that "loads on tanks due to liquids shall be represented by a hydrostatic distributed load" (p. 23). This is valid for concrete and steel tanks. The characteristic value of pressure is thereby determined by the height of the hydrostatic head z and the unit weight of the stored liquid γ – as shown in equation 10 (European Committee for Standardization, 2006a, p. 74).

$$p(z) = \gamma \cdot z \qquad with \qquad \gamma = \rho_w \cdot g \tag{10}$$

The distribution of the hydrostatic load over the height of a cylindrical tank can be observed in Figure 24. The pressure increases linearly depending on the height of the water column in the tank. The pressure is, furthermore, equally distributed to the tank's walls at the height z – as shown in the cross section of the cylinder A-A.

The following assessment of the two tank options – namely, steel and concrete – aims on finding the most economic option for the upper reservoir, including the optimal aspect ratio and number of tanks. Therefore, the quantities of the required materials are estimated based on the sustained loads. The calculations thereby focus solely on the containment of the hydrostatic load. It is assumed that the structures are not built in seismic areas and wind loads are not considered. Vertical stresses caused by the weight of the tank itself are well below the critical limits and therefore not part of this assessment.

Reinforced Concrete Upper Reservoir

The most commonly used option in the previously discussed examples is the reinforced concrete reservoir. For the assessment of this option, Eurocode 2 is applied as the guiding standard. The amount of required materials is based on the contained hydrostatic loads of the reservoir. The highest hydrostatic load is always expected at the bottom of the reservoir – as shown in Figure 24. The hydrostatic head becomes maximum at this location. This maximum load is therefore chosen as the reference load for the following calculations.

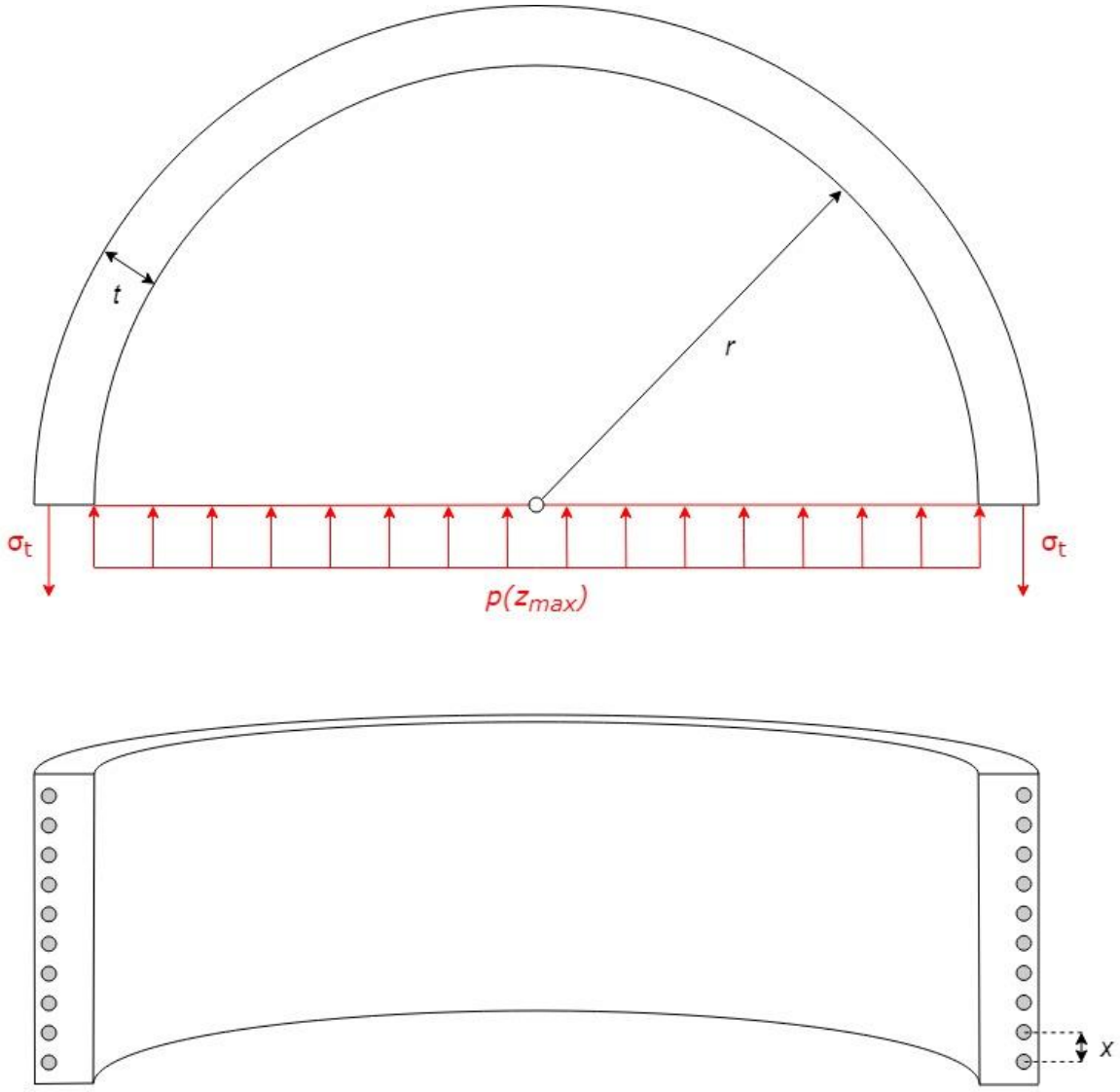

Figure 25a) (upper) Loads on cross section of cylindrical concrete tank wall, viewed from above. b) (lower) Schematic cross section of cylindrical concrete tank, side view – The gray filled cirlces show the locations of the steel tendons in the cross section. Note x is the center-to-center distance between the tendons.

Due to the low tensile strength of concrete, the hydrostatic load depicted in Figure 24 requires steel reinforcement to absorb the forces. The European Committee for Standardization (2004) furthermore states that steel reinforcement is not required when prestressing steel is used to put the concrete in compression. According to the European

Committee for Standardization (2006b) prestressing steel can be applied in liquid retaining structures to minimize cracking due to imposed deformations – in the current case through the hydrostatic load of the reservoir. Eurocode EN 1992-3:2006 (E) defines four tightness classes that represent different requirements for leakage. For the current case study, tightness class 2 is selected. Cracks that "pass through the full thickness of the section should generally be avoided" (European Committee for Standardization, 2006b, p. 10). Leakage is not desired for the reservoir as it might leave stains on the building's exterior or might even damage the building structure. To assure that cracks cannot pass through the full thickness of the reservoir wall, the compression zone within the section must be the lesser of 50 mm or 0.2 times the wall thickness t (European Committee for Standardization, 2006b).

If prestressing is applied, and the whole section remains in compression, no liner or sealant is required on the inside of the reservoir to achieve tightness class 2. When internal prestressing is used in cylindrical tanks, local failures due to the prestressing force can be avoided if the diameter of the duct containing the prestressing steel tendon does not exceed 0.25 times the reservoir wall thickness t. The prestressing force should also be evenly distributed on the wall of the reservoir, and the minimum tank wall thickness t for tightness class 2 is 150 mm. In the current case study horizontal prestressing is applied to contain the hydrostatic load of the upper reservoir. The location of the prestressing tendons can be viewed in the cross section in Figure 25b. They are colored grey, and each encircle the entire tank.

The prestressing tendons are assumed to take the entire hydrostatic load $p(z_{max})$ in the calculations. For this purpose, 7-wire prestressing steel strands following the prEN 10138-3:2000 standard by the European Committee for Standardization (2000) are selected. These strands are available in various standardized diameters and tensile strengths.

Given the hydrostatic head z, the tank radius r and the tensile strength of the strand R_m, the required cross-sectional area of prestressing steel tendon at the bottom of the tank can be calculated. The equilibrium condition for Figure 25a is

$$\uparrow: \quad F_p - 2 \cdot F_t = 0.$$

Whereas F_p is the compressive force caused by the maximum hydrostatic distributed load $p(z_{max})$, as defined in equation 11, multiplied by the affected surface – in the current case the tank diameter $2 \cdot r$ times the center-to-center spacing of the steel tendons x – as shown in Figure 25b. The partial factor γ_F is defined as 1.35 according to the European Committee for Standardization (2006a). It acts as a safety margin for the applied load. The compressive force is therefore defined as (European Committee for Standardization, 2006a, p. 74)

$$F_p = \gamma_F \cdot p(z_{max}) \cdot 2 \cdot r \cdot x \qquad with \qquad p(z_{max}) = \rho_w \cdot g \cdot z_{max}. \tag{11}$$

F_t represents the tensile force that affects the cross-section of the steel strands within the tank wall. The tensile force counteracts the hydrostatic force F_p. It is defined by the tensile stress σ_t and the cross-sectional area of the tendons $A_p{}'$. Due to the even distribution of the steel strands around the circular tank, the tensile force

$$F_t = A_p{}' \cdot \sigma_t$$

is defined by an equal cross-sectional area $A_p{}'$ of the tendons on both ends of the tank cross section as depicted in grey color in Figure 25b.

With the compressive force F_p and the tensile force F_t the equilibrium condition becomes

$$\gamma_F \cdot \rho_w \cdot g \cdot z_{max} \cdot 2 \cdot r \cdot x - 2 \cdot A_p{}' \cdot \sigma_t = 0.$$

Solving the equilibrium condition for the tensile stress on the prestressing steels strands σ_t results in

$$\sigma_t = \frac{\gamma_F \cdot \rho_w \cdot g \cdot z_{max} \cdot r \cdot x}{A_p{}'}. \quad (12)$$

The stress results from the hydrostatic load and includes the safety factor γ_F.

It must be assured that the tensile stress σ_t remains lower than the tensile strength of the steel strands R_m to avoid failure – as shown by the limiting condition for the tensile stress σ_t in the prestressing steel strand, equation 13

$$\sigma_t \leq R_m \quad (13)$$

Taken into consideration, the limiting condition results in equation 14 where the minimum required cross-sectional area of the prestressing steel strands is shown.

Using Equation 12 with $x = z_{max}$, inserting σ_t with R_m and dividing with factor 2, i.e:

$$A_p{}'_{total} \geq \frac{\gamma_F \cdot \rho_w \cdot g \cdot z_{max} \cdot r \cdot x}{2 \cdot R_m} \quad (14)$$

delivers the required cross-sectional area of prestressing steel over the entire height of the tank $A_p{}'_{total}$. According to W. Schick from BBV Systems GmbH, the factor ½ is included to represent the linear decline of required prestressing steel from the tank bottom to the top (personal communication, August 07, 2019). Multiplied by the circumference of the cylindrical tank – which also represents the length of the prestressing steel strands – the volume of the required tendons can be calculated. When multiplied by the density of steel $\rho_{steel} = 7850\ kg/m^3$, as found in European Committee for Standardization (2004, p. 40), the total weight of prestressing steel strands is identified.

There are many different methods of installing steel tendons. According to Geßner et al. (2017) they can be pre- or post-tensioned, directly bonded with the concrete or situated in ducts within the concrete, and they can be applied externally or internally. The costs of these different methods differ significantly. For the current assessment it is assumed that the steel tendons are post-tensioned and internally bonded with the concrete. A further, more detailed assessment might however suggest a different prestressing method as more feasible. The assumption is made for practical reasons. Moreover, the exact layout, number and diameter of the tendons will not be further examined in this study. Generally, it must be ascertained that the concrete needs to remain compressed at the highest hydrostatic load to avoid cracks through tensile stress. However, concrete compression may neither exceed the concretes stress limit to avoid cracks and brittle failure through compression when the tank is empty (European Committee for Standardization, 2004). This type of examination would be part of

a more detailed analysis but is not necessary for estimating the quantity of prestressing steel required for containing the hydrostatic load.

The amount of concrete that is required for the cylindrical tank wall, so that cracking is avoided, can be quantified by reversely applying the equation for minimum reinforcement areas as defined in Eurocode 2 by the European Committee for Standardization (2004, pp. 120-121). Considering that bonded prestressing tendons are used instead of horizontal reinforcement the equation becomes

$$\xi_1 \cdot {A_p}' \cdot \Delta\sigma_p = k_c \cdot k \cdot f_{ct,eff} \cdot A_{ct,h}.$$

The adjusted ratio of bond strength ξ_1 is $\sqrt{\xi}$ if only prestressing steel is applied to control cracking. The value for ξ is thereby 0.5 for post-tensioned strands bonded in C35/45 concrete as shown by the European Committee for Standardization (2004, p. 112). The recommended value for stress variation in prestressing tendons $\Delta\sigma_p = 100\ MPa$ is also chosen according to the European Committee for Standardization (2004, p. 81). The coefficient k_c takes account of the distribution of stress immediately before cracking occurs. For pure tension k_c is 1.0 which applies to the current case. The coefficient k is a factor that "allows for the effect of non-uniform self-equilibrating stresses, which lead to a reduction of restraint forces" (Bond et al., 2006, p. 76). For a wall thickness t below 300 mm, factor k is 1.0, and for a wall thickness t above 800 mm factor k is 0.65. Intermediate values are to be interpolated. According to Papula (2017, p. 84) they are calculated as

$$k(t) = 0.65 + \frac{1.0 - 0.65}{300\ mm - 800\ mm} \cdot (t - 800\ mm)$$

using Newtons linear interpolation. The mean value of tensile strength of the C35/45 concrete $f_{ct,eff} = f_{ctm} = 3.2\ MPa$ is chosen according to the European Committee for Standardization (2004, p. 29). Finally, if the above equation is solved for the horizontal area of concrete within the tensile zone $A_{ct,h}$ it becomes equation 15 – the required horizontal cross-sectional area of concrete within the tensile zone

$$A_{ct,h} = \frac{\sqrt{\xi} \cdot {A_p}' \cdot \Delta\sigma_p}{k_c \cdot k \cdot f_{ctm}} \tag{15}$$

Considering $k(t)$, however, suggests that $A_{ct,h}$ should be split into its components; the wall thickness t, and the tank height x – thereby neglecting that the prestressing tendons also lie within that cross-sectional area. This relation is shown in Figure 25. With these adjustments in place the equation becomes

$$\sqrt{\xi} \cdot {A_p}' \cdot \Delta\sigma_p = k_c \cdot k \cdot f_{ctm} \cdot t \cdot x \cdot \left(0.65 + \frac{1.0 - 0.65}{300\ mm - 800\ mm} \cdot (t - 800\ mm)\right).$$

Solving above equation for the wall thickness t is done by applying the quadratic formula as described by Papula (2017, p. 18). The required wall thickness for cylindrical concrete tanks t is finally calculated as shown in equation 16.

$$t = \frac{6050}{7} - \sqrt{\left(\frac{6050}{7}\right)^2 - \frac{\sqrt{\xi} \cdot {A_p}' \cdot \Delta\sigma_p}{k_c \cdot f_{ctm} \cdot x \cdot 0.0007}} \tag{16}$$

The European Committee for Standardization (2006b) recommends that the wall thickness of tanks complying with tightness class 2 should be at least 150 mm (p. 15). This minimum wall thickness is used if the wall thickness calculated in equation 16 lies below the limit. Multiplied by the tank height $x = z_{max}$ the required cross-sectional area of concrete over the entire height of the tank can be calculated. Furthermore, multiplied by the circumference of the cylindrical tank the volume of the required concrete is found.[1]

As vertical prestressing is not applied, vertical reinforcement is provided as recommended by the European Committee for Standardization (2006b). The recommendation for the cross-sectional area of vertical reinforcement $A_{s,v}$ is

$$0.002 \cdot A_{ct,v} \leq A_{s,v} \leq 0.04 \cdot A_{ct,v}$$

as defined by the European Committee for Standardization (2004, p. 163). The average value for $A_{s,v} = 0.021 \cdot A_{ct,v}$ is selected, whereas $A_{ct,v}$ represents the vertical cross-sectional area of concrete and is the product of the wall thickness t times the circumference of the cylindrical tank. Multiplied by the tank height $x = z_{max}$ the volume of required reinforcing steel is identified. Again, multiplied by the density of steel the mass of required reinforcing steel is found.

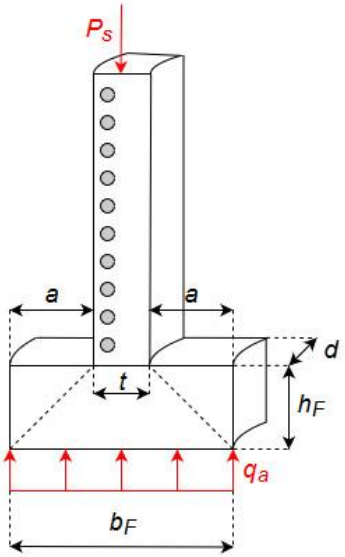

Figure 26 Tank wall plain concrete foundation with respective strains

The above calculations provide the quantity of all required materials for the cylindrical tank wall. The following examination focuses on the tank foundation and floor. The tank walls

[1] It must be noted that the above stated procedure for calculating the tank wall thickness is performed based on Eurocode 2. The ACI-373 guideline: "Design and Construction of Circular Prestressed Concrete Structures with Circumferential Tendons" provides further information on the detail design of circular tanks. The guideline suggests that a detailed calculation of the required concrete wall thickness depends strongly on many factors that go beyond the scope of the current study. The wall thickness, for instance, needs to be big enough to maintain the massive compression stresses that apply to the large tanks discussed in this study. Whether or not a minimum wall thickness of 150 mm and a concrete strength of C35/45 are sufficient to withstand these forces needs to be ascertained in a more detailed study. However, the current study is based on the assumptions stated above.

need to be supported by a wall foundation as shown in Figure 26. For the cylindrical tanks in this study, plain concrete wall footings are considered. The figure also shows the dimensions for plain foundations as described by Bond et al. (2006).

The purpose of the foundation is to distribute the load evenly into the ground while avoiding failure of the soil beneath the footing. Therefore, different types of underground have different properties. If hard rock is to be built on, foundations are not necessarily required. In the current case study the ground is assumed to consist of very stiff boulder clay with a presumed allowable bearing value of $q_a = 500\ kN/m^2$ as listed by Bond et al. (2006, p. 45). For the design of a wall foundation it is necessary to calculate the required area of footing in contact with the soil A. This can be achieved by following the *allowable stress design* method as described by Wight, Richart, and MacGregor (2012).

The specified load acting on the footing P_s needs to be distributed over the area A so that the allowable bearing value q_a of the soil is not exceeded. This correlation is depicted in Figure 26 and the required area of footing in contact with the soil A is calculated as shown in equation 17 (Wight et al., 2012, p. 814).

$$A \geq \frac{\sum P_s}{q_a} \tag{17}$$

The area of the footing is defined as $A = d \cdot b_F$, whereas d represents the thickness of the slice and b_F the width of the footing. In the current case study, the specific load P_s is defined by the weight of the wall and is calculated as

$$P_s = z_{max} \cdot t \cdot d \cdot g \cdot \rho_{ct}$$

with the density of concrete as $\rho_{ct} = 2300\ kg/m^3$ according to Wight et al. (2012, p. 30). Finally, the required width of the footing in contact with the soil b_F can be calculated as shown in equation 18.

$$b_F \geq \frac{z_{max} \cdot t \cdot g \cdot \rho_{ct}}{q_a} \tag{18}$$

With the width of the foundation b_F given, the depth of the footing h_F can be easily calculated considering the dimension relations in Figure 26 and the practice of designing the depth $h_F = a$ as described in Bond et al. (2006, p. 49). Multiplying the footings width b_F times the depth h_F times the circumference of the tank leads to the required volume of concrete for the wall foundation.

Besides the wall foundation, the concrete reservoir also needs a flat floor slab to prevent the water to seep into the ground. Following the design recommendations by Mohammed (2011) the slab is assumed to have a thickness of 150 mm. The required volume of the concrete for the slab can be easily calculated by multiplying the slab thickness times the circular ground area of the tank.

The load acting on the footing P_s highly depends on the height of the tank z. For small tank heights the load $P_{s,1}$ is small enough that an additional plain concrete foundation for the wall is not required. In these cases, the floor slab is sufficient to distribute the load into the ground. This relation is depicted in Figure 27. The image shows three different stages. On the left hand side, the simple slab foundation is sufficient as described above. The second figure

shows that the flat slab is required to protrude slightly so that the load distribution for $P_{s,2}$ can be accomplished, while the slab thickness remains at 150 mm. The image on the right hand side shows the third stage in which the load $P_{s,3}$ needs to be distributed into an even larger ground area. In this case it is not sufficient to simply extend the flat slab but rather increase the thickness of the wall footing.

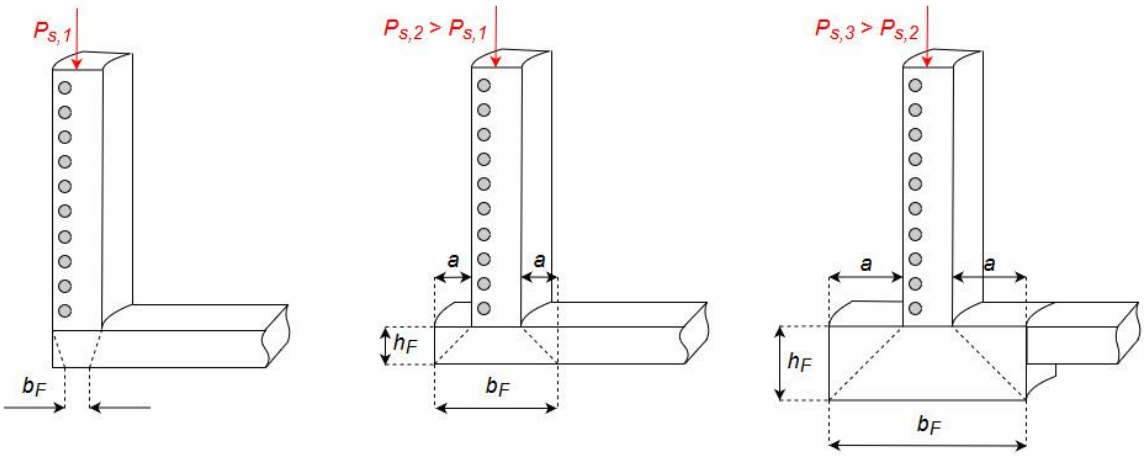

Figure 27 Wall foundation and floor slab for different loads $P_{s,1}$, $P_{s,2}$ & $P_{s,3}$

For the reinforcement of the floor slab, reinforcement mats are used. The cross-sectional area of reinforcement A_s that is required in the foundation and the slab is

$$0.0017 \cdot A_{ct} \leq A_s \leq 0.04 \cdot A_{ct}$$

for C35/45 concrete as listed by Bond et al. (2006, p. 49). The reinforcement mats may be selected accordingly. Also, the wall foundation requires reinforcement. Therefore, the average value $A_s = 0.02085 \cdot A_{ct}$ is considered for the vertical and horizontal cross-sections of the footing. This information and some further calculations that consider the tank geometry lead to the quantity of reinforcing steel that is required for the foundation and floor slab.

Steel Upper Reservoir

The second option for the upper reservoir of the proposed PHES system is the cylindrical steel tank. As opposed to the concrete tank, this system is composed of less different components and materials due to the fact that steel has a very high tensile strength. This makes the steel option easier to design. The guiding standard for steel structures is Eurocode 3. In particular Part 4-2 deals with the construction of tanks as published by the European Committee for Standardization (2007). The following assessment has the aim to identify the quantity of required materials using the same approach as for the concrete tank. Again, the highest hydrostatic load is expected at the bottom of the reservoir – as shown in Figure 24 – and therefore chosen as the reference load for the following calculations.

Different consequence classes exist for steel tanks, depending on the risk of failure for the storage of different liquids or gases. This reliability differentiation is important for the design process of tanks as operational safety needs to be assured. For tanks containing water the lowest consequence class 1 applies. For liquid induced loads the recommended value for the partial factor γ_F is defined as 1.35 – similar to the safety margin for the concrete tank

(European Committee for Standardization, 2007). Furthermore, the European Committee for Standardization (2007) defines the properties of the steels that may be used for tank structure. Structural steels according to EN 10025 may be used for this purpose. The effects of corrosion may always be considered by defining a corrosion allowance that is added to the thickness of the steel plates. In the current case, an isotropic cylindrical shell is assumed for the tank wall, composed of welded flat rolled steel sheet. Any structural reinforcement of the tank wall, by means of external stiffeners, is not considered in the current pre-feasibility study.

For the current assessment, the simplified design guideline by the European Committee for Standardization (2007) is applied. The design of the shell is mainly characterized by the steel plate thickness t_s. The steel plates need to withstand the hydrostatic loads. Therefore, the plate thickness needs to be determined accordingly. As shown in equation 19, the circumferential normal stress due to the liquid loads on the left hand side of the equation needs to comply with the design yield strength of steel $f_{y,d}$ (European Committee for Standardization, 2007, p. 46).

$$\gamma_F \cdot \rho_w \cdot g \cdot z_{max} \cdot \left(\frac{r}{t_s}\right) \leq f_{y,d} \tag{19}$$

Solving equation 19 for the steel plate thickness t_s results in

$$\frac{\gamma_F \cdot \rho_w \cdot g \cdot z_{max} \cdot r}{f_{y,d}} \leq t_s$$

with the partial factor γ_F, the density of water ρ_w, the gravity acceleration, the maximum water column height z_{max}, the radius r and the design yield strength of steel $f_{y,d}$. Multiplied by the circumference of the tank wall and the tank height this information provides the required quantity of steel for the tank shell.

Besides the reservoir wall, the system also requires a bottom plate to prevent water from seeping into the ground. Such a simple system can be viewed in Figure 28a. If butt welding is used to conjoin carbon steel bottom plates, the minimum nominal thickness t_b is 5 mm excluding the corrosion allowance (European Committee for Standardization, 2007, p. 50). Assuming a corrosion allowance of 3 mm the required thickness of the bottom plate totals 8 mm.

If the tanks diameter is larger than 12.5 meters, an additional base ring is required in the form of an annular plate, as described by the European Committee for Standardization (2007). This system is depicted in Figure 28b. The base ring has the purpose to provide stability to the tank shell to which it is attached. The minimum nominal thickness t_a of the base ring can be taken from equation 20 (European Committee for Standardization, 2007, p. 50).

$$t_a = max\left[\frac{t_s}{3} + 3\ mm\ ;\ 6\ mm\right] \tag{20}$$

The larger value in equation 20 is selected, and the corrosion allowance of 3 mm is added. The limiting value for the width of the base ring w_a is the lesser of the values shown in equation 21. It is the "distance from the inner edge of the annular base plate to the inner edge of the shell plate" (European Committee for Standardization, 2007, p. 51).

$$w_a = max\left[1.5 \cdot \left[\frac{f_{y,d} \cdot {t_a}^2}{\rho_w \cdot g \cdot z_{max}}\right]^{\frac{1}{2}} ; 500\ mm\right] \quad (21)$$

The foundation for the steel tank is implemented in reinforced concrete according to the design criteria of the European Committee for Standardization (2004). The same calculations apply as described for the wall footing of the concrete upper reservoir. In Figure 28 both systems – with and without base rings – are situated on a plain concrete foundation.

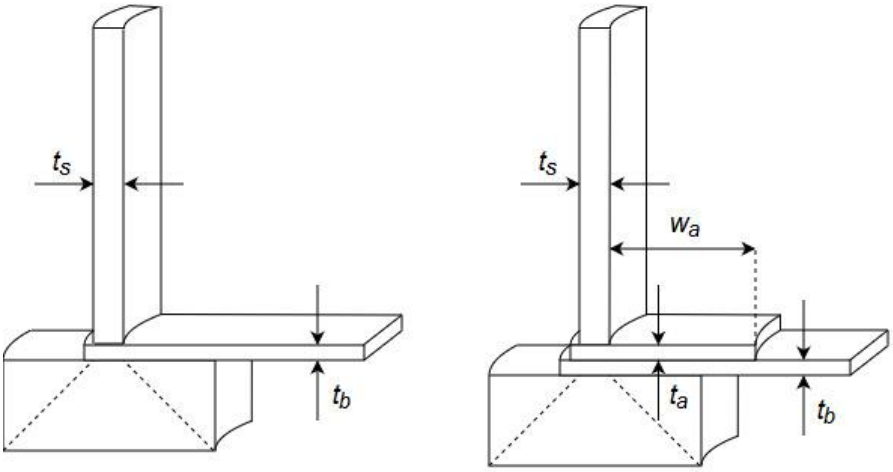

Figure 28a) (left) Bottom plate of a steel tank for diameters < 12.5 m. b) (right) Bottom plate and base ring for steel tanks with diameters > 12.5 m.

Considering the thickness and surface areas of the bottom plate, and if necessary, the base ring, the quantity of required steel can be easily found. For the plain concrete foundation, the required materials can be identified as explained in the previous subchapter.

Furthermore, the carbon steel components required for the cylindrical steel tank need to be protected against corrosion. The most common method for large steel tanks is the application of a paint coating to separate the steel surface from the water. This type of corrosion protection requires regular maintenance (WaterWorld, 2004).

5.2.4 Selecting Concepts for the other Subfunctions

Existing technologies are available for the other subfunctions shown in Figure 15 and therefore do not need to be examined as thoroughly as the upper reservoir of the proposed PHES system. In the following subchapters, available concepts will be chosen for the electromechanical equipment as well as the piping system.

Electromechanical Equipment & Powerhouse

According to Cavazzini, Santolin, Pavesi, and Ardizzon (2016) the electromechanical equipment includes two main items: “the mechanical equipment, including [pump-] turbine, automatic valve and regulation elements, and the […] electrical equipment” (p. 749), mainly including the transformer and the motor-generator. The latter is available from different

manufacturers in many different standardized sizes and can be ordered in the desired power class (Schulze, 2017). The same applies to the transformer. The motor efficiency can be set as $\eta_{motor} = 97\%$ and in reverse generator mode as $\eta_{gen} = 98\%$, whereas the transformer efficiency is $\eta_{trans} = 99.5\%$ either way (Giesecke et al., 2014, p. 721). The pump-turbine, however, requires a closer analysis. Figure 29 shows the application range of different types of turbines, whereas the hydrostatic head, the power output and the flow are plotted. The red line shows the application range of the options that are examined in the current case study. The intended power output is 4 MW and the lowest observed hydrostatic head of the current system is at 5 m when the upper reservoir is empty. The highest observed hydrostatic head is considered for a full upper reservoir. Pelton turbines are not considered in this study as they cannot be used in pumping mode due to their mechanical setup (Giesecke et al., 2014).

The ideal turbine is chosen by considering the desired power output and hydrostatic head. Figure 29 reveals that three types of turbines can be taken into account for the given height range at a power output of 4 MW: Kaplan turbines for the tank heights from 10 m to 60 m, and diagonal Dériaz turbines for tank heights from 20 m to 130 m (Giesecke et al., 2014). Another option for the proposed PHES system is the application of pumps as turbines (PaT). The pumps in question are double suction pumps within a height range of 30 m to 130 m (Morabito & Hendrick, 2019). If several multistage pumps are operated in parallel, the available head of a 4 MW system can even reach 500 m as described by Orchard and Klos (2009). All three options, namely Kaplan, Dériaz and PaT systems, will be considered in the current case study and the most economic option will be selected. Reversible Francis turbines are out of reach for the current study as they are only available for power ranges above 5 MW according to Morabito, de Oliveira e Silva, and Hendrick (2019).

Kaplan turbines are axial flow turbines that are applied at low and medium hydrostatic heads. Different types of setups are possible – vertical and horizontal – and they are mostly used for small-scale hydro power plants. The Kaplan turbine has adjustable impellers allowing for a large range of admission at high efficiency (Giesecke et al., 2014, p. 591). The efficiency of Kaplan turbines differs between turbine and pumping mode. In turbine mode the efficiency is approximately $\eta_t = 93{\sim}95\ \%$ and in pumping mode it is considered $\eta_p = 75{\sim}85\ \%$ as estimated by Giesecke et al. (2014, p. 587).

According to Morabito et al. (2019) the diagonal flow Dériaz turbine can be considered a hybrid technology that fills the gap between Francis and Kaplan turbines. It is very well suited for the use as a pump-turbine, covering a wide range of partial load conditions. This is due to the combination of adjustable runner blades and guide vanes resulting in high efficiencies over a large range of admission. This makes the Dériaz pump-turbine well suited for the current case study with its large head variation during the charging and discharging of the upper reservoir. Morabito et al. (2019) describe the 3MW case study *Naussac II* in France that uses a Dériaz pump-turbine with a turbine efficiency of $\eta_t = 92.8\ \%$ and a pumping efficiency of $\eta_p = 85.5\ \%$. Hence, the efficiencies of Kaplan and Dériaz pump-turbines are within the same range. Generally, the Dériaz turbine has not been described a lot in the literature and is not deployed very often.

Deploying pumps as turbines is often considered in micro-hydropower applications when the investment costs for conventional hydropower units are relatively high. Pumps are usually standardized, so they can be purchased “off the shelf” at low cost.

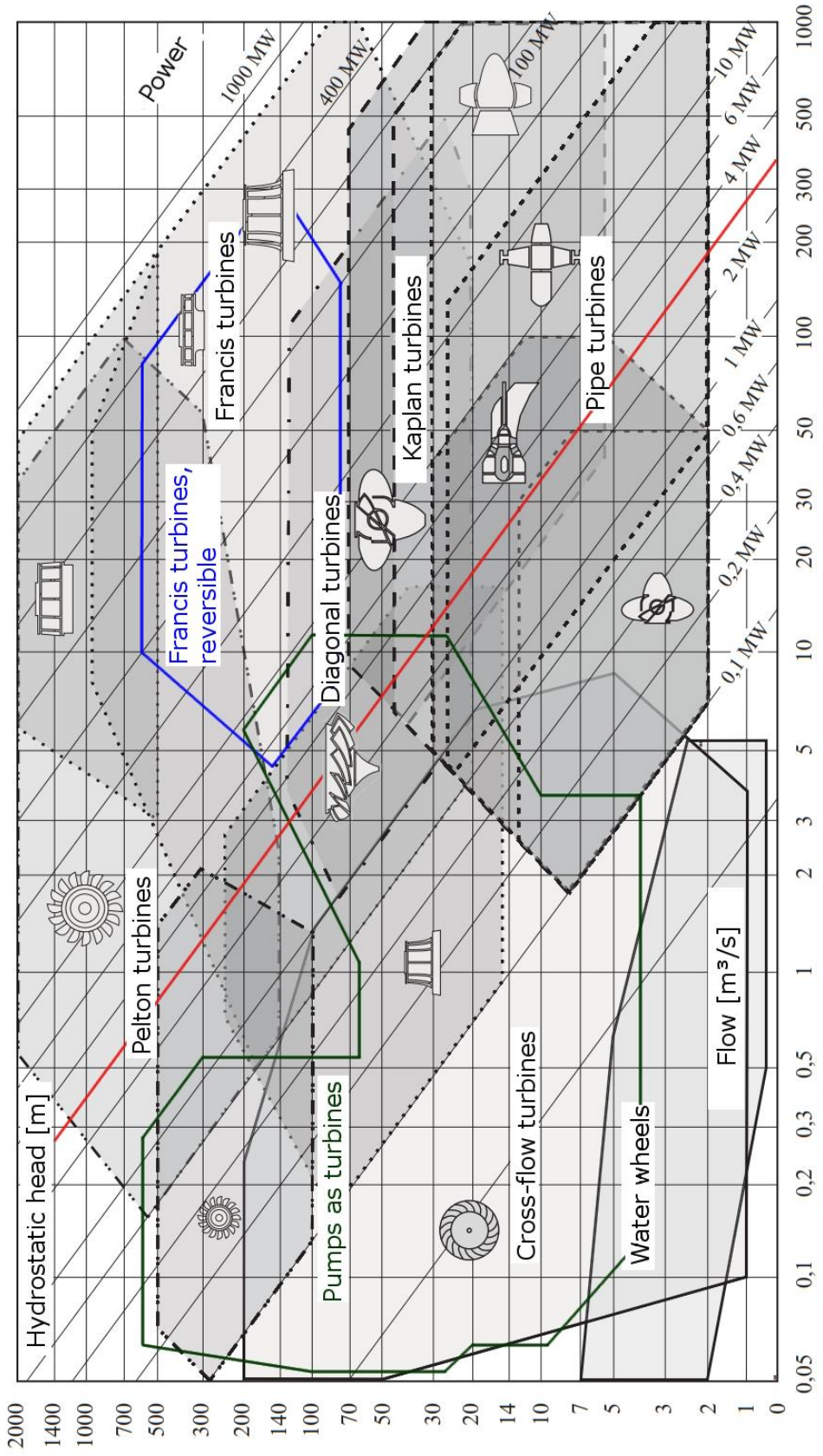

Figure 29 Turbine application chart – Flow rate over hydrostatic head. Adapted from Giesecke et al. (2014, p. 534), Morabito et al. (2019, p. 4) & Morabito and Hendrick (2019, p. 571).

As pumps do not have adjustable guide vanes for adapting to load fluctuations, they operate at lower efficiency if the hydrostatic head varies a lot – as it is the case for the current proposed PHES system. This is a drawback to the PaT system. However, operating many pumps in parallel allows for an extended range. Fluctuating water supply can then be controlled by connecting or disconnecting single pump units (Orchard & Klos, 2009). Furthermore, Morabito and Hendrick (2019) describe how they used a variable frequency driver (VFD) in their case study *le quartier Negundo* in Froyennes, Belgium to adjust the rotational speed of the pump-turbine. This allows for an operation at high efficiency under changing working conditions. Despite the variation in available head, the PaT-system achieved an efficiency of over $\eta_{t,p} = 70\ \%$ in the pumping and turbine mode.

Once the most suitable machinery has been selected, the electromechanical equipment needs to be encased in a powerhouse to protect it from external influences. The powerhouse design is mainly based on the size of the equipment, making a simple dimensioning of the components necessary. Again, the dimensions of the motor-generator are easy to find and of small magnitude, so that the size of the pump-turbine is used as the main reference for the dimensions of the powerhouse. A very simple approach is performed to identify the quantity of required materials for the powerhouse. Therefore, only the amount of concrete and reinforcing steel will be determined. Other materials are neglected. All walls are assumed to have a thickness of 200 mm and slabs are assumed to have a thickness of 250 mm. In total, four walls and three floor slabs are considered that together form a cube with two stories and a concrete roof.

At the heart of the powerhouse design is the size of the largest component of the pump-turbine. For the Kaplan turbine that is the width of the inflow shaft as calculated according to the pre-dimensioning guideline by Giesecke et al. (2014, pp. 601-607).

For the Dériaz turbine, the largest dimension of the turbine is the width of the volute casing as calculated according to Giesecke et al. (2014, pp. 611-614). It is thereby assumed that the components of the Dériaz turbine, except for the impeller, are similar to those of the Francis turbine as stated by Giesecke et al. (2014). The dimensions of the PaT system can be found in manufacturer datasheets, as pumps are usually standardized (DAB Water Technology, 2015, p. 232). A distance of 5 m around the turbine is then added to the dimension of the largest component to ensure enough space for the other electromechanical equipment and to allow access to the components. The quantity of concrete and reinforcement steel is then calculated according to the Eurocode 2 standard as described by the European Committee for Standardization (2004).

Piping System

The piping system includes two subsystems: the penstock and the tailrace. The penstock connects the upper reservoir to the pump-turbine and the tailrace connects the pump-turbine to the lower reservoir – as shown in Figure 5. In the current case study, the lower reservoir is assumed to be an existing, natural water body and the powerhouse is to be located as close as possible to the lower reservoir. Giesecke et al. (2014) states that precautions need to be undertaken to remove sand, flotsam and suspended matter from the intake water. Any solids can cause abrasive damage to the surfaces of the machine elements that are in contact with unclean water. This especially applies to the pump-turbine and can reduce its lifetime considerably. Therefore, the intake water needs to pass a grill and a sand trap before it enters the powerhouse through the tailrace pipe.

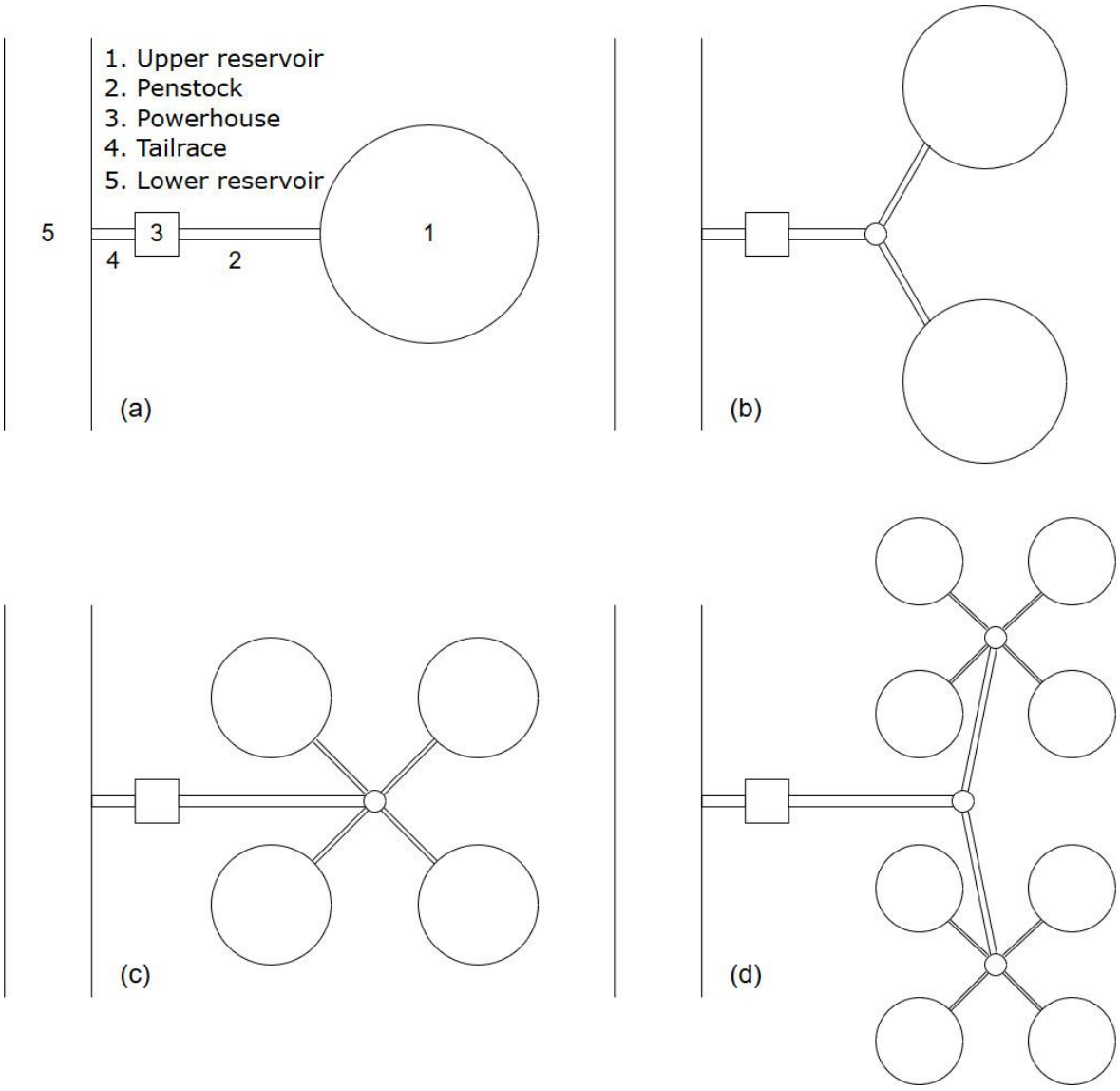

Figure 30 Schemetaic piping layout for (a) one upper reservoir tank, (b) two upper reservoir tanks (c) four upper reservoir tanks and (d) eight upper reservoir tanks – view from above.

The penstock of the current system is characterized by its length. Depending on the layout of the system, whether it has one, two, four or eight upper reservoir tanks, the distance covered by the penstock piping varies strongly. This correlation can be viewed in Figure 30. The piping for a system with only one upper reservoir tank can be very short depending on the distance between the tank and the powerhouse. If two tanks are considered, also two different pipe diameters will have to be calculated: one for the tank outlets and one for the powerhouse inlet – assuming that only one pump-turbine is to be installed. This layout requires the connection of the two smaller pipes into one large pipe. This connection will not be designed in detail in the current pre-feasibility study. The same applies to the layouts with four tanks and eight tanks. These systems require even more different pipe diameters and a more complex piping system. However, only a rough estimation of piping material and costs is made in this study.

Conventional steel water pipes following the EN 10255 standard are used for the piping system in the current case study. Technical information, including the standardized pipe

diameters and wall thicknesses of the pipes, is gathered from the datasheets of the steel manufacturer Salzgitter Mannesmann Stahlhandel (2015).

The required inner diameter of a pipe d_i depends on the flow rate Q and the velocity v of the flow as defined by the continuity equation and shown in equation 22 (Giesecke et al., 2014, p. 248).

$$d_i = 1.128 \cdot \sqrt{Q/v} \quad with \quad Q = \frac{V}{time} \tag{22}$$

According to Giesecke et al. (2014), the most economic velocity within the piping system is usually in the range of $v = 1{\sim}7\ m/s$ (p. 248). For the current case study, a value of $v = 7m/s$ is chosen. The flow rate Q is defined by the volume of water V that needs to enter or exit the upper reservoir, as calculated in equation 9, within the predefined timespan for one cycle $time = 4\ h$, as found in the requirements list in chapter 5.1.

Besides the pipe diameter, the required wall thickness of the pipe needs to be identified. This can be accomplished by following the EN 13480-3 standard for the design and calculation of metallic industrial piping as published by the European Committee for Standardization (2002). The minimum required wall thickness for a straight pipe excluding allowances and tolerances is thereby calculated as shown in equation 23 (European Committee for Standardization, 2002, p. 22).

$$e = \frac{p_c \cdot D_o}{2 \cdot f \cdot z_{jc} + p_c} \quad with \quad p_c = p(z_{max}) \cdot \gamma_F \tag{23}$$

The calculation pressure p_c is based on the hydrostatic load at maximum head $p(z_{max})$, as defined in equation 10, times the safety margin $\gamma_F = 1.35$. The outer diameter of the pipe D_o is selected from a standardized data table and is based on the required inner diameter of the pipe as calculated in equation 22. For the joint coefficient, a value of $z_{jc} = 1$ is used under the assumption of seamless and fully tested pipes. The design stress f at the design temperature is calculated as

$$f = min\left\{\frac{R_{eH\,t}}{1.5}\ ;\ \frac{R_{p0.2\,t}}{1.5}\ ;\ \frac{R_m}{2.4}\right\}$$

according to the European Committee for Standardization (2002). The minimum option for f is chosen from the equation above. The minimum upper yield strength at the calculation temperature $R_{eH\,t}$, the yield strength at the calculation temperature $R_{p0.2\,t}$, and the tensile strength of the utilised steel S195T are therefore gathered from the steel datasheet by Salzgitter Mannesmann Stahlhandel (2015). With the minimum required wall thickness e at hand, the ordered thickness e_{ord} can be identified. The ordered thickness includes all tolerances and a corrosion allowance c_0. If the manufacturer expresses the value of tolerance c_1 as a percentage $x_{\%}$ of the ordered thickness e_{ord}, it can be calculated as in equation 24 (European Committee for Standardization, 2002, p. 18).

$$e_{ord} \geq (e + c_0 + c_2) \cdot \frac{100}{(100 - x_{\%})} \tag{24}$$

The thinning allowance c_2 is neglected in the current study. The ordered thickness represents the final thickness of the ordered steel pipe. It needs to fulfill equation 24 and is chosen from

a standardized table by Salzgitter Mannesmann Stahlhandel (2015). The table also lists the weights of the according pipes per meter. With this information and length of the pipes, the total quantity of steel can be identified.

A detailed calculation is foregone for the pipe efficiency. Losses through friction are considered to be very low in compliance with Giesecke et al. (2014), assuming the pipe efficiency to be $\eta_{pipe} = 99\%$ (p. 721).

5.2.5 Overall Concept Variants

Finally, a set of concept variants can be examined based on the preliminary assessment. For the upper reservoir a variation of the tank height (10m – 130m), tank number (one, two, four or eight) and tank material (concrete or steel) is performed. The pump-turbines in question are either Kaplan, Dériaz or Pumps as Turbines. The selection of pump-turbines thereby also depends on the tank height of the upper reservoir. The size of the powerhouse depends on the size of the pump-turbine and the layout of the piping system varies depending on the tank height and tank number.

Table 7 Examined concept variants

Variable	Variants	Number of variants
Tank height	10 m 20 m 30 m 40 m 50 m 60 m 70 m 80 m 90 m 100 m 110 m 120 m 130 m	13
Tank number	One tank Two tanks Four tanks Eight tanks	4
Tank material	Concrete Steel	2
Turbine type	Kaplan Dériaz Pump as Turbine	3
		312 variants in total

A total number of 312 concept variants are examined in the current study as shown in Table 7. The main selection criteria are the total cost of the system, the system efficiency, the area requirement, and the architectural design. All other requirements discussed in the task clarification in chapter 5.1 are assumed to be met by the preselection of all above variants. The assessment is performed in a Microsoft Excel sheet.

The following chapters are dedicated to selecting the most favorable solution from the options stated above.

5.2.6 Techno-Economic Analysis

Based on the concept variants shown in Table 7, a techno-economic analysis is performed for the variants in order to determine the most feasible option. Pahl et al. (2007) recommend the economic analysis of the concept variants because the investment costs for the system are an important selection criteria. Low costs have also been defined one of the most important requirements for the current case study.

Table 8 Techno-economic data for engineering design study

	Unit	Value	Reference
Concrete C35/45	€/m^3	138.5	CEMEX (2018)
Reinforcing steel bars	€/to	955	Grosschädl Stahl (2019)
Reinforcing steel mats	€/to	1613	Jücker Stahlhandel (2019)
Prestressing steel strands	€/to	850	(J. Rüther, Westfälische Draht-industrie GmbH, personal communication, June 03, 2019)
Hot-rolled steel plates	€/to	1080 ~ 1150	Jücker Stahlhandel (2019)
Steel pipe, EN 10255	€/to	1300	(Schwarzkopf, Salzgitter Mannesmann Stahlhandel, personal communication, July 29, 2019)
Share of material costs in total civil work costs	%	26	Statistisches Bundesamt (2018)
Building land, small city	€/m^2	360.38	Statistisches Bundesamt (2019b)
German value added tax	%	19	European Union (2019)

In order to determine the most economic concept variant for the innovative pumped hydro scheme, the general cost structure of PHES projects needs to be found. A breakdown of the capital costs for hydropower projects is performed by IRENA (2012). The working paper describes the civil works of a project as the major contributor to a hydropower plant. These civil works include the dam and reservoir construction, as well as tunnels, canals and the construction of the powerhouse. According to the Statistisches Bundesamt (2018) the cost structure of civil works is characterized by the following shares: the actual material costs only make up for 26% of the civil work costs, whereas labor costs account for 28%. Another 33% of the civil costs is allocated to subcontractors and 13% of the civil costs are other costs. IRENA (2012) furthermore describes the electromechanical equipment as an important cost factor. The engineering, procurement and construction (EPC), as well as the owner's cost are assumed to be part of the civil costs for subcontractors and other costs as described above.

For the current case study, it is assumed that the site access infrastructure and the grid connection are already available and easy to implement.

Due to the fact that the plant is to be constructed in an urban setting, where area is scarce and the price for land is considerably high, the costs for building land are also considered in the current case study. It is therefore assumed that the PHES plant is located in a small German city with 200,000 to 500,000 inhabitants with a buy price for building land of 360.38 €$_{2018}$/m^2 (Statistisches Bundesamt, 2019b). The area requirement of the upper reservoir tanks and the powerhouse are considered for the cost calculation of the building land.

The prices for the required construction materials are gathered or estimated based on real-world data. Where possible, cost data for construction materials is taken from industry pricelists and directly from manufacturers to ensure plausible results for the techno-economic analysis. All prices are inflation-adjusted to €$_{2018}$ and exclude the German value added tax (VAT). A summary of the techno-economic data for the current analysis can be viewed in Table 8.

The following bullet list summarizes the different cost components that are part of the capital expenditure for the proposed innovative pumped storage scheme:

- Civil works;
    - Material;
    - Labor;
    - Subcontractors;
    - Other;
- Electromechanical equipment;
- Building land;
- Value added tax.

The costs for material are calculated based on the material quantities that are identified as described in the previous chapters - 5.2.3 and 5.2.4. The costs for labor, subcontractors and other are then calculated as a bulk cost item, based on the share of material costs in the total civil work costs (26%). The electromechanical equipment is calculated as described in the subchapter below. Finally, the VAT is added to the total capital cost in the end of the cost assessment. The building land is then calculated by considering the space requirements for the proposed PHES plant as identified in the chapters 5.2.3 and 5.2.4. No VAT is due for building land. Other taxes for land are neglected in the current study.

Pre-Selection Upper Reservoir

The most suitable concept for the upper reservoir can be chosen at an early stage due to the unambiguous results obtained from the techno-economic comparison between the concrete and the steel reservoir. While the cheapest option for the concrete tank is calculated to cost € 1,980,000, the cheapest steel reservoir for a system with the same energy capacity causes

costs of € 13,070,000. This difference in capital expenditure for the upper reservoir is very high and justifies the pre-selection of the reinforced concrete reservoir for the final concept selection.

Pre-Selection Electromechanical Equipment

The cost calculation for the electromechanical equipment for Kaplan, Dériaz and pumps as turbines is performed according to statistical cost estimation models by Cavazzini et al. (2016) and Alzohbi (2018). The model by Cavazzini et al. (2016) "decomposes the cost of the electromechanical equipment, including ex-works market prices of turbine, automatic valve, regulation elements and alternator, into three terms." (p. 749). The net head z_{max} $[m]$, the design flow rate Q $[l/s]$ and the design power NP $[kW]$ are considered by their model.

According to Cavazzini et al. (2016) the costs for Kaplan turbines can therefore be calculated as

$$C_{Kaplan}[€_{2016}] = 139318.161 \cdot {z_{max}}^{0.02156} + 0.06372 \cdot Q^{1.45636} + 155227.37 \cdot NP^{0.11053} - 302038.27.$$

The simulation of the real costs of power plants has shown that the above correlation has an average error equal to 8.1% and a standard deviation of 8.8%. The simulation can therefore be considered accurate enough for an estimate of the real costs in the current pre-study.

No specific cost estimation model was found for the Dériaz turbine. As described in chapter 5.2.4, the components of the Dériaz turbine, except for the impeller, are similar to those of the Francis turbine (Giesecke et al., 2014). It is therefore assumed that the costs of Dériaz turbines are comparable to those of Francis turbines. According to Cavazzini et al. (2016) the costs for Francis turbines can be calculated as

$$C_{Francis}[€_{2016}] = 190.37 \cdot {z_{max}}^{1.27963} + 1441610.56 \cdot Q^{0.03064} + 9.62402 \cdot NP^{1.28487} - 1621571.28.$$

For the simulation model of Francis turbines, the average error equals 10.6% and the standard deviation is 4.4%.

Alzohbi (2018) analyzed a range of 73 centrifugal pumps and developed a new correlation for the cost of pumps as turbines. Unlike the previous cost models, her correlation is based only on the net head z_{max} $[m]$ and the design power NP $[kW]$ of the plant. The cost of the electromechanical equipment of PaT's is calculated as

$$C_{PaT}[€_{2018}] = 1355.6 \cdot NP^{0.8296} \cdot {z_{max}}^{-0.1035}.$$

The model is only valid for a head range of $25\ m \leq z_{max} \leq 200\ m$, and a power range of $P \leq 550\ kW$. For the current PHES system with 4 MW it is therefore assumed that eight 500 kW centrifugal pumps are used. The average observed error of the model is 2 % and the standard deviation is 14.6%.

Based on the three cost correlation models described above, the cost for the electromechanical equipment of the three different technology approaches is calculated for

all observed tank heads. The results can be viewed in Appendix IX. Based on these calculated costs, a preselection can be performed. The pumps as turbines option is an unviable option for a 4 MW PHES system. The simulated costs for such a system are significantly higher than for equivalent Dériaz or Kaplan systems. Furthermore, the powerhouse needs to be much bigger for the PaT system as eight single units are to be installed, taking up more space. This increases the civil work costs as well as the building land costs. That is why only Kaplan and Dériaz turbines are considered in the final concept selection.

5.3 Outcome

Based on the previous chapters, the engineering design study is finalized. At the end of this chapter, a final concept variant is chosen from the remaining principle solution variants. Following the recommendations by Pahl et al. (2007), a separate economic and technical evaluation is performed in the following subchapters, followed by a conclusion and the selection of a final concept for the innovative PHES system.

5.3.1 Economic Evaluation

With all pre-selections made, the techno-economic analysis can be performed, regarding the assumptions stated in chapter 5.2.6. The results are depicted in Figure 31. The numerical results are shown in Appendix X to Appendix XIII.

Each data point in Figure 31 represents one of the final concept variants, whereas the head range of the Kaplan and Dériaz turbines is considered. For Kaplan turbines a maximum head of 60m can be realized for a 4 MW system – as depicted in the turbine application chart in Figure 29. For Dériaz turbines this maximum is 130m.

The first noticeable observation is that the $CAPEX$ of the PHES system decreases with increased height of the upper reservoir for all configurations. This is mainly due to the required volume of the upper reservoir for different hydrostatic heads as described in equation 9. The higher the hydrostatic head is, the less water volume is required for the same energy storage capacity. This has an immediate effect on the amount of required material for the system and decreases the required flow rate to charge and discharge the upper reservoir(s) – as considered in equation 22. The latter allows lower costs for the electromechanical equipment. Furthermore, the required radius of the upper reservoir(s) decreases at same total volume when the tank height increases, causing the costs for building land to decrease simultaneously. The lowest capital expenditures are therefore expected for the maximum possible tank head of the respective configurations.

A further observation that strikes attention is the large gap between the configurations with eight upper reservoir tanks and the other systems with one, two and four tanks. This applies to both options: with Kaplan and with Dériaz turbine. While the configurations with one, two and four tanks lie within a very small range in terms of total $CAPEX$, the eight tank configurations lie approximately € 2 million above that in each case. This observation can be traced back to the design of the upper reservoir tank. In particular to the required wall thickness of the concrete reservoir.

As stated in the engineering design study in subchapter 5.2.3, the European Committee for Standardization (2006b) recommends that the wall thickness of tanks complying with tightness class 2 should be at least 150 mm (p. 15). This minimum wall thickness is used if the wall thickness calculated in equation 16 lies below the limit. For the proposed PHES systems with one, two and four tanks this minimum wall thickness is complied with and the calculated value can be chosen for the design. For the systems with eight tanks this does not apply. The calculated value for the wall thickness, according to equation 16, lies well below the minimum value. Therefore, the minimum value of 150 mm must be chosen for each observed tank height, making the eight-tank option less feasible than the other options. The benefits of the theoretically decreased wall thickness requirement cannot be considered due to the consideration of the construction standard.

All observed Kaplan and Dériaz configurations lie within the same range in terms of capital expenditure for the maximum tank height. The cost-difference of the different options is only marginal and is less than € 250,000. Due to the proximity of the results of the configurations with one, two and four tanks and with Dériaz or Kaplan equipment, all six options are considered in the final concept selection.

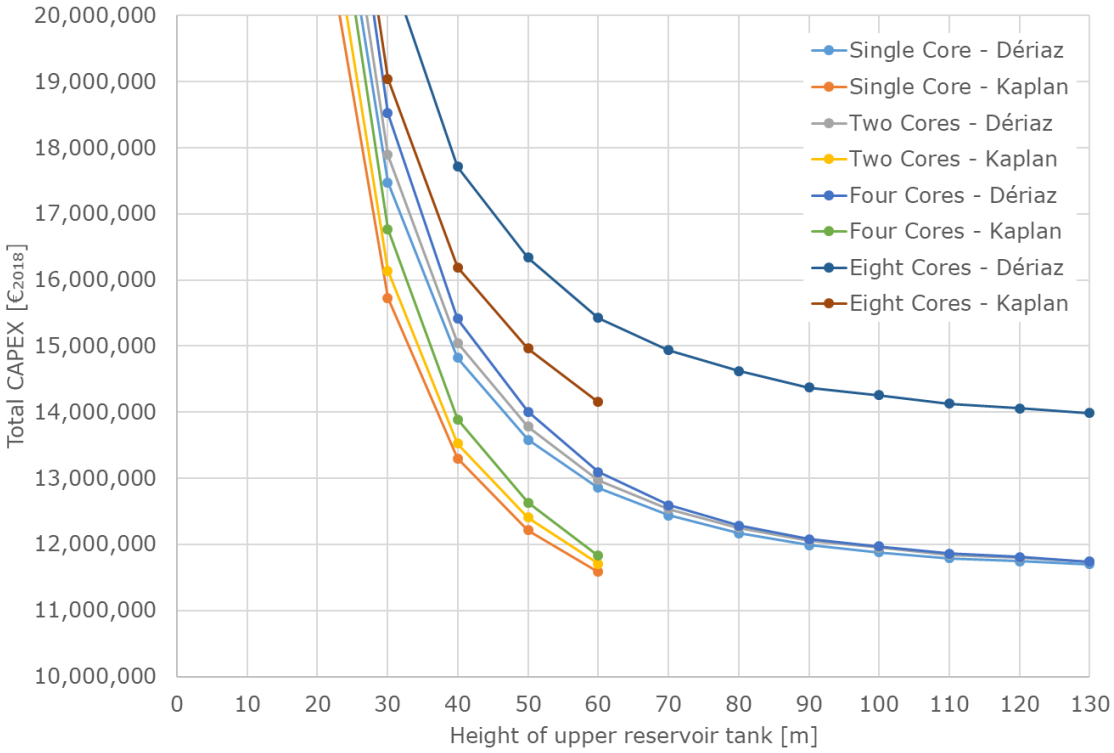

Figure 31 Total $CAPEX$ for different concept variants over the tank height

The capital expenditure is considered the only economic criteria for the final selection because all other economic quantities are assumed to be similar for all pre-selected options. The difference in the $LCOE$ is only determined through the $CAPEX$.

The $CAPEX$ of the observed options can be viewed in Table 9. For the further assessment it is scaled "using the 0-4 scale proposed in VDI Guideline 2225" (Pahl et al., 2007, p. 195). The lowest achievable $CAPEX$, for the "Kaplan, 60m, 1 tank"-option, is thereby assigned the highest grade 4, while the highest $CAPEX$, for the "Kaplan, 60m, 4 tanks"-option, is

assigned the grade 3.5, as the values are very close to each other. Intermediate values are interpolated.

Table 9 Economic criteria of pre-selected options

	CAPEX [€2018]	CAPEX [0-4]	R_e	Rank
Kaplan, 60m, 1 tank	11,586,583	4.00	1.000	**1**
Kaplan, 60m, 2 tanks	11,705,386	3.75	0.938	3
Kaplan, 60m, 4 tanks	11,827,062	3.50	0.875	6
Dériaz, 130m, 1 tank	11,698,517	3.77	0.942	2
Dériaz, 130m, 2 tanks	11,735,778	3.69	0.922	4
Dériaz, 130m, 4 tanks	11,741,002	3.68	0.920	5

The economic rating R_e is a share that represents the proximity to the optimum value. It is determined by dividing the total of achieved points by the number of maximum achievable points. The best economic rating is achieved by the single-tank Kaplan option. The rank of the options is also defined in the table.

5.3.2 Technical Evaluation

The technical evaluation is based on the non-economic requirements for the desired PHES plant. The efficiencies of the different options are assumed to be similar, as the only difference is within the piping system and no large losses are expected here. The only requirements left to consider are the area requirement, the architectural appeal and the synergies with other systems as described in chapter 5.1. The architectural appeal and the availability of synergies are assumed to correlate with the tank radius.

Table 10 Area requirement and tank radius of pre-selected options

	Area requirement [m^2]	Tank radius [m]
Kaplan, 60m, 1 tank	3,999	34.7
Kaplan, 60m, 2 tanks	3,999	24.5
Kaplan, 60m, 4 tanks	3,999	17.4
Dériaz, 130m, 1 tank	1,187	16.7
Dériaz, 130m, 2 tanks	1,187	11.8
Dériaz, 130m, 4 tanks	1,187	8.3

The basic idea behind this is that a slender structure may be considered more appealing to the viewer than a huge tank of a bulky appearance. Furthermore, slender tanks are somewhat easier to integrate into the architectural design of a building, making the identified synergies with the structural design of a building easier to implement.

Table 10 shows the calculated values for the area requirement and tank radius of the observed options. Again, the 0-4 scale is used to assign comparable values for the final assessment. The area requirement of the Kaplan systems is assigned a grade 2, while the Dériaz systems are assigned a grade 3. The largest tank radius, the "Kaplan, 60m, 1 tank"-option, is assigned the lowest grade 1, while the smallest tank radius, for the "Dériaz, 130m, 4 tanks"-option, is

assigned the grade 4. Intermediate values are interpolated. The assigned values can be viewed in Table 11.

Table 11 Technical criteria of pre-selected options

	Area requirement [0-4]	Tank radius [0-4]	Total	R_t	Rank
Kaplan, 60m, 1 tank	2	1.00	3.00	0.3750	6
Kaplan, 60m, 2 tanks	2	1.97	3.97	0.4957	5
Kaplan, 60m, 4 tanks	2	2.64	4.64	0.5798	4
Dériaz, 130m, 1 tank	3	2.70	5.70	0.7131	3
Dériaz, 130m, 2 tanks	3	3.17	6.17	0.7711	2
Dériaz, 130m, 4 tanks	3	3.50	6.50	0.8125	**1**

The total points are then calculated so that the technical rating R_t can be identified. Similar to the economic rating, the technical rating is a share that represents the proximity to the optimum value. It is determined by dividing the total of achieved points by the number of maximum achievable points for each option. The rank of the options is also shown in the table. The Dériaz option with four tanks is the preferred option from the technical point of view. Figure 31 Total $CAPEX$ for different concept variants over the tank height

5.3.3 Final Concept Selection

The final selection is performed by applying the rating method recommended by Pahl et al. (2007). For a better overview the strength diagram in Figure 32 is used to depict the technical and economic ratings (Pahl et al., 2007). Due to the very small variation of the $CAPEX$, the economic rating does not make a very large difference between the different options.

The technical rating however is influenced by the area requirement of the plant and the tank diameter. For these requirements the variation between the six observed options are considerable. The area requirement of all three Kaplan options is more than three times higher than the area requirement for the Dériaz options. This is an important decision criteria in a city where space is scarce. Furthermore, the radius of the upper reservoir tanks is much larger for the Kaplan options, making an integration into the urban environment rather difficult. It can be considered desirable to have bigger number of tanks with smaller diameters that can be integrated into building structures than one large tank that stands for itself and takes up a lot of space. This correlation is very well depicted in Figure 32.

The single pre-selected concept variants appear in the same order as they are listed in Table 11 from left to right in the figure below. It becomes apparent that the last option – the Dériaz turbine with four tanks of 130m height – can be considered the most desirable option. Although it is the second most expensive, this option has technical advantages that make it more suitable for the integration into the urban built environment. The option has been calculated to be only 154,000 €$_{2018}$ more expensive than the cheapest option at a total capital expenditure of 11.74 million €$_{2018}$.

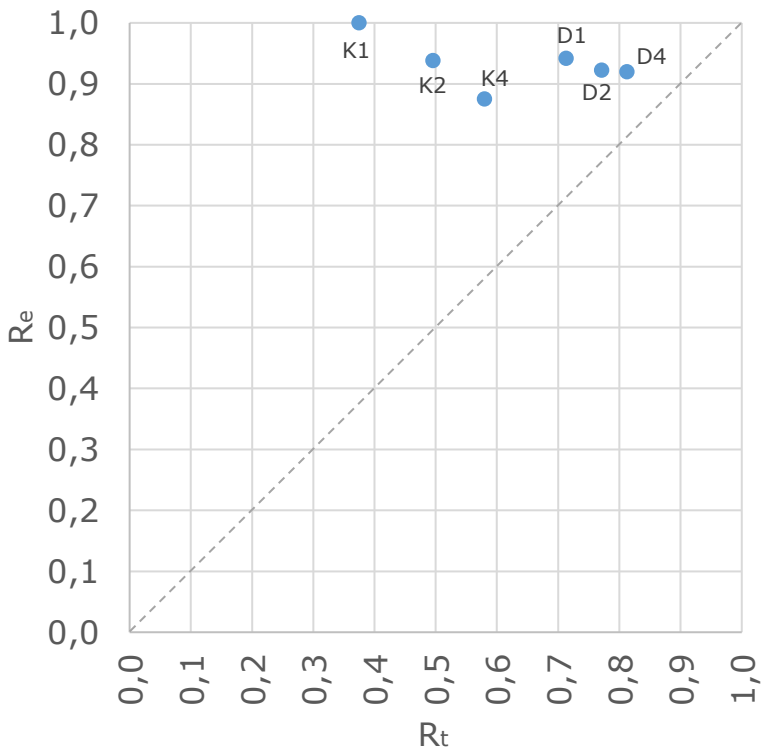

Figure 32 Comparison of the technical and economic ratings of the pre-selected options

According to Giesecke et al. (2014, p. 44) the inaccuracy of the investment costs of pre-feasibility studies lies within a range of ±20-25%, putting the cost difference of around 1.3 % into perspective.

6 Economic Study

The economic study has the aim to compare the $LCOE$ of the proposed innovative pumped hydro design from the previous chapter 5, with other energy storage plants and the SCCT baseline scenario. The other energy storage plants include the three small-scale PHES case studies in buildings, as described by de Oliveira E Silva and Hendrick (2016), Fonseca and Schlueter (2013) and Schulze (2017), as well as lithium-ion battery systems and power-to-gas-to-power systems – both, current and future systems.

6.1 Assumptions

All assumptions made previously for the economic study are summarized in Table 12. The assumptions #1 to #4 are valid for the entire $LCOE$ model and all examined technology cases. The assumptions #5 and #6 are valid for small-scale energy storage systems. The electricity costs are thereby defined as in chapter 4.1.2. Assumption #7 is valid for all energy storage systems, while the natural gas price – assumption #8 – is valid for the SCCT baseline scenario only.

Table 12 Assumptions for the economic study

		Unit	Value
#1	Corporate tax rate	%	30
#2	Discount rate (WACC, real)	%	3.23
#3	Exchange rate, US$ > € (2018)	-	0.8475
#4	Residual value, share of CAPEX	%	5
#5	Electricity costs, charge	€$_{2018}$/MWh	34.98
#6	Electricity costs, discharge	€$_{2018}$/MWh	51.94
#7	Sum of levies, electricity	€$_{2018}$/MWh	6.71
#8	Natural gas price	€$_{2018}$/MWh	24.81
#9	Capacity factor, small-scale storage	-	0.16

Assumption #9 is new and characterizes the current economic comparison study. It defines the capacity factor for all small-scale energy storage systems which are to be analyzed in the economic study. It is assumed that every small-scale storage system discharges electricity into the grid for four hours per day, on 350 days a year, as described in chapter 4.1.2. The remaining 15 days are considered as a buffer for maintenance and for days that do not allow an economic operation of the plant. For better comparison, SCCT plants are also modelled with the capacity factor described above. Large-scale hydro plants are excluded from this operational mode as they usually have a much longer discharging cycle and a much higher capacity factor. They are simply not designed for this type of short-cycle operation.

6.2 Input Data

The input data is case-specific and therefore needs to be discussed separately for each technology case.

Table 13 Input data for different storage systems and the SCCT baseline scenarios

Technology Case	CAPEX [€]	OPEX [€]	CF	η_{total} [%]	M [years]
#1 SCCT baseline scenario 1 – 94 MW	59,130,000	1,140,000	0.08	37	50
#2 SCCT baseline scenario 2 – 94 MW	59,130,000	1,720,000	0.16	37	50
#3 Proposed innovative PHES – 4 MW	11,740,000	411,000	0.16	74	50
#4 Goudemand residence PHES – 1.5 kW	45,820	1,604	0.16	35	50
#5 Torre Confinanzas PHES – 30.1 kW	142,000	4,971	0.16	32.5	50
#6 Wesermühlen PHES – 0.23 MW	3,347,000	117,100	0.16	80	50
#7 Lithium-ion battery system, 2016 – 1 MW	2,977,000	39,410	0.16	95	6
#8 Lithium-ion battery system, 2030 – 1 MW	1,184,000	15,670	0.16	97	11
#9 P2G2P system, 2020 – 1 MW	6,707,000	335,300	0.16	31.8	36
#10 P2G2P system, 2030 – 1 MW	5,064,000	253,200	0.16	37.7	43
#11 Average large-scale PHES – 560 MW	456,100,000	15,960,000	0.31	80	50

Table 13 shows a summary of the input data gathered for the different energy storage technologies. The $CAPEX$ and $OPEX$ values are rounded to four significant digits. All monetary values are inflation-adjusted to €$_{2018}$.

With the input data at hand, the levelized cost of energy for the different systems can be calculated as described in chapter 3.1. In the following subchapters the assumptions made in Table 13 are discussed in detail for each technology case.

6.2.1 Simple-Cycle Combustion Turbine Baseline

For the simple-cycle combustion turbine two different scenarios are considered: scenario 1 is modelled with a capacity factor of 0.08 as described in the economic pre-study in chapter 0. Scenario 2 is modelled with a capacity factor of 0.16, reflecting the conditions described in the previous subchapter and allowing for a fair comparison with the energy storage technologies. The different capacity factors furthermore affect the operational expenditure of the SCCT plant. All other assumptions remain the same for both scenarios. The input data for the technology is described below.

Nameplate Power Capacity

The 94 MW SCCT baseline plant is based on a real facility located in Darmstadt, Germany (Krein, 2011).

Total Efficiency

The total efficiency $\eta_{total} = 37\%$ of the plant is chosen according to Obi et al. (2017), as this value represents an average for single-cycle combustion turbines.

Capital Expenditure

The plant operator Entega – formerly known as HSE – invested 55 million Euros in the plant back in 2010. Inflation-adjusted to 2018, the $CAPEX$ is considered to be € 59,130,000 (HSE, 2010).

Operational Expenditure

The $OPEX$ is calculated as shown in equation 4 with the data provided by Obi et al. (2017). The fixed operational expenditure $OPEX_{fixed,n}$ is therefore considered to be 5,969 €/MW and the variable operational expenditure $OPEX_{variable,n}$ is 8.79 €/MWh – after exchange from US dollars to Euros and inflation-adjustment to 2018. Considering the plants nameplate power capacity $NP = 94\,MW$ and the annual energy production NRG_n as calculated in equation 7, two different values for the $OPEX$ are determined for the different capacity factors $CF_1 = 0.08$ and $CF_1 = 0.16$. The annual operational expenditure for scenario 1 ($OPEX_1$) is calculated as € 1,140,000 and for scenario 2 ($OPEX_2$) as € 1,720,000.

System Lifetime

As already stated in the economic pre-study in subchapter 4.1.1, the German energy agency dena (2010) estimates the system lifetime of gas turbines at 50 years, based on average values from real-life simple-cycle combustion turbine plants.

6.2.2 Proposed Innovative Pumped Hydro System

The input data for the proposed innovative PHES system is taken directly from the engineering design study in chapter 5.2.6.

Nameplate Power Capacity

The nameplate power capacity of the proposed PHES system has been defined as 4 MW in the economic pre-study.

Total Efficiency

The total efficiency of the proposed PHES system can be calculated by considering the efficiencies of all subsystems. Giesecke et al. (2014, p. 721) state the efficiency of the subsystems in pumped hydro facilities. The subsystems are also shown in Figure 15. The transformer has an estimated efficiency of 99.5%, and the electricity passes through the transformer twice. The motor-generator usually has two different efficiencies for each function. In motor mode it has an estimated efficiency of 97% and in generator mode 98%. For the piping system a loss of 1% is assumed making the efficiency of the piping 99%. Finally, the Dériaz pump-turbine efficiency varies depending on the operation mode, and is given by Morabito et al. (2019, p. 6), based on a case study in France. For the pumping mode the efficiency is 85.5% and in turbine mode it is 92.8%. The total efficiency can finally be calculated as 74%.

Capital Expenditure

The capital expenditure of the final concept – the Dériaz option with four 130m high upper reservoir tanks – is € 11,740,000.

Operational Expenditure

The operational expenditure of the proposed PHES is assumed to be 3.5% of the $CAPEX$ which is within the range of typical values according to Giesecke et al. (2014).

System Lifetime

The system lifetime of the proposed PHES plant in the current study is 50 years according to the Bundesministerium der Finanzen (1995).

6.2.3 Other Pumped Hydro Systems

Four different pumped hydro systems are analyzed in the current economic study: the three different case studies of micro-scale PHES in buildings, as described in chapter 2.3.1, and the average large-scale system. For PHES systems, no big technological progress is expected by 2030 due to the fact that pumped hydro is a mature technology.

Nameplate Power Capacity

The nameplate power capacity of each PHES technology case is described below.

#4 Goudemand Residence

According to de Oliveira E Silva and Hendrick (2016) the Goudemand residence case study has a nameplate power capacity of 1.5 kW.

#5 Torre Confinanzas Complex

The nameplate power capacity of the proposed PHES in a tall building by Fonseca and Schlueter (2013) totals 30.1 kW. It comprises 16 identical 1.4 kW turbines set up in parallel in the first circuit and 7 identical 1.1 kW turbines set up in parallel in the second circuit of the system.

#6 Wesermühlen

Schulze (2017) states that the nameplate power capacity of his Wesermühlen case study PHES is 0.23 MW.

#11 Average large-scale PHES

For the large-scale PHES the average power capacity of the examined large-scale PHES plants in the pre-study is considered. It is identified as 560 MW by evaluating all 24 plants with a power capacity larger than 10 MW and built after the year 2000.

Total Efficiency

The total efficiency of each PHES technology case is described below.

#4 Goudemand Residence

de Oliveira E Silva and Hendrick (2016) state the total system efficiency of their small-scale case study at 35%.

#5 Torre Confinanzas Complex

The total system efficiency of the case study Caracas in Venezuela is stated as 30 to 35% (Fonseca & Schlueter, 2013). For the current study the intermediate value 32.5% is chosen.

#6 Wesermühlen

Schulze (2017) assumes a total system efficiency of 80% for his case study.

#11 Average large-scale PHES

The average system efficiency for large-scale PHES systems, 80%, is assumed for the average large PHES system (Obi et al., 2017).

Capital Expenditure

The capital expenditure of each PHES technology case is described below.

#4 Goudemand Residence

The $CAPEX$ of the Goudemand residence PHES system is 45,820 €$_{2018}$ considering the system case 1 with an upper and a lower reservoir as described by de Oliveira E Silva and Hendrick (2016).

#5 Torre Confinanzas Complex

Fonseca and Schlueter (2013) state the capital expenditure for their system at 142,000 €$_{2018}$ after inflation-adaption and applying the $ / € exchange rate.

#6 Wesermühlen

Schulze (2017) concludes that the investment costs for his PHES in an abandoned silo building amount to 3,347,000 €$_{2018}$.

#11 Average large-scale PHES

The average $CAPEX$ of large-scale PHES systems is identified as 456.1 million €$_{2018}$ in the economic pre-study.

Operational Expenditure

The operational expenditure of each PHES technology case is assumed to be 3.5% of the $CAPEX$ which is within the range of typical values according to Giesecke et al. (2014).

System Lifetime

The system lifetime of all PHES plants in the current study is 50 years according to the Bundesministerium der Finanzen (1995).

6.2.4 Lithium-Ion Battery System

The current study focuses on the NMC/LMO cell chemistry for the examined lithium-ion battery systems, as described in 2.3.2. Two different scenarios are considered for the lithium-ion battery storage option. The first scenario is characterized by the conditions and the state of art in the year 2016 – in this study referred to as the current scenario. The second scenario reflects the forecasted technological progress by the year 2030. This allows for the consideration of potential technological change that might increase the future feasibility of the lithium-ion battery technology.

Nameplate Power Capacity

The nameplate power capacity of the lithium-ion systems is assumed to be 1 MW for both scenarios.

Total Efficiency

The total efficiency of lithium-ion battery systems is only expected to increase slightly by 2030. The values for both scenarios are defined below.

#7 Lithium-ion 2016

The current state of the art allows NMC/LMO lithium-ion batteries with total system efficiencies of 95% (IRENA, 2017).

#8 Lithium-ion 2030

According to IRENA (2017) the total system efficiency of lithium-ion batteries will increase to 97% by 2030.

Capital Expenditure

The $CAPEX$ of lithium-ion battery systems is expected to decrease strongly by 2030. The values for both scenarios are defined below.

#7 Lithium-ion 2016

The authors in IRENA (2017) find that the current energy installation costs of lithium-ion batteries lie within the range of 200 to 840 US$/kWh. For the NMC/LMO cell chemistry an average value of 420 US$/kWh is identified. Multiplied by the energy storage capacity of the system, 4MWh, the energy installation costs can be calculated. Tsiropoulos, Tarvydas,

and Lebedeva (2018) furthermore point out that the battery pack only accounts for 50% of the total costs of an energy-designed grid-scale stationary storage system. Thus, the specified energy installation costs are doubled to receive the final $CAPEX$ for the lithium-ion battery storage system in 2016. It is calculated as 2,977,000 €$_{2018}$.

#8 Lithium-ion 2030

For 2030, the authors in IRENA (2017) find that the energy installation costs of NMC lithium-ion batteries will have an average value of 167 US$/kWh. Multiplied by the energy storage capacity of the system, 4MWh, the energy installation costs can be calculated. Again, the $CAPEX$ is doubled to receive the total system costs for the lithium-ion battery storage system in 2030. It is calculated as 1,184,000 €$_{2018}$.

Operational Expenditure

The $OPEX$ for both lithium-ion battery system scenarios are described below.

#7 Lithium-ion 2016

For the current lithium-ion storage system, the operational expenditure is calculated according to the U.S. Energy Information Administration (2019). The report states the fixed and variable operational costs for general battery storage systems in 2018. $OPEX_{variable}$ is given as 7.26 US$$_{2018}$/MWh and $OPEX_{fixed}$ as 36.32 US$$_{2018}$/kW/year. After applying equation 4 the total operational expenditure is calculated as 39,410 €$_{2018}$.

#8 Lithium-ion 2030

For 2030 the operational expenditures are calculated based on the share of the $OPEX$ to $CAPEX$ in 2016 as the U.S. Energy Information Administration (2019) does not provide future estimates of the operation and maintenance costs. The share is identified to be 1.38%. Thus, the $OPEX$ of lithium-ion battery systems for 2030 is estimated to be 1.38% of the capital expenditure in 2030 – 15,670 €$_{2018}$.

System Lifetime

The system lifetime of battery storage systems can be identified in two ways. The cycle life defines how often a battery can go through a full charging and discharging cycle, whereas the calendar life describes how many years a battery system is expected to last if the cycle life is not exceeded (IRENA, 2017). The smaller of both values is to be considered as the final systems lifetime. The system lifetime for both scenarios is identified below.

#7 Lithium-ion 2016

According to IRENA (2017) the cycle life of NMC/LMO lithium-ion batteries in 2016 is 2000 cycles. Considering the operation mode of the current case study, the system goes through 350 cycles per year, leading to an expected lifetime of 5.71 years. The calendar life of the same battery system is identified as 12 years, so the smaller value is the cycle lifetime. The 2016 system therefore has a system lifetime of 5.71 years.

#8 Lithium-ion 2030

According to IRENA (2017) the cycle life of NMC/LMO lithium-ion batteries in 2030 is approximately 4000 cycles. Considering the operation mode of the current case study the cycle lifetime is 11.43 years. The calendar life of the same battery system is identified as 18

years in 2030, so the smaller value is the cycle lifetime again. The 2030 system therefore has a system lifetime of 11.43 years.

6.2.5 Power to Gas to Power

Many different energy storage technologies are available that are based on converting power into any form of fuel (Sterner & Stadler, 2017). The current study focuses on power to gas to power (P2G2P) because the option is comparable with other energy storage technologies that have electricity as an input and output. Furthermore, the study analyses PEMEC systems as described in 2.3.3. As for the lithium-ion systems before, two different scenarios are considered for the P2G2P option. The first scenario is characterized by the conditions and the state of art in the year 2020 – in this study referred to as the current scenario. The second scenario reflects the forecasted technological progress by the year 2030. This allows for the consideration of potential technological change that might increase the future feasibility of the P2G2P technology.

Nameplate Power Capacity

The nameplate power capacity of the P2G2P systems is assumed to be 1 MW. This means that the fuel cell has a power output of 1 MW into the grid.

Total Efficiency

The total efficiency of the P2G2P system depends on the efficiencies of the sub-processes. The main components of the P2G2P system are the PEM electrolyzer, the pressurized tank that stores the produced hydrogen, the compressor, the balance of plant equipment and the PEM fuel cell – as described in 2.3.3.

#9 P2G2P 2020

In 2020 the PEM electrolyzer is assumed to have an efficiency of 74.5% (Schmidt et al., 2017), whereas the PEM fuel cell has a much lower efficiency of 45% after the interpolation of values in IEA (2015). The International Energy Agency also provides the efficiencies for the compressor at 95%, and the storage tank at 100%. The total efficiency of the P2G2P system is therefore defined as 31.8%.

#10 P2G2P 2030

In 2030 the PEM electrolyzer is assumed to have an efficiency of 81% (Schmidt et al., 2017), whereas for the PEM fuel cell an efficiency of 49% is found after interpolating the efficiencies in 2015 and 2050 (IEA, 2015). The efficiencies for the compressor and the storage tank remain at the 2020 levels because of the maturity level of these subsystems. The total efficiency of the P2G2P system is therefore defined as 37.7%.

Capital Expenditure

The $CAPEX$ of the P2G2P systems in 2020 and 2030 is calculated below for both scenarios.

#9 P2G2P 2020

According to Schmidt et al. (2017) PEMEC electrolyzers have a capital cost between 1,000 and 1,950 $€_{2016}/kW_{el}$ in 2020. The average value 1,475 $€_{2016}/kW_{el}$ is used for the current study. The engineering company Fichtner (2014) states that PEMEC fuel cells can be assumed to have the same costs as electrolyzers. Therefore, the same cost data is used.

Fichtner (2014) also assumes balance of plant costs of 65 €$_{2014}$/kW$_{el}$. The hydrogen technology roadmap by the IEA (2015) states that pressurized tanks with a storage capacity of 0.1-10 MWh have average capital costs of 8,000 US$$_{2015}$/MWh. Finally, the compressor costs 70 US$$_{2015}$/kW$_{H2}$ (IEA, 2015).

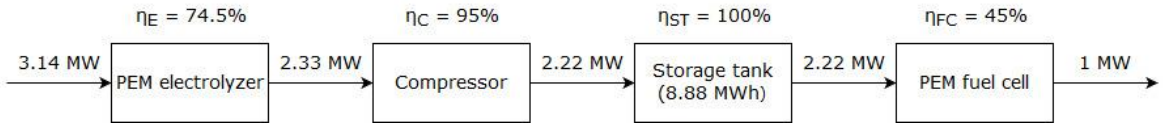

Figure 33 Flow chart of the P2G2P process in 2020 with efficiencies and power capacities

The final $CAPEX$ is based on the costs described above and the required size of the components. Figure 33 depicts the system components and the power capacity of each component after considering the efficiencies of the subsystems. The total system efficiency needs to be considered to estimate the required power capacity of the PEM electrolyzer. The fuel cell has a power output of 1 MW, so the electrolyzer needs an electrical power capacity of 3.14 MW. The compressor costs are based on the equivalent power capacity of hydrogen that enters the compressor. For 2020 that power capacity is 2.33 MW. The storage capacity of the tank is 8.88 MWh based on the charging cycle duration of 4 hours and the power input of 2.22 MW. The balance of plant cost is based on the power output 1 MW.

After considering all variables and cost components, a total capital expenditure of 6,707,000 €$_{2018}$ is identified for a P2G2P system in the year 2020.

#10 P2G2P 2030

According to Schmidt et al. (2017) PEMEC electrolyzers are expected to decrease their capital costs by 2030. A $CAPEX$ between 850 and 1,650 €$_{2016}$/kW$_{el}$ is expected. The average value 1,250 €$_{2016}$/kW$_{el}$ is used for the current study. The same applies to PEMEC fuel cells. The balance of plant cost is not expected to decrease significantly and remain at 65 €$_{2014}$/kW$_{el}$. The same applies to the hydrogen storage tanks with average capital costs of 8,000 US$$_{2015}$/MWh, and the compressor with costs of 70 US$$_{2015}$/kW$_{H2}$ (IEA, 2015).

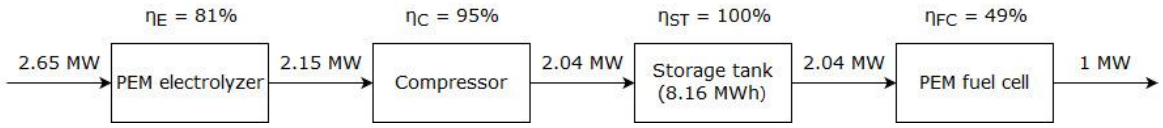

Figure 34 Flow chart of the P2G2P process in 2030 with efficiencies and power capacities

The final $CAPEX$ is based on the costs described above and the required size of the components. Figure 34 depicts the system components and the power capacity of each component after considering the efficiencies of the subsystems in 2030. The total system efficiency needs to be considered to estimate the required power capacity of the PEM electrolyzer. The fuel cell has a power output of 1 MW, so the electrolyzer needs an electrical power capacity of 2.65 MW. The compressor costs are based on the equivalent power capacity of hydrogen that enters the compressor. For 2030 that power capacity is 2.15 MW. The storage capacity of the tank is 8.16 MWh based on the charging cycle duration of 4

hours and the power input of 2.04 MW. The balance of plant cost is based on the power output 1 MW.

After considering all variables and cost components a total capital expenditure of 5,064,000 €$_{2018}$ is identified for a P2G2P system in the year 2030.

Operational Expenditure

The operational expenditure of P2G2P systems is approximately 5% of the $CAPEX$ in 2020 and 2030 (IEA, 2015).

System Lifetime

The system lifetime of the P2G2P systems in 2020 and 2030 is defined below for both scenarios.

#9 P2G2P 2020

In her comparison study, Jülch (2016) defines the electrolyzer lifetime as the financial lifetime of a P2G2P storage system. This assumption is adopted for the current case study. According to Schmidt et al. (2017), the electrolyzer lifetime of P2G2P plants in 2020 lies within the range of 41,000 to 60,000 hours. For the current study 50,500 hours are chosen as the average value. Assuming that the storage system discharges electricity into the grid for four hours per day, on 350 days a year, as defined in 6.1, the system lifetime can be expected to be 36 years.

#10 P2G2P 2030

By 2030 the electrolyzer lifetime is expected to increase to 40,000 to 80,000 hours with an average lifetime of 60,000 hours. Under the same assumptions as stated above, a system lifetime of 43 years can be expected for the P2G2P system in 2030.

7 Environmental Study

The environmental study is performed based on the observed energy storage systems and has the aim to put the proposed, innovative PHES system into perspective by comparing its environmental impacts with those of the other systems. The following subchapters set the framework for the environmental study that is performed using the life cycle assessment software openLCA.

7.1 Goal and Scope

The goal and scope definition of the environmental study for selected energy storage systems is performed in the subchapters below.

7.1.1 Goal

The current study aims at examining and comparing the environmental impact of energy storage systems that can be situated in the urban built environment. Besides these small-scale systems, one large-scale pumped hydro system will also be assessed to demonstrate the effect of economies of scale. This study is supposed to show that energy storage systems have a considerably lower environmental impact than their currently used alternative: natural gas peaking plants. Simple-cycle combustion turbines will therefore be included in this environmental study. Furthermore, the results of this study aim to support the decision-making process of electricity providers and building owners who currently seek to install small-scale energy storage systems in their premises in the urban built environment.

7.1.2 Scope

The assessment focuses on the environmental consequences of change within the life cycle. Therefore, the current simple cycle combustion turbine baseline scenario is replaced by energy storage technologies. The method is, therefore, consequential. The energy storage technologies examined in this study are lithium ion battery systems and power to gas to power systems. For these systems an assessment of only the current state of art will be performed due to data restrictions. Furthermore, large-scale pumped hydro plants will be examined as well as the formerly established innovative pumped hydro scheme in the urban built environment.

Two scenarios will be examined in this study. The first scenario assumes that the storage systems are charged using the German electricity mix, and in the second scenario the systems are charged with electricity from 100% wind.

In compliance with other life cycle assessment studies of energy storage systems, the functional unit of the current environmental study is one kilowatt hour (1 kWh) of electricity distributed to the grid (Abdon et al., 2017). The study focuses on the manufacturing phase of the electricity distribution service. The system boundaries include the raw material

extraction, the manufacturing of the energy storage systems und the electricity storage and discharge phase. A cutoff point is established at the output of the storage systems. Thus, the electricity distribution network is not included in this study (Oliveira et al., 2015). The systems end-of-life and disposal are also not regarded in this assessment. The type of study therefore is cradle to gate. This environmental study is mostly drawn from public industry data included in the ecoinvent 3.5 database. Following the definition of Agarwal et al. (2012) it can be considered a non-ISO desk study with the purpose of delivering good estimations rather than a detailed analysis.

The impact assessment method used in this study is the ILCD 2011 midpoint method according to the European Commission Joint Research Centre Institute for Environment and Sustainability (2012). The study examines the impact category "Climate change - ILCD 2011 Midpoint" with the reference unit kg CO_2 eq. Furthermore, the LCIA method "Cumulative exergy demand" with the three impact categories "non-renewable energy resources, fossil", "non-renewable energy resources, metals" and "non-renewable energy resources, minerals" is used (Hischier et al., 2010). The reference unit for the resource depletion impact is MJ eq. Although the "land use" impact will not be assessed in this analysis, it will be discussed briefly in the discussion chapter. This study uses the open source software openLCA 1.8.0 by GreenDelta, Berlin.

7.2 Life Cycle Inventories of Selected Technologies

The current subchapter introduces the inventories for the SCCT baseline scenario, and the examined energy storage technologies as described previously. The life cycle inventories of the current environmental study are mainly based on the available data from the ecoinvent database, version 3.5.

For each storage technology two different scenarios are analyzed as discussed in the previous chapter 7.1: the charging electricity for the first scenario is assumed to be the German electricity mix from 2014 – "market for electricity, high voltage | electricity, high voltage | APOS,U - DE" – according to the ecoinvent 3.5 database. The second scenario assumes the electricity for charging to come from German wind turbines. Therefore, the dataset "electricity production, wind, 1-3MW turbine, onshore | electricity, high voltage | APOS,U - DE" is chosen, according to the ecoinvent 3.5 database (Wernet et al., 2016).

Whenever material datasets are selected from the ecoinvent 3.5 database, the global market average is chosen as the provider. Furthermore, the electricity outputs of each option are adjusted to the functional unit 1 kWh.

7.2.1 Life Cycle Inventory of Simple-Cycle Combustion Turbine Baseline

The simple-cycle combustion turbine scenario is based on the 10 MW_e natural gas electricity production gas turbine from the ecoinvent 3.5 database – "electricity production, natural gas, 10MW | electricity, high voltage | APOS,U - DE". According to Wernet et al. (2016) the module includes fuel input, infrastructure, and emissions to air.

The flowchart of the product system is shown in Figure 35. The electricity production unit requires a continuous flow of natural gas to enable the operation of the plant. The gas turbine construction is also accounted for in the life cycle assessment of the dataset. The gas turbine generates electricity but also causes various emissions that are considered in the current study.

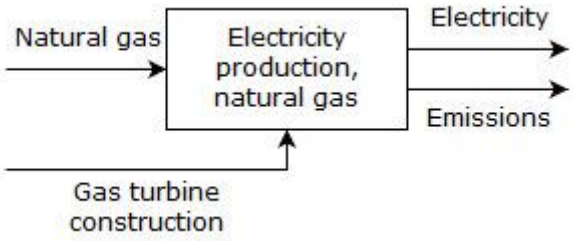

Figure 35 Flowchart of the SCCT set-up

No additional adjustments are required for the chosen dataset. It is already adjusted to the power output of 1 kWh.

7.2.2 Life Cycle Inventory of Proposed Innovative Pumped Hydro System

The proposed, innovative PHES system is modelled in openLCA using a simplified approach. Only the main contributors are acknowledged in the model. These main contributors are assumed to be the concrete and steel used in the construction process of the PHES, as these materials, by far, make up for the largest amount of materials used for the plant. Namely, the concrete and reinforcing steel for the construction of the upper reservoir and the powerhouse are considered, as well as the prestressing steel strands for the upper reservoir, also the steel required for the piping system.

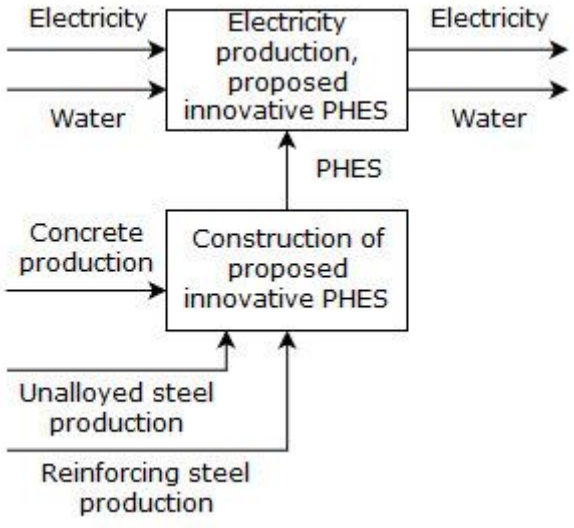

Figure 36 Flowchart of the proposed innovative PHES system set-up

The total quantities of the considered materials can be viewed in Table 14. The ecoinvent 3.5 datasets “market for concrete, 35MPa | concrete, 35MPa | APOS,U”, “market for

reinforcing steel | reinforcing steel | APOS,U" and "market for steel, unalloyed | steel, unalloyed | APOS,U" are used (Wernet et al., 2016). The datasets include the average transportation distances of the materials. All other materials required for the PHES plant, including the production and operation of the electromechanical equipment, are neglected in the current environmental study.

The flow of materials and energy is shown in Figure 36. Electricity is sourced from either the German electricity mix or from wind turbines as described above. The water is taken from a natural water body, passes through the pump-turbine twice and is released back into the water body. The construction of the PHES system is acknowledged as described above.

Table 14 Total quantities of materials for the construction of the proposed PHES system

	Unit	Value
Concrete C35/45	m^3	4,888
Reinforcing steel	kg	827,400
Prestressing steel, unalloyed	kg	897,000
Piping steel, unalloyed	kg	38,180

All data is adjusted to the functional unit 1 kWh of output electricity. Therefore, the efficiency of the proposed PHES system, $\eta_{total} = 74\%$, is considered – as discussed in chapter 6.2.2 – leading to a required input electricity of 1.538 kWh. The total material demand for the PHES construction itself needs to be scaled down to 1 kWh of generated electricity. The 4 MW plant has a lifetime of 50 years, or 70,080 hours if the capacity factor $CF = 0.16$ is considered. If operated for one hour, the plant generates 4000 kWh of energy. That is 4000 times the functional unit 1 kWh. Thus, the total number of 1 kWh-cycles the plant operates in its system lifetime is

$$4000 \cdot 70{,}080h = 280.32 \cdot 10^6.$$

The PHES item, that accounts for the construction of the site, needs to be divided by this total number of cycles to represent the normalized value for the functional unit of 1 kWh.

7.2.3 Life Cycle Inventory of Large-scale Pumped Hydro System

For the large-scale pumped hydro system, a dataset is readily available from the ecoinvent 3.5 database.

The dataset "electricity production, hydro, pumped storage | electricity, high voltage | APOS,U - DE" represents a pumped storage plant in Germany in the year 2012. The dataset is thereby based on 52 reservoir plants in Switzerland. The use of pump energy (high voltage electricity), lubricant oil, water volume that passes through the turbine and the emissions of greenhouse gases from the reservoir are accounted in the dataset (Wernet et al., 2016).

Figure 37 depicts the flow of products and the elementary flows. The plant construction is also regarded in the life cycle assessment of the dataset. The origin of the input electricity depends on the scenario as explained above. Only the emissions from the decomposition of biomass in the reservoir are considered in the dataset.

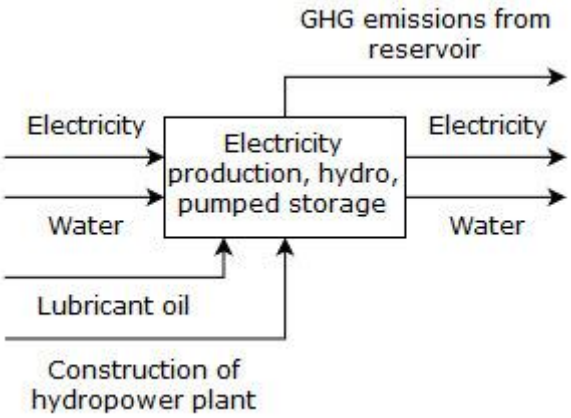

Figure 37 Flowchart of the large-scale pumped hydro set-up

No additional adjustments are required for the chosen dataset. It is already adjusted to the power output of 1 kWh.

7.2.4 Life Cycle Inventory of Lithium Ion Battery Systems

The LCA model for the lithium-ion battery system is also very simple and based on the ecoinvent dataset "market for battery, Li-ion, rechargeable, prismatic | battery, Li-ion, rechargeable, prismatic | APOS,U" and includes the estimated transport distances as well as the battery production, for which the dataset "battery production, Li-ion, rechargeable, prismatic | battery, Li-ion, rechargeable, prismatic | APOS,U" is used (Wernet et al., 2016). This dataset includes the battery pack with 14 single cells, a steel casing, a battery management system and cables. The battery pack is originally intended for the use in electric vehicles. However, it is assumed that it can also be scaled up to stationary use. The actual battery cell production is accounted for by including the dataset "battery cell production, Li-ion | battery cell, Li-ion | APOS,U - RoW" (Wernet et al., 2016).

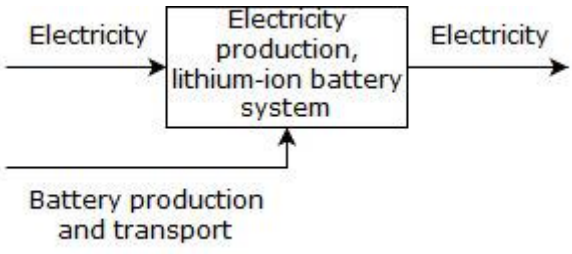

Figure 38 Flowchart of the lithium-ion battery system set-up

The battery has an electricity input from a varying source, depending on the observed scenario described above, and an electricity output. The emissions all relate back to the production phase of the battery pack as well as the transport of the system as shown in Figure 38.

All data for the lithium-ion battery system is adjusted to the functional unit 1 kWh of output electricity. Therefore, the efficiency of the system, $\eta_{total} = 95\%$, is considered – as discussed in chapter 6.2.4 for the 2016 scenario – leading to a required input electricity of 1.053 kWh. Also, the total material demand for the battery production and transport needs

to be scaled down to 1 kWh of generated electricity. One kilogram of the utilized battery pack contains 0.5886 kg of pure battery cells with a specific energy of 0.2 kWh / kg as stated by IRENA (2017, p. 74). Therefore, the energy storage capacity of the battery pack is calculated as 0.1177 kWh. Thus, for the functional unit of 1 kWh, 8.49 kg of the battery pack are required.

However, the environmental burden is distributed equally over the system life. For the 2016 battery system the system lifetime is 2000 cycles as described in chapter 6.2.4. The required battery pack weight needs to be divided by this total number of cycles to represent the normalized value for the functional unit of 1 kWh.

7.2.5 Life Cycle Inventory of Power to Gas to Power Systems

The power to gas to power system is modelled based on a separation into the electrolyzer and the fuel cell. The ecoinvent database 3.5 provides a dataset for the fuel cell, namely "market for fuel cell, stack polymer electrolyte membrane, 2kW electrical, future | fuel cell, stack polymer electrolyte membrane, 2kW electrical, future | APOS,U". The market dataset sources the fuel cells from Switzerland and the rest of the world. The analyzed PEM fuel cells have a power rating of 2 kW electrical and the dataset includes the most important production materials and also accounts for the systems transport.

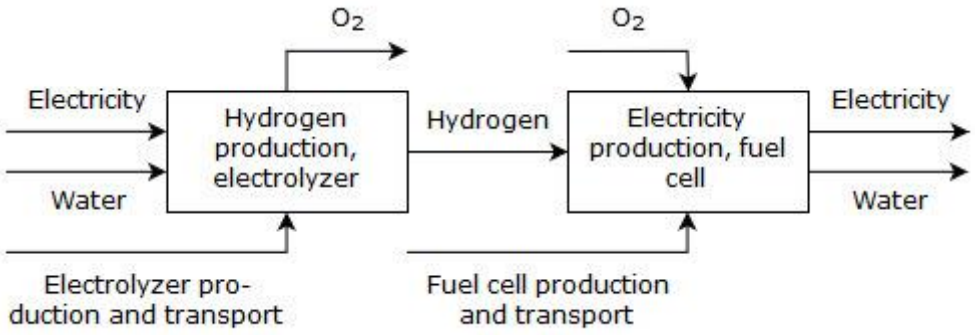

Figure 39 Flowchart of the power to gas to power system set-up

However, the ecoinvent database does not provide a dataset for the electrolysis process. The life cycle inventory is therefore sourced from Maack (2008) and modelled in openLCA using the ecoinvent 3.5 database (Wernet et al., 2016). The inventory for the electrolyzer includes all material and energy flows necessary to produce hydrogen. The output is scaled to 1kg of hydrogen. The following components are considered by Maack (2008): the electrolyzer, a diaphragm compressor, the storage module, walls and foundation, other components and the material and energy flows required for operation. For the current study the output is adjusted from 1kg of hydrogen to one electrolyzer item, accounting for the manufacturing of the electrolyzer.

As described in chapter 2.3.3, the hydrogen production process requires electricity that is sourced from either the German mix or wind turbines – depending on the observed scenario. Furthermore, water is required in the process, splitting it up into hydrogen and oxygen (O_2), as displayed in Figure 39. The electrolyzer production and transportation includes the diaphragm compressor, the storage module, walls and foundation and other components as described previously. The produced hydrogen then reacts with oxygen again to form water

and generate electricity in the fuel cell. The fuel cell production and transportation are also accounted for in the model.

All data for the P2G2P system is adjusted to the functional unit 1 kWh of output electricity. The electricity input into the electrolyzer as well as the hydrogen input into the fuel cell depends on the system efficiencies. The subprocess efficiencies and total power in- and outputs are depicted in Figure 33 in the economic study. The 2020 scenario is considered in the environmental study. The required energy in- and outputs are determined based on this information. The electricity input is calculated as 3.14 kWh after considering the total system efficiency of 31.8%. The hydrogen output from the PEM electrolyzer is 2.22 kWh. The material dataset for the electrolyzer is given per kilogram of produced hydrogen. That equals an energy content of 33.3 kWh according to the lower heating value (IDEALHY, 2019). That is 15 times as much as the required 2.22 kWh. The PEM electrolyzer item therefore needs to be divided by 15 to represent the normalized value for the functional unit of 1 kWh.

The same procedure is applied to the fuel cell. The total material demand for the fuel cell needs to be scaled down to 1 kWh of generated electricity. The fuel cell power output is stated as 2kW and the system has a lifetime of 50,500 cycles as stated in chapter 6.2.5. If operated for one hour, the plant generates 2 kWh of energy. That is twice the functional unit 1 kWh. Thus, the total number of 1 kWh-cycles the plant operates in its system lifetime is

$$2 \cdot 50{,}500h = 101{,}000.$$

The fuel cell item, that accounts for its production, needs to be divided by this total number of cycles to represent the normalized value for the functional unit of 1 kWh.

8 Results and Discussion

The Engineering Design Study reveals that the Dériaz turbine option with four 130 m high upper reservoir tanks has the biggest combined technical and economic potential. This option is now to be compared with the other energy storage technologies that were examined in the previous chapters, as well as the baseline scenario – the simple-cycle combustion turbine plant. The following assessment is divided into the results of the economic feasibility study and the environmental study. Finally, a combined rating is performed.

8.1 Economic Feasibility

Based on the findings in the economic study (chapter 6), the final analysis is performed. The levelized cost of electricity is therefore found for all examined options and the results are discussed. Furthermore, a sensitivity analysis and Monte Carlo simulation are performed in order to account for the uncertainty of the model.

Table 15 LCOE of the examined energy storage technologies

	Technology Case	**LCOE (50th percentile) [€$_{2018}$/MWh]**
#1	SCCT baseline scenario 1 – 94 MW (CF=0.08)	121.33
#2	SCCT baseline scenario 2 – 94 MW (CF=0.16)	95.63
#3	Proposed innovative PHES – 4 MW	150.83
#4	Goudemand residence PHES – 1.5 kW	1580.95
#5	Torre Confinanzas Complex PHES – 30.1 kW	304.42
#6	Wesermühlen PHES – 0.23 MW	720.25
#7	Lithium-ion battery system, 2016 – 1 MW	347.70
#8	Lithium-ion battery system, 2030 – 1 MW	71.99
#9	Power-to-gas-to-power system, 2020 – 1 MW	502.62
#10	Power-to-gas-to-power system, 2030 – 1 MW	370.69
#11	Large-scale PHES – 560 MW	41.74

The final levelized costs of energy from the comparison model are shown in Table 15. They are calculated based on the assumptions and definitions in chapter 3.1 and chapter 6 and represent the 50th percentile of all $LCOE$ values gathered from the Monte Carlo simulation. The results are discussed in the following subchapters.

8.1.1 Sensitivity Analysis

As the $LCOE$ results in Table 15 are strongly based on assumptions and numerous input parameters, it is recommended to analyze the impact of the different inputs on the result. Therefore, a sensitivity analysis is performed, similar to that done by Obi et al. (2017), varying the capacity factor, total efficiency, $CAPEX$, $OPEX$, system lifetime, discount rate,

the natural gas price for the SCCT baseline scenario and the electricity charge price, discharge price and sum of levies for the energy storage technologies. All variables are varied by ±15%. The results of this analysis are described for the particular technologies in the following subchapters.

Table 16 Most sensitive variables determined in sensitivity analysis – ranked in order

SCCT Baseline	PHES Systems	Lithium-Ion Battery Systems	P2G2P Systems
Total Efficiency	Capacity Factor	Capacity Factor	Capacity Factor
Natural Gas Price	CAPEX	System Lifetime	OPEX
Capacity Factor	OPEX	CAPEX	CAPEX
CAPEX	Total Efficiency	Electricity Price Discharge	Total Efficiency
		Total Efficiency	
		Electricity Price Charge	

Table 16 provides an overview over the most sensitive variables of the different technology cases as described below. The variables are ranked from most to least sensitive (up-down).

Simple Cycle Combustion Turbine Baseline Scenario

The LCOE of the SCCT baseline scenario is particularly sensitive to the systems total efficiency and the natural gas price as shown in Figure 40.

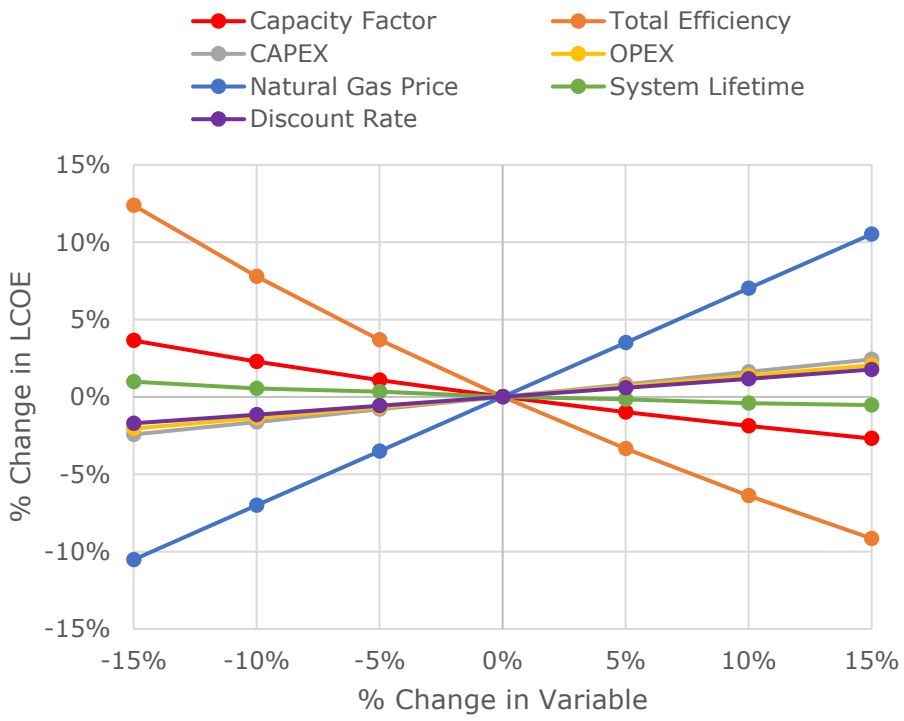

Figure 40 LCOE Sensitivity for SCCT baseline scenario 2

A 15% decrease of the total efficiency results in a 12.4% increase of the LCOE. A 5% change of the natural gas price results in a 3.5% change in the LCOE.

The $CAPEX$ and $OPEX$ have a much smaller impact on the LCOE. This is due to the fact that the operating fuel costs of gas turbines strongly outweigh the initial capital costs. The total efficiency, capacity factor, discount rate and system lifetime show non-linear dependence on the LCOE, while the over variables show linear behavior around the baseline LCOE – as also noticed by Obi et al. (2017).

Pumped Hydro Energy Storage Systems

The $LCOE_{Storage}$ of pumped hydro systems is strongly dependent on the capacity factor and the $CAPEX$ as shown in Figure 41. A 15% decrease of the capacity factor results in a 17.1% increase of the $LCOE_{Storage}$. A 5% change of the $CAPEX$ approximately results in a 5% change in the $LCOE_{Storage}$. Furthermore, the $OPEX$ and the total efficiency have a considerable but much smaller impact than the $CAPEX$ and the capacity factor. The electricity charge and discharge price also have an impact, but the change of the $LCOE_{Storage}$ remains around 5% if these variables are varied by 15%. The same applies to the discount rate. The high dependence on the capacity factor is due to the fact that operating the plant more often does not have a significant effect on the operational costs as the "fuel" of hydropower plants is available for free. However, hydro plants are very capital intensive giving the $CAPEX$ such a strong influence on the $LCOE_{Storage}$.

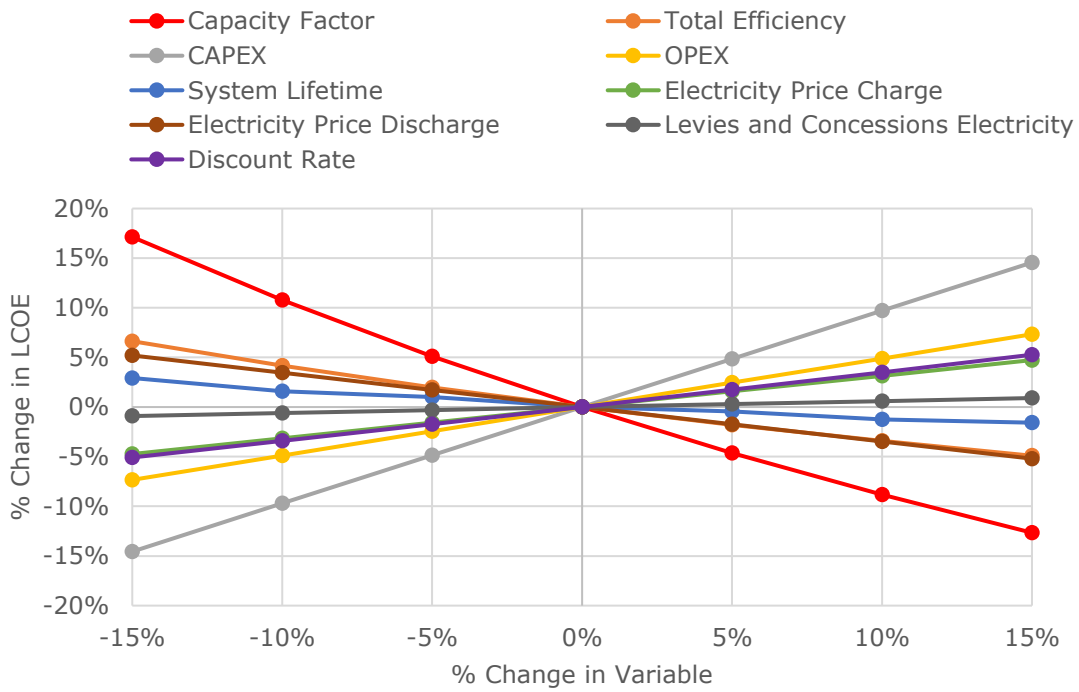

Figure 41 $LCOE_{Storage}$ Sensitivity for proposed innovative PHES system

The electricity prices for charging and discharging as well as the levies and concessions are linear dependent on the $LCOE_{Storage}$. The other variables are as described for the SCCT baseline scenario.

Lithium-Ion Battery Storage Systems

The $LCOE_{Storage}$ changes of lithium-ion battery systems are considerably higher than for PHES systems. Besides the capacity factor and the $CAPEX$, the system lifetime of lithium-ion batteries also has a significant influence on the $LCOE_{Storage}$. A 15% decrease of the capacity factor results in a 20% increase of the $LCOE_{Storage}$, whereas a 15% decrease of the system lifetime will result in an 18% increase of the $LCOE_{Storage}$.

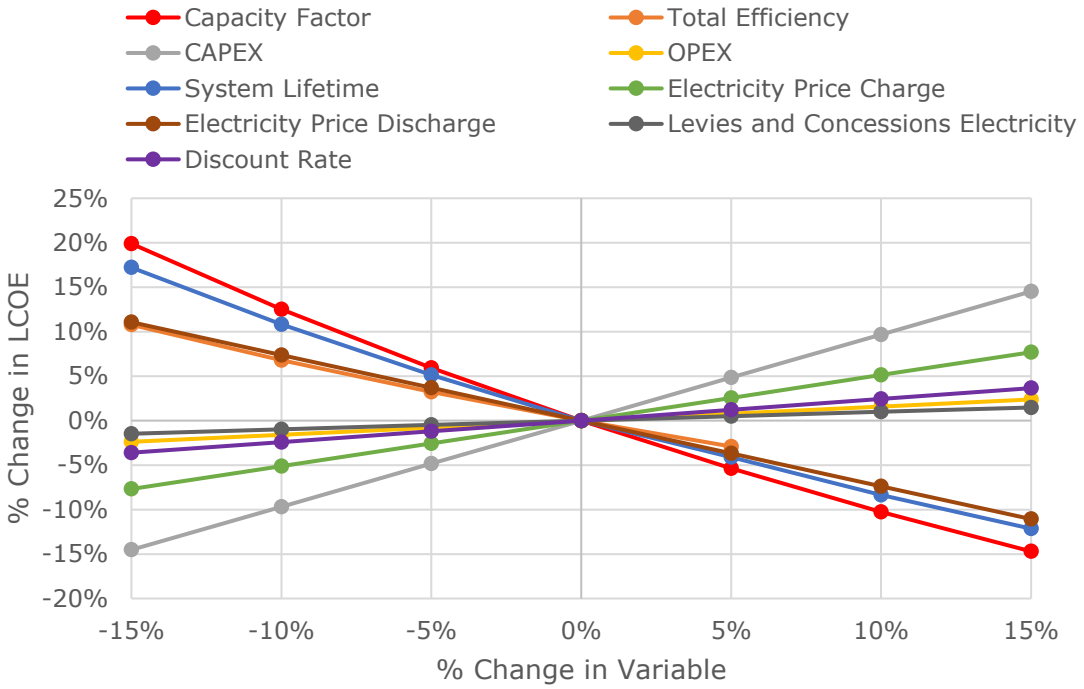

Figure 42 $LCOE_{Storage}$ Sensitivity for lithium-ion battery system in 2030

Again, a 5% change of the $CAPEX$ approximately results in a linear 5% change in the $LCOE_{Storage}$. Furthermore, the electricity price for charging and discharging have a comparably strong influence on the result. The total efficiency of lithium-ion battery is already very high and cannot be higher than 100% which is why an increase of 10% and higher is not possible. Technically, the total efficiency of lithium-ion batteries is very stable as it only depends on very few components.

Power to Gas to Power Systems

The $LCOE_{Storage}$ of power to gas to power systems is particularly sensitive to the capacity factor as shown in Figure 43. A 15% decrease of the capacity factor results in a 15% increase of the $LCOE_{Storage}$. The $OPEX$ has the second largest impact on the systems $LCOE_{Storage}$ which is due to the high operational expenditure compared to the other storage systems. The $CAPEX$ and the total efficiency both change the $LCOE_{Storage}$ by 5% if the variables are varied by 15%. All other variables change the $LCOE_{Storage}$ only slightly.

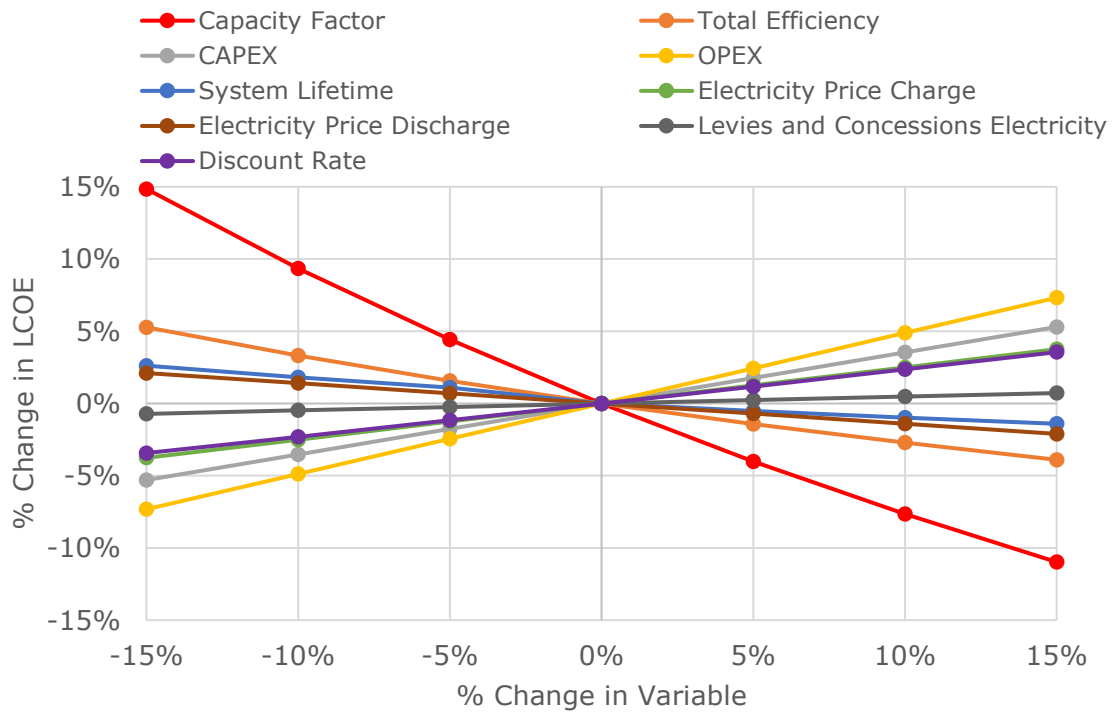

Figure 43 $LCOE_{Storage}$ Sensitivity for power-to-gas-to-power system in 2030

Figure 43 reveals that the P2G2P system is not particularly sensitive to a lot of variables – the capacity factor being an exception.

8.1.2 Monte Carlo Simulation

With the results from the sensitivity analysis at hand, it is possible to determine the uncertainty of the model by applying a variation to the most sensitive parameters, as described by Obi et al. (2017). This is achieved by performing Monte Carlo simulations. Each variable is thereby varied within a standard deviation. The standard deviation for each case is based on the literature as described in the following subchapters. 10,000 trials are performed in order to determine the characteristic uncertainty of each examined scenario.

The results of each examined scenario – including the three case studies for PHES systems in buildings – are shown in Figure 44. Figure 45 shows a closeup of the results for systems with an LCOE below 600€/MWh. For the current analysis, boxplots are chosen to depict the results from the Monte Carlo simulations. According to Galarnyk (2018) boxplots display five characteristic numbers derived from the 10,000 trails of the Monte Carlo simulation: the minimum value, the 25th percentile Q1, the median (or 50th percentile), the 75th percentile Q3 and the maximum value. If the actual minimum value is an outlier, the minimum value is instead defined by $Q1 - 1.5 \cdot IQR$, with the interquartile range (IQR) being $Q3 - Q1$. Also, if the actual maximum value is an outlier, the maximum value is instead defined as $Q3 + 1.5 \cdot IQR$. While the interquartile range is displayed by a box, with its left border representing Q1 and the right border representing Q3, the median is characterized by the line in the center of the box. The minimum and maximum values are represented by whiskers that depict the range of values. Outliers are not depicted in the figure. The results are discussed in the following subchapters for the single scenarios.

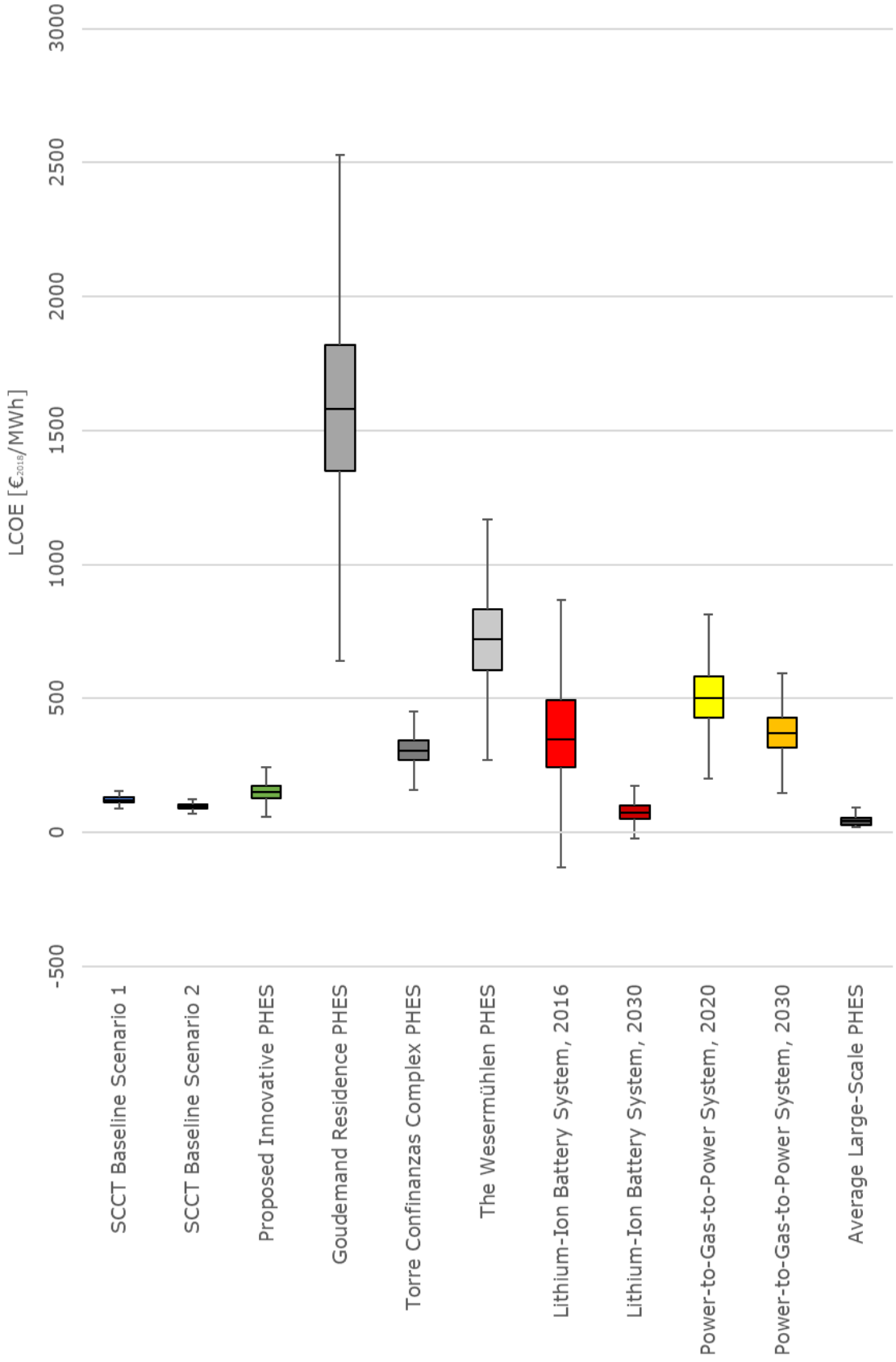

Figure 44 Results from Monte Carlo Simulation for all Scenarios

Simple Cycle Combustion Turbine Baseline Scenario

The capacity factor of the simple-cycle combustion turbine in scenario 1 is set at 0.08 which represents the real-life value determined by NREL (2018). In scenario 2, the SCCT baseline is assumed to have a capacity factor of 0.16 align with the storage technologies – for reasons of better comparison. For the Monte Carlo analysis, the total efficiency, natural gas price and the capital expenditure are subjected to variation for both scenarios. For the total efficiency a standard deviation of 10% around the original value is assumed, representing the efficiency range of modern SCCT plants as described by Boyce (2012). The same standard deviation – 10% around the original value – is assumed for the natural gas price in accordance with the natural gas forecast prices of the next decade as published by The World Bank (2019b). The capital expenditure of SCCT plants is also varied by 10% around the original value as recommended by Obi et al. (2017).

With these assumptions, the median value for the SCCT baseline scenario 1 is found to be 121 €$_{2018}$/MWh. The 25th percentile is 114 €$_{2018}$/MWh and the 75th percentile is found to be 129 €$_{2018}$/MWh. The minimum value is 87 €$_{2018}$/MWh and the maximum value is 178 €$_{2018}$/MWh.

The median value for the SCCT baseline scenario 2 is found to be 96 €$_{2018}$/MWh. The 25th percentile is 89 €$_{2018}$/MWh and the 75th percentile is found to be 102 €$_{2018}$/MWh. The minimum value is 67 €$_{2018}$/MWh and the maximum value is 151 €$_{2018}$/MWh. As expected, the LCOE of scenario 2 is lower of that of scenario 1 because the plant is operated more hours per year.

Generally speaking, the uncertainty of both SCCT baseline scenarios is low and the LCOE within the same range as in the comparison study performed by Obi et al. (2017).

Proposed Innovative PHES

With a set capacity factor of 0.16 – as for all storage technologies in the Monte Carlo simulation – the total efficiency is assumed to have a standard deviation of 10% around the determined value, as proposed by Obi et al. (2017). For the $CAPEX$, a standard deviation of ±22.5% is assumed in accordance with the uncertainty of pre-feasibility studies as described by Giesecke et al. (2014, p. 44). The $OPEX$ is subjected to a standard deviation of 40% as the range of operational expenditures varies a lot for PHES plants, as described by Giesecke et al. (2014, p. 81).

The proposed innovative PHES performs well compared to the baseline scenarios. With the assumptions stated above, the median value for the proposed innovative PHES is found to be 151 €$_{2018}$/MWh. The 25th percentile is 127 €$_{2018}$/MWh and the 75th percentile is found to be 173 €$_{2018}$/MWh. The minimum value is 26 €$_{2018}$/MWh and the maximum value is 302 €$_{2018}$/MWh. The wider range of the results from the Monte Carlo simulation are due to the larger variance of variables and due to the fact that the PHES plant is based on the current pre-feasibility study that is subject to larger uncertainty in terms of project costs. The cost uncertainty for PHES plants can be considered much higher than that for standardized SCCT plants. While SCCT plants can be delivered and set up anywhere with only marginal differences, each PHES system varies strongly. This is reflected in the higher determined uncertainty. However, of all PHES plants in buildings, the innovative PHES plant proposed in the current study stands out positively with a significantly lower LCOE.

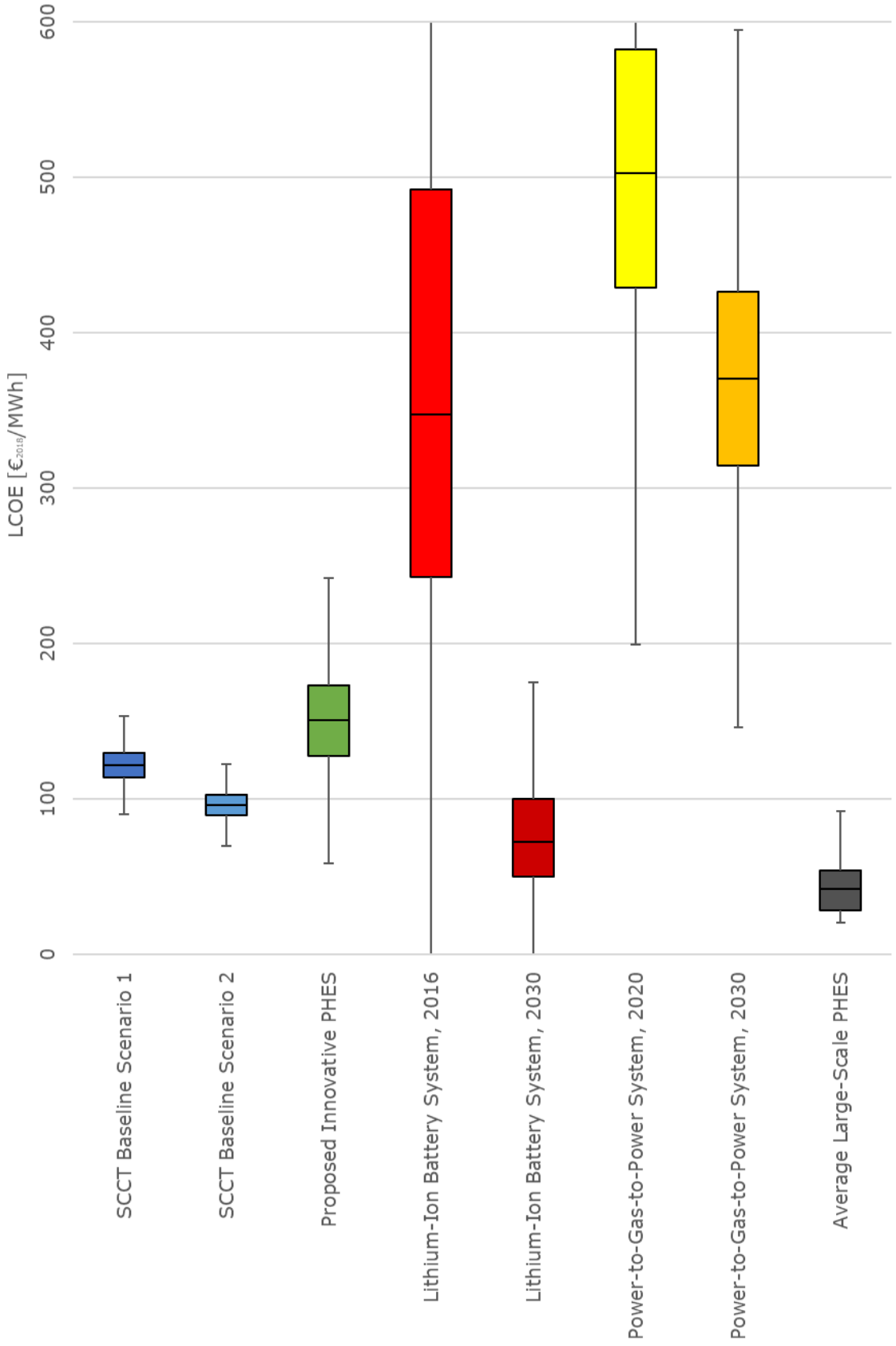

Figure 45 Closeup of results from Monte Carlo Simulation for selected scenarios: For lithium-ion battery systems the whiskers do not fit the graph due to high volatility and low probability extreme events.

PHES in Building Case Studies

Also, the three examined PHES systems in buildings are assessed in the Monte Carlo simulation. They are adapted to a capacity factor of 0.16 and the same assumptions are applied as for the proposed innovative PHES described above. However, they do not perform as well as the proposed PHES system as shown in Figure 44.

Especially the micro-scale PHES system in the Goudemand residence scores a very high LCOE of 1581 €$_{2018}$/MWh (median value). This is the highest LCOE of all examined options. The variation of results is accordingly wide-spread because the standard deviation is given in percent, resulting in a high variation for high values. The 25th percentile for the Goudemand residence is 1347 €$_{2018}$/MWh and the 75th percentile is found to be 1819 €$_{2018}$/MWh. The minimum value is 142 €$_{2018}$/MWh and the maximum value is 2897 €$_{2018}$/MWh. Among the case studies of PHES systems in buildings, the proposed Torre Confinanzas Complex PHES scores best with a median LCOE of 304 €$_{2018}$/MWh. The proposed Wesermühlen PHES system achieves a median LCOE of 720 €$_{2018}$/MWh which is second most expensive compared to the other examined systems.

Lithium-Ion Battery Systems

The lithium-ion battery systems are subject to the strongest variations, compared to the other options – although they are considered to have the same operation schedule as the PHES systems. This is due to the fact that the system lifetime, the $CAPEX$, $OPEX$, as well as the electricity charge and discharge price are subjected to variations in the Monte Carlo simulation. The standard deviation for the system lifetime is set as 35%, and for the capital expenditure a value of 40% is chosen according to the technology variations described by the IRENA (2017, p. 78). The operational expenditures for lithium-ion battery systems are comparatively low and the variation is not expected to be high, which is why 10% is chosen as the standard deviation (U.S. Energy Information Administration, 2019). The efficiency is already close to 100% and no great variation is expected so that the original value is not varied in the simulation. The standard deviations of the electricity charge and discharge prices are defined as 13.5% which is based on historical data provided by the Fraunhofer-Gesellschaft (2019a). These assumptions are valid for both scenarios – the current scenario (2016) and the future scenario (2030).

The results from the Monte Carlo simulation of the 2016 lithium-ion battery system cover a wide range. The median is calculated as 348 €$_{2018}$/MWh which can be considered very high compared to the SCCT baseline scenario. The 25th percentile for the 2016 scenario is 242 €$_{2018}$/MWh and the 75th percentile is found to be 492 €$_{2018}$/MWh. The minimum value is -132 €$_{2018}$/MWh and the maximum value is 374 €$_{2018}$/MWh. The negative minimum value can be considered a side-effect of the high efficiency of the battery storage system. If the high efficiency is combined with a very low electricity charge price and a high electricity discharge price, the system can technically be operated at profit. This, however, is very unlikely as the normal distribution of the LCOE implies.

It is worth noting that the short system lifetime of lithium-ion battery systems has an important influence on the results. A longer lifetime – as it applies to PHES systems – means that the energy storage project has more time to recover its capital expenditure. For lithium-ion batteries this implies that the high investment costs are spread over a very short system lifetime, resulting in a high LCOE$_{Storage}$.

The 2030 lithium-ion battery system shows massive improvements compared to the 2016 system. This is due to the expected technology improvements within the next decade. With a median of 72 €$_{2018}$/MWh the 2030 system is by far less expensive than the baseline scenario and clearly beats the LCOE of the proposed innovative PHES system. Only the average large-scale PHES system remains less expensive than the 2030 lithium-ion battery system. The 25th percentile for the 2030 scenario is 50 €$_{2018}$/MWh and the 75th percentile is found to be 100 €$_{2018}$/MWh. The minimum value is -25 €$_{2018}$/MWh and the maximum value is 75 €$_{2018}$/MWh. The negative minimum value appears for the same reason as described for the 2016 system. Generally, the range of variation is smaller for the 2030 system due to the lower calculated $LCOE_{Storage}$ values.

Power to Gas to Power Systems

For the Monte Carlo analysis, the operational expenditure, total efficiency and the capital expenditure are subjected to variation for both examined scenarios – the current 2020 scenario and the future 2030 scenario. For the operational expenditure and the total efficiency, a standard deviation of 10% each is assumed. The $CAPEX$ of power to gas to power systems is expected to vary strongly, as described by the IEA (2015), justifying a standard deviation of 60% for the capital expenditure.

The LCOE of both power to gas to power scenarios is considerably higher than that of the lithium-ion battery system, the proposed innovative PHES system and the SCCT baseline scenario. Also, the difference between the current P2G2P scenario and the future P2G2P scenario is much smaller than for the lithium-ion system. The median of the 2020 scenario is 503 €$_{2018}$/MWh compared to the median of the 2030 scenario of 371 €$_{2018}$/MWh. Although the decline is considerable in absolute terms, it still does not make the P2G2P technology feasible. The reason for the high LCOE of the P2G2P systems can be found in an extremely low total system efficiency paired with very high capital costs and the highest operational expenditures among all examined options at 5% of the $CAPEX$.

Average Large-Scale PHES

For the assessment of the average large-scale PHES system no Monte Carlo analysis is performed. Instead the values from the single case studies (larger than 10 MW), as described in the economic pre-study, are gathered and analyzed. The median LCOE for the large-scale PHES plants analyzed in the pre-study of this thesis is found to be 42 €$_{2018}$/MWh. The 25th percentile is 28 €$_{2018}$/MWh and the 75th percentile is found to be 54 €$_{2018}$/MWh. The minimum value is 20 €$_{2018}$/MWh and the maximum value is 92 €$_{2018}$/MWh. Figure 45 reveals that the distribution of values is skewed towards the higher LCOE. There seems to be a lower limit that marks the minimum achievable LCOE for PHES plants – no matter the size. As already described in the economic pre-study, the LCOE depends strongly on the capacity of the plant. The range of values that are higher than the 75th percentile likely come from smaller PHES plants. The large-scale PHES plants remain the cheapest option for medium- and long-term power system flexibility – even in 2030 – once again proving the concept of economies of scale.

8.2 Environmental Feasibility

Based on the assumptions in chapter 7, an environmental assessment is performed using the LCA software openLCA version 1.8. The impact categories *climate change impact* as well as *non-renewable exergy resources, fossil*, *non-renewable exergy resources, metals* and *non-renewable exergy resources, minerals* are examined. Thereby, two basic scenarios are considered. In the first scenario, the energy storage systems are assumed to store energy from the German energy mix, and in the second scenario the energy storage system utilizes energy from wind power sources. The results from the first scenario are depicted in Figure 46. The results from the second scenario are shown in Figure 47.

8.2.1 Results for German Electricity Mix Scenario

The first scenario shows some surprising results. It becomes apparent that the SCCT baseline scenario performs very well in comparison with the energy storage technologies that are charged by the German electricity mix. While the SCCT scenario even scores best in the *non-renewable exergy resources, metals* and the *non-renewable exergy resources, minerals* impact categories, it has among the lowest *climate change impact* – only beaten by the lithium-ion battery system. Even though the SCCT process itself operates on natural gas, it is only ranked second highest in the *non-renewable exergy resources, fossil* impact category. It is outranked by the P2G2P system. The reason for the good rank in the *climate change impact* category is that SCCT plants only burn natural gas which causes lower greenhouse gas emissions than coal- and lignite-fired power plants. The latter make up for a large proportion of the German electricity mix in 2014 causing PHES plants and P2G2P plants to be responsible for higher greenhouse gas emissions than the SCCT baseline scenario. SCCT plants are much less resource-intensive in terms of minerals and metals, which is reflected in the according resource depletion impact categories. SCCT plants can be considered a competitive choice for the first scenario from an environmental viewpoint.

The four energy storage technologies show a relatively consistent behavior in all four impact categories. It must be noted, that the largest share of environmental burden in the impact categories *climate change impact* and *non-renewable exergy resources, fossil* for all four technologies can be allocated to the use of the German electricity mix with its high share of power from coal and lignite combustion. The P2G2P system thereby stands out, having the highest environmental burden in all four examined impact categories. The reason for this can be considered the extremely low efficiency of such facilities compared with the other storage technologies. Having a low efficiency results in a high need of input energy from the German electricity grid. The opposite applies to the lithium-ion battery system. Its high efficiency makes it rank best in the impact categories *climate change impact* and *non-renewable exergy resources, fossil*. In the *non-renewable exergy resources, metals* impact category, however, lithium-ion battery systems prove very resource-intensive compared to PHES systems.

The examined PHES systems have surprisingly similar results. In all four impact categories the environmental impact of the proposed innovative PHES system is only slightly higher than the average large-scale PHES system. This makes perfect sense, as the large-scale system profits from economies of scale, decreasing the systems impact per kWh. For the *non-renewable exergy resources, metals* category this difference is slightly higher which is most likely due to the high requirement of prestressing steel for the proposed PHES system.

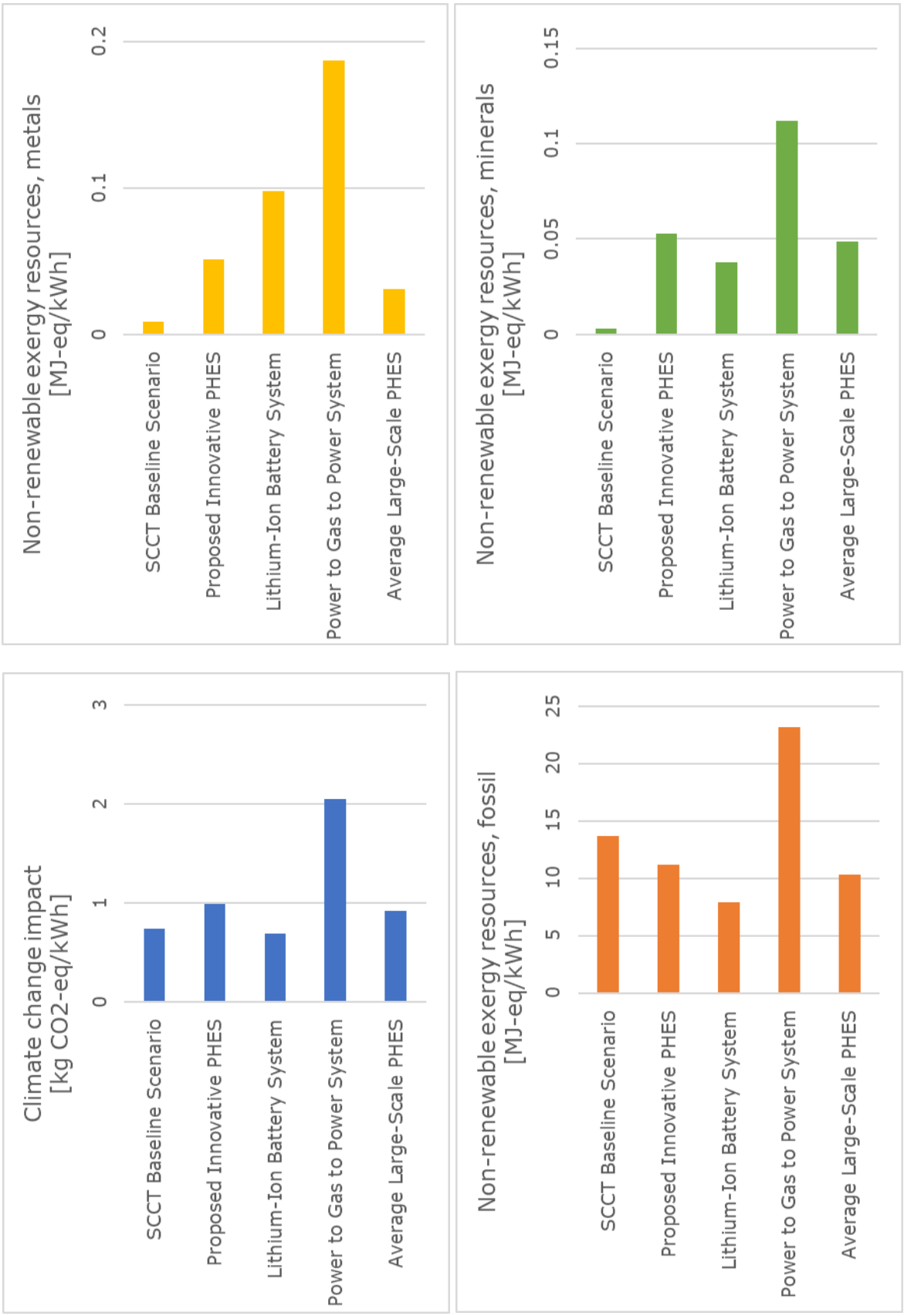

Figure 46 Results from the environmental assessment of the energy storage options, charged by the German electricity mix, and the SCCT baseline scenario

The higher need of minerals for the reservoir construction is reflected in the *non-renewable exergy resources, minerals* category. In this category, the PHES systems outweigh the lithium-ion battery system. Among the three small-scale storage systems, the lithium-ion battery can be considered to have the lowest environmental impact, with only one exception: the metal resource depletion impact of lithium-ion systems is considerably higher than for the other technologies. The numerical results for the German electricity mix scenario can be viewed in Appendix XIV.

8.2.2 Results for Onshore Wind Turbines Scenario

A significant difference can be observed in the second scenario. While all four storage technologies have a much smaller environmental impact in the categories *climate change impact*, *non-renewable exergy resources, fossil*, and *non-renewable exergy resources, minerals*, the depletion of *non-renewable exergy resources, metals* increases slightly for all four storage systems. This difference can be explained by the nature of wind turbines that now provide the charging electricity for the storage systems. During the operation of these wind turbines, no carbon emissions are produced, and no fossil resources are depleted – neglecting lubricating oil. Also, less minerals are required for the construction of wind turbines compared to the other generating technologies that provide electricity to the power grid. However, the metal requirements for building wind turbines can be considered slightly higher per kWh than for conventional plants, explaining the higher resource depletion of metals.

Again, the power to gas to power energy storage technology, by far, has the highest environmental impact in all four categories. As described before, this can be explained by the low efficiency of the system, but also by the material requirements of the technology itself. In contrast to the first scenario, the lithium-ion battery system scores less well compared to the proposed innovative solution. This proves that the very high efficiency of lithium-ion systems has an especially positive effect compared to the other storage systems when the charging electricity comes from the mainly fossil-fired German electricity mix. If wind energy is utilized to charge the system, the system efficiency plays a much smaller role for the *climate change impact* and the *non-renewable exergy resources, fossil* impact. This is why the proposed innovative PHES plant scores better than the lithium-ion battery system in these categories. Again, the large-scale PHES plant scores slightly lower than the proposed innovative PHES facility in all categories. And again, for the *non-renewable exergy resources, metals* category this difference is slightly higher which is due to the high requirement of prestressing steel for the proposed PHES system.

In the second scenario, the large-scale PHES plant scores the overall best results, with one exception: the *non-renewable exergy resources, minerals* impact of the large-scale PHES system is slightly higher than that of lithium-ion battery systems. Among the small-scale systems, the proposed innovative PHES system scores the best. Only in the *non-renewable exergy resources, minerals* it has a marginally higher impact than the lithium-ion battery system. However, this marginal difference is outweighed by the considerably larger *non-renewable exergy resources, metals* depletion of the lithium-ion system compared to the proposed innovative PHES system.

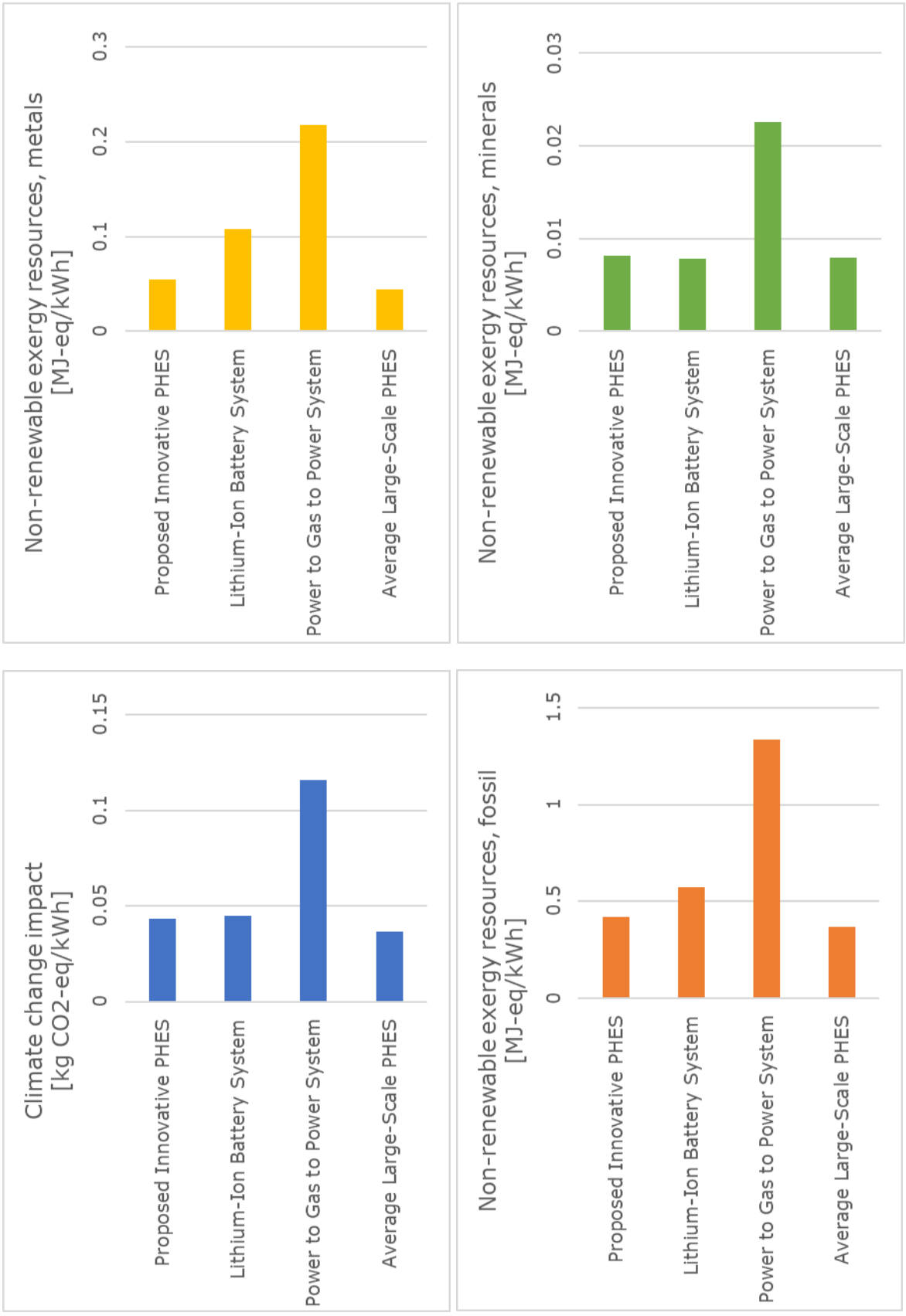

Figure 47 Results from the environmental assessment of the energy storage options, charged by electricity from onshore wind turbines

8.3 Combined Feasibility

The proposed innovative PHES system, developed in the engineering design study in chapter 5, scores overall good results in the combined technical, economic and environmental analysis of the different storage systems. In terms of $LCOE_{Storage}$ it achieves much better results than all other examined small-scale PHES systems in buildings, but also beats the current lithium-ion battery system and the current and future scenario of the P2G2P system. However, its median $LCOE_{Storage}$ is considerably higher than that of the SCCT baseline scenario rendering it unfeasible under the current legislation and market conditions. Nevertheless, the Monte Carlo analysis detects an uncertainty range that could potentially allow the proposed PHES system to lie within the same range as the baseline scenarios. The proposed innovative PHES option therefore remains an interesting solution that should not be excluded from further assessments.

Considering the expected technical improvements by 2030, the only serious small-scale storage competitor for the proposed PHES system is the future lithium-ion battery system. This storage option scores an even better $LCOE_{Storage}$ than both SCCT baseline scenarios. If the expected improvements can be realized, small-scale PHES systems will no longer be economically feasible. The cheaper battery storage options will be chosen instead. Large-scale pumped hydro systems, however, are expected to remain the cheapest power system flexibility option – even in 2030. The economies of scale remain the dominating factor for energy storage systems.

The combination of economic and environmental results confirms that P2G2P systems are not a feasible option for medium-term power to power storage systems. Neither the current systems, nor the anticipated future systems have good scores in terms of $LCOE_{Storage}$. In all four impact categories and both examined scenarios of the environmental study, the power to gas to power system by far scored the worst results. The main reason is considered to be the lowest efficiency among the examined options.

The environmental feasibility of storage systems vs the SCCT baseline scenario varies strongly depending on the source of charging electricity. If the German electricity mix is used, the *climate change impact* and the *non-renewable exergy resources, fossil* impact of the storage systems lies within a similar range. For this first scenario, lithium-ion battery systems can be considered to have the lowest environmental impact of all examined storage systems. The only exception is the resource depletion of metals, where lithium-ion systems score much higher than the SCCT baseline scenario and the assessed PHES systems. For the *climate change impact*, the *non-renewable exergy resources, fossil* depletion and the *non-renewable exergy resources, minerals* depletion, lithium-ion systems show the best results in the comparison.

In scenario two of the environmental assessment, power from wind turbines is used to charge the storage systems. The result is an overall much lower *climate change impact*, *non-renewable exergy resources, fossil* impact and *non-renewable exergy resources, minerals* impact of the storage systems compared to the SCCT baseline. When the charging power comes from renewable sources, system efficiencies have a smaller effect on the environmental impact. Therefore, the proposed innovative PHES system scores better than the lithium-ion battery in three out of four examined impact categories. The only exception

is the resource depletion of minerals, where PHES systems score marginally higher than the lithium-ion system.

It becomes apparent that lithium-ion battery systems and the proposed innovative PHES system are close competitors in the current analysis. If realized today, and when the charging electricity comes from wind power sources, the proposed innovative PHES system is in favor. If, however, the anticipated future progress of the lithium-ion technology is considered and power from charging comes from the German electricity mix, the lithium-ion battery makes the race.

9 Conclusions

The German Energiewende will require great efforts and a blend of different technologies and policies to be successful. The increasing demand for energy system flexibility is among the largest challenges. The growing share of power from variable renewable energy sources asks for technical solutions that allow their integration into the energy system – because supply and demand of electrical power must always be in balance. An important strategy to achieve this requirement is the implementation of energy storage utilities. Energy storage systems store excess energy from the grid when renewables supply more than consumers demand, and feed back into the grid when the demand is high, and supply is low. Among all energy storage systems, PHES plants are the oldest and most mature technology. At a large-scale they have already been implemented over 100 years ago. The aim of the current study is to systematically implement a small-scale PHES design that can be integrated into the urban built environment in a way that is technically, economically and environmentally feasible.

The first research question focuses on the smallest feasible size of small-scale PHES systems: How small can a pumped hydro system be while remaining economically feasible? – The economic pre-study reveals that the smallest feasible size of a PHES power plant lies in the single figure MW-range – representing a major challenge for a small-scale facility that is supposed to be integrated into a building system. 4 MW is identified as the power capacity that is large enough to operate at similar costs as the simple-cycle combustion turbine baseline scenario.

The second research question focuses on the technical implementation of a PHES system in a building: How can an economically feasible pumped hydro energy storage system be implemented in the urban built environment? – Despite the challenge, the product innovation approach is applied to find a suitable design that fulfills the technical and economic requirements. The assessment of existing technical solutions and analogies leads to the following basic concept: a set of four large water towers with a total height of 130m and a tank radius of 8.3m each. The basic idea is that these water towers are utilized as basic construction elements which can be integrated into a buildings structure while also taking structural loads from the building. These structural synergies could potentially reduce overall construction costs and increase the economic viability of the PHES system. Notwithstanding, the embodiment and detail design were not part of the current thesis. The results gained from this study only act as a proof of concept and require further developments. Among the open questions are: Which method should be applied to construct the concrete towers? Which particular prestressing method should be applied to absorb the weight of the stored water? A more detailed technical design study would also include the analysis of wind and seismic loads on the structure. Besides, the choice of the pump-turbine system should be analyzed in more detail due to the simplifications that have been made in the current study. Also, the effect of the large head-variation on the pump-turbine system, due to the upper reservoir, needs to be further examined. A sophisticated frequency control system is likely to be required for such a system.

The third research question addresses the economic and environmental feasibility of the proposed system: How does the proposed PHES plant in the urban built environment compare to other PHES systems, lithium-ion battery systems and power to gas to power (P2G2P) systems in terms of economic and environmental feasibility? – The economic analysis finds that the proposed innovative PHES system has a median $LCOE_{Storage}$ of ~150 €$_{2018}$/MWh. Although this value lies above the SCCT baseline scenario at ~120 €$_{2018}$/MWh, the uncertainty of the pre-feasibility study allows for an optimistic view on this result. Besides, a higher price on CO_2-emissions could drastically shift the results of the SCCT baseline scenario in favor of the small-scale PHES system. Currently, the ETS system in Europe sells CO_2 emission allowances at below 30 €/tonCO_2 (Markets Insider, 2019). This price, however, is expected to increase in the years to come. Also, it is worth mentioning that system-relevant SCCT power plants receive subsidies from the German government for their important power system flexibility services. It is very likely that such required system flexibility services will be rewarded in the future electricity grid, potentially rendering the proposed innovative PHES system feasible within the years to come.

As a matter of fact, the proposed PHES system has a much lower levelized cost of electricity storage than all other small-scale systems that are retrospectively integrated into buildings. Power to gas to power systems are not at all suitable for medium-term power to power applications, neither currently nor in 2030. Current lithium-ion battery systems are still expensive today but can become potential future competitors of small-scale PHES systems. In fact, the anticipated progress of the lithium-ion technology puts great pressure on the proposed innovative PHES system. However, the assessment has shown that large-scale PHES systems remain the cheapest option to store bulk energy for medium to long-term. And although these systems require a lot more space than the proposed innovative PHES plant, the environmental impact in terms of climate change impact and resource depletion impact per kWh remains slightly lower.

An important difference has been found between the two scenarios that were assessed in the environmental impact study. If the German electricity mix is considered as the source of charging electricity, energy storage technologies do not bring great advantages from an environmental viewpoint. If, however, the charging electricity comes from renewable sources, energy storage systems score very well despite their low efficiencies. In the future electricity mix with a 100% share of renewable energy, the proposed PHES plant shows an overall low environmental impact compared to P2G2P systems and is comparable with lithium-ion systems.

In conclusion, the current study reveals that the proposed innovative PHES system has considerable potential, even though strong competition comes from the lithium-ion battery system with its anticipated future developments. It is likely that the battery industry will find ways to reduce or eliminate harmful or rare substances from their lithium-ion battery production. For pumped hydro systems, however, no future improvements are expected. For the proposed PHES system to remain a competitive option in 2030, all examined synergies need to be further analyzed for their cost saving potential. Besides, any additional natural elevation differences between upper and lower reservoir will easily increase the feasibility of the proposed PHES system. As of today, the legal framework around energy storage systems in Germany can be considered counterproductive with regards to system flexibility. Energy storage plants are considered electricity end consumers, obliging the operators to pay the according fees which often leads to an unprofitable operation of the utilities. A better regulation and unbureaucratic exemption from levies and concessions, but also the rapid

adoption of a carbon price covering all energy sectors, and the introduction of a rewards-scheme for the provision of grid services are required to promote energy storage technologies that could soon be the backbone of the German power system flexibility strategy.

References

Abdon, A., Zhang, X. J., Parra, D., Patel, M. K., Bauer, C., & Worlitschek, J. (2017). Techno-economic and environmental assessment of stationary electricity storage technologies for different time scales. *Energy, 139*, 1173-1187. doi:10.1016/j.energy.2017.07.097

Agarwal, S., Tanger, K., Linich, D., Madsen, J., Nicholson, A., & Martin, L. (2012). Enhancing the value of life cycle assessment. Retrieved from https://www2.deloitte.com/us/en/pages/operations/articles/enhancing-the-value-of-life-cycle-assessment.html

AllgäuStrom. (2019). Multitalent Pumpspeicherkraftwerk, Planung für das Allgäu. Retrieved from https://www.allgaeustrom.de/energie-zukunft/multitalent-pumpspeicherkraftwerk-planung-fuer-das-allgaeu/

Alzohbi, G. (2018). The cost of electromechanical equipment in a small hydro power storage plant. *Journal of Energy Systems, 2*(4), 238-259. doi:10.30521/jes.457288

American Petroleum Institute. (2012). API 650: Welded Steel Tanks for Oil Storage. In (Vol. API Standard 650). Washington, D.C.

Aneke, M., & Wang, M. H. (2016). Energy storage technologies and real life applications - A state of the art review. *Applied Energy, 179*, 350-377. doi:10.1016/j.apenergy.2016.06.097

Ardizzon, G., Cavazzini, G., & Pavesi, G. (2014). A new generation of small hydro and pumped-hydro power plants: Advances and future challenges. *Renewable & Sustainable Energy Reviews, 31*, 746-761. doi:10.1016/j.rser.2013.12.043

Atrill, P., & McLaney, E. J. (2014). *Accounting and finance for non-specialists* (Ninth Edition. ed.). New York: Pearson.

Atrill, P., & McLaney, E. J. (2017). *Accounting and finance for non-specialists* (Tenth edition. ed.). Harlow, England ; New York: Pearson.

Barbir, F. (2005). PEM electrolysis for production of hydrogen from renewable energy sources. *Solar Energy, 78*(5), 661-669. doi:https://doi.org/10.1016/j.solener.2004.09.003

Barry, D. (2018). Kidston Renewable Energy Hub fast tracked Retrieved 24. July 2019, from North Queensland Register https://www.northqueenslandregister.com.au/story/5676629/kidston-renewable-energy-hub-fast-tracked/

BDEW. (2016). Energieverbände fordern faire Wettbewerbsbedingungen für Energiespeicher [Press release]. Retrieved from

https://www.bdew.de/presse/presseinformationen/energieverbande-fordern-faire-wettbewerbsbedingungen-fur-energiespeicher/

BDEW. (2019). *BDEW-Strompreisanalyse Januar 2019 Haushalte und Industrie*. Retrieved from Berlin: https://www.bdew.de/energie/strom-und-gaspreisanalysen-januar-2019/

Berk, J. B., & DeMarzo, P. M. (2011). *Corporate finance* (2nd ed.). Boston, MA: Prentice Hall.

Birkhofer, H., & Kloberdanz, H. (2017). *Produktinnovation*. Technische Universität Darmstadt. Darmstadt.

Bond, A. J., Brooker, O., Harris, A. J., Harrison, T., Moss, R. M., Narayanan, R. S., & Webster, R. (2006). *How to design concrete structures using Eurocode 2*. Camberley: The Concrete Centre.

Bösch, M. E., Hellweg, S., Huijbregts, M. A. J., & Frischknecht, R. (2006). Applying cumulative exergy demand (CExD) indicators to the ecoinvent database. *The International Journal of Life Cycle Assessment, 12*(3), 181. doi:10.1065/lca2006.11.282

Boyce, M. P. (2012). *Gas turbine engineering handbook* (4th ed.). Amsterdam ; Boston: Elsevier/Butterworth-Heinemann.

Breeze, P. A. (2005). *Power generation technologies*. Oxford: Newnes.

AfA-Tabelle für den Wirtschaftszweig "Energie- und Wasserversorgung", BStBl I 1995, 144 C.F.R. (1995).

Bundesnetzagentur. (2019). Market data visuals. Retrieved 20. August 2019 https://www.smard.de/en/marktdaten/5542?marketDataAttributes=%7B%22resolution%22:%22hour%22,%22from%22:1535925600000,%22to%22:1536529500000,%22moduleIds%22:%5B1001225,1004067,1004068,5000410%5D,%22selectedCategory%22:null,%22activeChart%22:true,%22style%22:%22color%22,%22region%22:%22DE%22%7D

Cavazzini, G., Santolin, A., Pavesi, G., & Ardizzon, G. (2016). Accurate estimation model for small and micro hydropower plants costs in hybrid energy systems modelling. *Energy, 103*, 746-757. doi:https://doi.org/10.1016/j.energy.2016.03.024

CEMEX. (2018). Preisliste Transportbeton, Spezialbaustoffe und Betonförderung. Retrieved 26. July 2019 https://www.cemex.de/produkte/beton/preislisten

Chen, A. (2018). Elon Musk wants cobalt out of his batteries — here's why that's a challenge. Retrieved 06. August 2019, from Vox Media https://www.theverge.com/2018/6/21/17488626/elon-musk-cobalt-electric-vehicle-battery-science

DAB Water Technology. (2015). Centrifugal Pumps Technical Catalogue. In.

de Oliveira E Silva, G., & Hendrick, P. (2016). Pumped hydro energy storage in buildings. *Applied Energy, 179*, 1242-1250. doi:10.1016/j.apenergy.2016.07.046

dena. (2010). *Kurzanalyse der Kraftwerksplanung in Deutschland bis 2020 (Aktualisierung). Annahmen, Ergebnisse und Schlussfolgerungen*. Retrieved from Berlin: https://www.dena.de/fileadmin/dena/Dokumente/Pdf/9108_Studie_Kurzanalyse_der_Kraftwerksplanung_in_D_bis_2020.pdf

Dennerlein, B. (2018). Definition: Absetzung für Abnutzung (AfA). Retrieved from https://wirtschaftslexikon.gabler.de/definition/absetzung-fuer-abnutzung-afa-27877/version-251519

Deutsche Welle. (2019). Germany to stop using coal by end of 2038. Retrieved from https://p.dw.com/p/3CETE

DN Tanks. (2019). How we build dependability into every tank. Retrieved 13. July 2019 https://www.dntanks.com/resources/brochures/

Dörr, H., Kröger, K., Köppel, W., Burmeister, F., Senner, J., Nitschke-Kowsky, P., . . . F., G. (2016). Untersuchungen zur Einspeisung von Wasserstoff in ein Erdgasnetz. *Energie-, Wasser-Praxis*(11), 50-59.

Entega AG. (2019). Spitzenlast-Gasturbine - Gasturbinenkraftwerk in Darmstadt. Retrieved 20. August 2019 https://www.entega.ag/geschaeftsfelder/erzeugung/konventionelle-energien/spitzenlast-gasturbine/

EPEXSPOT. (2018). Market Data - Day-Ahead Auction. Retrieved 18. January 2019, from epexspot https://www.epexspot.com/en/market-data/dayaheadauction

European Central Bank. (2019). ECB euro reference exchange rate: US dollar (USD). Retrieved 23. July 2019, from European Central Bank https://www.ecb.europa.eu/stats/policy_and_exchange_rates/euro_reference_exchange_rates/html/eurofxref-graph-usd.en.html

European Commission Joint Research Centre Institute for Environment and Sustainability. (2012). *Characterisation factors of the ILCD Recommended Life Cycle Impact Assessment methods. Database and supporting information*. Luxembourg: Publications Office of the European Union.

European Committee for Standardization. (2000). Prestressing steels - Part 3: Strand. In (Vol. prEN 10138-3:2000). Brussels: European Committee for Standardization.

European Committee for Standardization. (2002). Metallic industrial piping - Part 3: Design and calculation. In (Vol. EN 13480-3:2002 (E)). Brussels: European Committee for Standardization,.

European Committee for Standardization. (2004). Eurocode 2: Design of concrete structures - Part 1-1: General rules and rules for buildings. In (Vol. EN 1992-1-1:2004 (E)). Brussels: European Committee for Standardization,.

European Committee for Standardization. (2006a). Eurocode 1 - Actions on structures - Part 4: Silos and tanks. In (Vol. EN 1991-4:2006 (E)). Brussels: European Committee for Standardization.

European Committee for Standardization. (2006b). Eurocode 2 - Design of concrete structures - Part 3: Liquid retaining and containment structures. In (Vol. EN 1992-3:2006 (E)). Brussels: European Committee for Standardization,.

European Committee for Standardization. (2007). Eurocode 3 - Design of steel structures - Part 4-2: Tanks. In (Vol. EN 1993-4-2: 2007 (E)). Brussels: European Committee for Standardization.

European Union. (2019). VAT rules and rates. Retrieved 27. July 2019 https://europa.eu/youreurope/business/taxation/vat/vat-rules-rates/index_en.htm

Färber, R. (2016). Gaildorf Windstrom aus dem Wasserspeicher. *Schwäbisches Tagblatt*. Retrieved from https://www.tagblatt.de/Nachrichten/Windstrom-aus-dem-Wasserspeicher-307583.html

Fichtner. (2014). *Erstellung eines Entwicklungskonzeptes Energiespeicher in Niedersachsen*. Retrieved from Stuttgart: https://docplayer.org/5174810-Erstellung-eines-entwicklungskonzeptes-energiespeicher-in-niedersachsen.html

Fonseca, J. A., & Schlueter, A. (2013). Novel approach for decentralized energy supply and energy storage of tall buildings in Latin America based on renewable energy sources: Case study - Informal vertical community Torre David, Caracas - Venezuela. *Energy, 53*, 93-105. doi:10.1016/j.energy.2013.02.019

Franco Podio, Gilfredo Cavagnolo, & Cipriano, E. M. (2012). Simplified Method for Estimating the Cost of Plant Equipment. *Hydro Review, 20*(6).

Frankel, T. C. (2016, 30. September 2016). The cobalt pipeline: Tracing the path from deadly hand-dug mines in Congo to consumers' phones and laptops. *The Washington Post*. Retrieved from https://www.washingtonpost.com/graphics/business/batteries/congo-cobalt-mining-for-lithium-ion-battery/?

Fraunhofer-Gesellschaft. (2019a). Energy Charts: Jährliche Börsenstrompreise in Deutschland. Retrieved 23. August 2019, from Fraunhofer-Institut für Solare Energiesysteme ISE https://www.energy-charts.de/price_avg_de.htm?year=2019&price=nominal&period=annual

Fraunhofer-Gesellschaft. (2019b). Energy Charts: Jährlicher Anteil erneuerbarer Energien an der Stromerzeugung in Deutschland. Retrieved 20. August 2019, from Fraunhofer-Institut für Solare Energiesysteme ISE https://energy-charts.de/ren_share_de.htm?year=all&source=ren-share&period=annual

Galarnyk, M. (2018). Understanding Boxplots. Retrieved 23. August 2019, from Medium - Towards Data Science https://towardsdatascience.com/understanding-boxplots-5e2df7bcbd51

Geßner, S., Niedermeier, R., Ahrens, M. A., Hegger, J., Fischer, O., & Mark, P. (2017). I Spannbetonbau - Entwicklung, Bemessung und Konstruktion. In *Beton-Kalender 2017: Spannbeton, Spezialbetone*: Ernst & Sohn GmbH & Co. KG.

GFA. (2013). Pumpspeicherkraftwerk Lägerdorf vorerst auf Eis. Retrieved 24. July 2019, from Gesellschaft zur Förderung der Abwassertechnik e.V. http://www.gfa-news.de/webcode.html?wc=20130410_001

Giesecke, J. r., Heimerl, S., & Mosonyi, E. (2014). *Wasserkraftanlagen Planung, Bau und Betrieb* (6., aktualisierte und erw. Aufl. ed.).

Godina, R., Rodrigues, E., Matias, J., & Catalão, J. (2015). *Sustainable energy system of El Hierro Island*.

Gridflex Energy. (2019). Projects. Retrieved from http://gridflexenergy.com/projects/

Grosschädl Stahl. (2019). Lagerpreisliste. Retrieved 27. July 2019, from Franz Großschädl Stahlgroßhandel GesmbH https://www.grosschaedl.at/wp-content/uploads/2018/09/Lagerpreisliste-Betonstahl.pdf

Guise, D. (1991). *Design and technology in architecture* (Rev. ed.). New York: Van Nostrand Reinhold.

Heimerl, S., & Kohler, B. (2017). Aktueller Stand der Pumpspeicherkraftwerke in Deutschland. *WasserWirtschaft, 10 | 2017*.

Hischier, R., Weidema, B., Althaus, H.-J., Bauer, C., Doka, G., Dones, R., . . . Nemecek, T. (2010). *Implementation of Life Cycle Impact Assessment Methods. ecoinvent report No. 3, v2.2*. Dübendorf: Swiss Centre for Life Cycle Inventories.

HSE. (2010). HSE investiert 55 Millionen Euro in Darmstadt [Press release]. Retrieved from https://web.archive.org/web/20141221114308/http://www.hse.ag/presse/pressemeldungen/meldung/detail/11-06-2010-hse-investiert-55-millionen-euro-in-darmstadt.html

Hülsmann, S., Harby, A., & Taylor, R. (2015). The Need for Water as Energy Storage for Better Integration of Renewables. Policy Brief # 01/2015. Retrieved from https://www.hydropower.org/policy-brief-the-need-for-water-as-energy-storage-for-better-integration-of-renewables

IDEALHY. (2019). Liquid Hydrogen Outline Why liquefy hydrogen? Why IDEALHY? Retrieved 03. August 2019 https://www.idealhy.eu/index.php?page=lh2_outline

IEA. (2015). Technology Roadmap Hydrogen and Fuel Cells. Retrieved 30. July 2019, from International Energy Agency https://webstore.iea.org/technology-roadmap-hydrogen-and-fuel-cells

IEA. (2018). Status of Power System Transformation 2018 - Advanced Power Plant Flexibility. Retrieved 20. August 2019, from International Energy Agency https://webstore.iea.org/status-of-power-system-transformation-2018

illwerke vkw. (2019). Obervermuntwerk II. Retrieved 24. July 2019, from illwerke vkw AG https://www.illwerkevkw.at/obervermuntwerk-ii.htm

IRENA. (2012). Renewable Energy Technologies: Cost Analysis Series - Hydropower. *1: Power Sector*(3/5).

IRENA. (2017). *Electricity Storage and Renewables: Costs and Markets to 2030*. Retrieved from Abu Dhabi: https://www.irena.org/publications/2017/Oct/Electricity-storage-and-renewables-costs-and-markets

IUB Engineering Ltd. (2013). Refurbishment of Niederwartha Pumped Storage Power Plant Dresden/Germany. Retrieved 24. July 2019 https://www.engineering-group.ch/references/projekte/detail/refurbishment-of-niederwartha-pumped-storage-power-plant-dresden-germany.html

Janjanin, M., & Schumann, P. (2016). Pumpspeicher-Projekt zu den Akten gelegt. *Südwest Presse*. Retrieved from https://www.swp.de/suedwesten/landkreise/alb-donau/pumpspeicher-projekt-zu-den-akten-gelegt-22913617.html

Jücker Stahlhandel. (2019). Preis- / Lagerliste. Retrieved 27. July 2019, from Jücker GmbH & Co. Stahlhandels KG https://stahlhandel-juecker.de/preislisten/

Jülch, V. (2016). Comparison of electricity storage options using levelized cost of storage (LCOS) method. *Applied Energy, 183*, 1594-1606. doi:10.1016/j.apenergy.2016.08.165

Kaczynski, J. r. (1994). *Stauanlagen, Wasserkraftanlagen* (2., überarb. Aufl. ed.).

Karlo. (2007). Wassersilo Tübingen. In Wassersilo_Tuebingen.jpg (Ed.). https://de.wikipedia.org/wiki/Wassersilo_T%C3%BCbingen.

Katsaprakakis, D. A., Christakis, D. G., Pavlopoylos, K., Stamataki, S., Dimitrelou, I., Stefanakis, I., & Spanos, P. (2012). Introduction of a wind powered pumped storage system in the isolated insular power system of Karpathos–Kasos. *Applied Energy*, *97*, 38-48. doi:https://doi.org/10.1016/j.apenergy.2011.11.069

KPMG. (2018). *Cost of Capital Study 2018*. Retrieved from https://home.kpmg/de/en/home/insights/2018/10/kapitalkostenstudie-2018.html

KPMG. (2019). Corporate tax rates table. Retrieved from https://home.kpmg.com/xx/en/home/services/tax/tax-tools-and-resources/tax-rates-online/corporate-tax-rates-table.html

Krein, J. (2011). *Gasturbinenkraftwerk Darmstadt*. Retrieved from Darmstadt:

Kusakana, K. (2015). Feasibility analysis of river off-grid hydrokinetic systems with pumped hydro storage in rural applications. *Energy Conversion and Management, 96*, 352-362. doi:https://doi.org/10.1016/j.enconman.2015.02.089

Levine, J. G., & Barnes, F. S. (2011). *Large energy storage systems handbook*. Boca Raton: CRC Press.

Liebherr. (2017). Höchste Windkraftanlagen der Welt: Max Bögl baut mit Liebherr-Mobilkran modernen Energiespeicher. Retrieved from https://www.liebherr.com/de/deu/aktuelles/news-pressemitteilungen/detail/h%C3%B6chste-windkraftanlagen-der-welt-max-b%C3%B6gl-baut-mit-liebherr-mobilkran-modernen-energiespeicher.html

Maack, M. (2008). *Generation, of the energy carrier HYDROGEN In context with electricity buffering generation through fuel cells*. Retrieved from http://www.needs-project.org/

Manolakos, D., Papadakis, G., Papantonis, D., & Kyritsis, S. (2004). A stand-alone photovoltaic power system for remote villages using pumped water energy storage. *Energy, 29*(1), 57-69. doi:10.1016/j.energy.2003.08.008

Markets Insider. (2019). CO2 European Emission Allowances - Price Commodity. Retrieved 17.09.2019 https://markets.businessinsider.com/commodities/co2-european-emission-allowances

Matthews, J. S., Major (1969). Westcoast Building under construction - 1333 West Georgia Street. In f27df9f2-da39-4702-ba6a-eee91cfdddf4-A25260.jpg (Ed.).

Max Bögl Wind AG. (2019a). Gaildorf als Vorreiter für Stromspeicher. Retrieved from https://www.mbrenewables.com/pilotprojekt-gaildorf/

Max Bögl Wind AG. (2019b). Naturstromspeicher. Retrieved from https://www.naturspeicher.de/de/naturstromspeicher.php

Merritt, F. S., & Ambrose, J. E. (1990). *Building engineering and systems design* (2nd ed.). New York: Van Nostrand Reinhold.

Mitanis, M. (2017). The Rich and Variegated History of The Qube. Retrieved from https://vancouver.skyrisecities.com/news/2017/06/rich-and-variegated-history-qube

Mohammed, H. J. (2011). Economical Design of Water Concrete Tanks. *European Journal of Scientific Research, 49*(4), 510-520.

Moles, P., Parrino, R., & Kidwell, D. S. (2011). *Corporate finance* (European ed. ed.). Chichester: Wiley.

Morabito, A., de Oliveira e Silva, G., & Hendrick, P. (2019). Deriaz pump-turbine for pumped hydro energy storage and micro applications. *Journal of Energy Storage, 24*, 100788. doi:https://doi.org/10.1016/j.est.2019.100788

Morabito, A., & Hendrick, P. (2019). Pump as turbine applied to micro energy storage and smart water grids: A case study. *Applied Energy, 241*, 567-579. doi:https://doi.org/10.1016/j.apenergy.2019.03.018

Mutschmann, J., Stimmelmayr, F., & Fritsch, P. (2011). *Taschenbuch der Wasserversorgung* (15., vollst. überarb. und aktualisierte Aufl. ed.).

Nevada Hydro. (2019). Lake Elsinore Advanced Pumped Storage - Power from nature. Retrieved from http://leapshydro.com/

NREL. (2018). Annual Technology Baseline - Natural Gas Plants. Retrieved 23. July 2019, from NREL - national renewable energy labatory of the U.S. Department of Energy https://atb.nrel.gov/electricity/2018/index.html?t=cg

Obi, M., Jensen, S. M., Ferris, J. B., & Bass, R. B. (2017). Calculation of levelized costs of electricity for various electrical energy storage systems. *Renewable & Sustainable Energy Reviews, 67*, 908-920. doi:10.1016/j.rser.2016.09.043

OECD. (2019a). Inflation forecast (indicator) (Publication no. 10.1787/598f4aa4-en). Retrieved 15 January 2019

OECD. (2019b). Producer price indices (PPI) (indicator) (Publication no. 10.1787/a24f6fa9-en). Retrieved 22. July 2019 https://data.oecd.org/price/producer-price-indices-ppi.htm#indicator-chart

Oliveira, L., Messagie, M., Mertens, J., Laget, H., Coosemans, T., & Van Mierlo, J. (2015). Environmental performance of electricity storage systems for grid applications, a life cycle approach. *Energy Conversion and Management, 101*, 326-335. doi:https://doi.org/10.1016/j.enconman.2015.05.063

Orchard, B., & Klos, S. (2009). Pumps as turbines for water industry. *World Pumps, 2009*(8), 22-23. doi:https://doi.org/10.1016/S0262-1762(09)70283-4

Organic power International SL. (2013). MAREX Delivery of predictable, clean, base load electricity from Wind Power in Mayo to supply 1.5% of total UK annual power demand. In. Palma de Mallorca Islas Baleares, Spain.

Pahl, G., Beitz, W., Blessing, L. n., Feldhusen, J. r., Grote, K.-H., & Wallace, K. (2007). *Engineering Design A Systematic Approach*. In. Retrieved from http://scans.hebis.de/HEBCGI/show.pl?19410312_toc.html

Papula, L. (2017). *Mathematische Formelsammlung für Ingenieure und Naturwissenschaftler* (12., überarbeitete Auflage ed.). Wiesbaden: Springer Vieweg.

Patel, S. (2013). Spain Inaugurates 2-GW Pumped Storage Facility. *POWER Magazine*.

Perlan. (2019). About Perlan. Retrieved from https://perlan.is/about-perlan/

POWER Engineering. (2011). Alstom to supply a 207 MW turbine to Salamonde pumped storage plant in Portugal. Retrieved 24. July 2019 https://www.power-eng.com/articles/2011/06/alstom-to-supply-a.html

Rehman, S., Al-Hadhrami, L. M., & Alam, M. M. (2015). Pumped hydro energy storage system: A technological review. *Renewable and Sustainable Energy Reviews, 44*, 586-598. doi:https://doi.org/10.1016/j.rser.2014.12.040

Rufer, A. (2018). *Energy Storage Systems and Components*. Boca Raton: Taylor & Francis Group.

Sabihuddin, S., Kiprakis, A., & Mueller, M. (2015). A Numerical and Graphical Review of Energy Storage Technologies. *Energies, 8*, 172-216. doi:10.3390/en8010172

Sadik, O. (2019). Ergebnisse der Kohlekommission: Interview mit Greenpeace-Geschäftsführer Martin Kaiser - Kohleausstieg ist beschlossen. Retrieved 24. August 2019, from Greenpeace e. V. https://www.greenpeace.de/themen/klimawandel/kohleausstieg-ist-beschlossen

Salzgitter Mannesmann Stahlhandel. (2015). Lieferprogramm für Stahlrohre. In.

Sandia National Laboratories. (2019). DOE Global Energy Storage Database. Retrieved 20. March 2019, from U.S. Department of Energy https://www.energystorageexchange.org/projects

Schmidt, O., Gambhir, A., Staffell, I., Hawkes, A., Nelson, J., & Few, S. (2017). Future cost and performance of water electrolysis: An expert elicitation study. *International Journal of Hydrogen Energy, 42*(52), 30470-30492. doi:https://doi.org/10.1016/j.ijhydene.2017.10.045

Schulze, J. (2017). Energiespeicherung als Nutzungsperspektive für leerstehende Bauwerke? : Eine typologische und fallbezogene Untersuchung am Beispiel des Industrie- und Militärbaus. In. Darmstadt.

Statistisches Bundesamt. (2018). Produzierendes Gewerbe - Kostenstruktur der Unternehmen im Baugewerbe. Retrieved 27. July 2019, from Statistisches Bundesamt (Destatis) https://www.destatis.de/GPStatistik/receive/DEHeft_heft_00083509

Statistisches Bundesamt. (2019a). Erzeugerpreisindex gewerblicher Produkte Retrieved 22. July 2019, from Statistisches Bundesamt (Destatis) https://www.destatis.de/DE/Themen/Wirtschaft/Preise/Erzeugerpreisindex-gewerbliche-Produkte/_inhalt.html

Statistisches Bundesamt. (2019b). Preise - Kaufwerte für Bauland. Retrieved 27. July 2019, from Statistisches Bundesamt (Destatis) https://www.destatis.de/DE/Themen/Wirtschaft/Preise/Baupreise-Immobilienpreisindex/Publikationen/Downloads-Bau-und-Immobilienpreisindex/kaufwerte-bauland-vj-2170500183244.pdf?__blob=publicationFile&v=2

Steinwender, T. (2016). Rellswerk power station – Vorarlberger Illwerke AG. *World of PORR - Information for pros*.

Sterner, M., & Stadler, I. (2017). *Energiespeicher Bedarf, Technologien, Integration* (2 ed.).

Sugawara, H., Narita, K., & Sik Kim, M. (2019). COOLING EFFECT BY URBAN RIVER.

Ter-Gazarian, A. (2011). *Energy Storage for Power Systems* (2nd ed. ed.). London: Institution of Engineering and Technology.

The European Commission. (2016a). Investment Project EIPP-20160047 - Hydro Pump Storage in Greece – Amfilochia. Retrieved 24. July 2019, from The European Commission https://ec.europa.eu/eipp/desktop/en/projects/project-32.html

The European Commission. (2016b). Investment Project EIPP-20160049 - Amari Hybrid Energy Project at Crete. Retrieved 24. July 2019 https://ec.europa.eu/eipp/desktop/en/projects/project-33.html

The World Bank. (2019a). Pumped Storage Technical Assistance Project. Retrieved 24. July 2019, from The World Bank http://projects.worldbank.org/P112158/upper-cisokan-pumped-storage-hydro-electrical-power-1040-mw-project?lang=en&tab=overview

The World Bank. (2019b). World Bank Commodities Price Data (The Pink Sheet). Retrieved 23. July 2019, from The World Bank https://www.worldbank.org/en/research/commodity-markets

Tisue, S. (2008). Knights of Columbus Headquarters. In Knights_of_Columbus_headquarters.jpg (Ed.).

TPF. (2019). Project - Foz Tua Hydroelectric. Retrieved 24. July 2019, from TPF S.A. https://tpf.eu/projects/foz-tua-hydroelectric/

Tsiropoulos, I., Tarvydas, D., & Lebedeva, N. (2018). *Li-ion batteries for mobility and stationary storage applications Scenarios for costs and market growth* (978-92-79-97254-6). Retrieved from Luxembourg:

U.S. Energy Information Administration. (2013). *Updated Capital Cost Estimates for Utility Scale Electricity Generating Plants*. Retrieved from Washington, DC: https://www.eia.gov/outlooks/capitalcost/

U.S. Energy Information Administration. (2019). Cost and Performance Characteristics of New Generating Technologies, Annual Energy Outlook 2019. Retrieved 30. July 2019, from U.S. Energy Information Administration https://www.eia.gov/outlooks/aeo/assumptions/pdf/table_8.2.pdf

Vattenfall. (2019). Niederwartha. Retrieved 24. July 2019, from Vattenfall AB https://powerplants.vattenfall.com/en/niederwartha

Wahlquist, C. (2018). South Australia's Tesla battery on track to make back a third of cost in a year *The Guardian*. Retrieved from

https://www.theguardian.com/technology/2018/sep/27/south-australias-tesla-battery-on-track-to-make-back-a-third-of-cost-in-a-year

Wang, G., Wang, D., Trenberth, K. E., Erfanian, A., Yu, M., Bosilovich, Michael G., & Parr, D. T. (2017). The peak structure and future changes of the relationships between extreme precipitation and temperature. *Nature Climate Change, 7*, 268. doi:10.1038/nclimate3239

Wassersilo Tübingen. (n.d., 21. December 2018). Retrieved from https://de.wikipedia.org/w/index.php?title=Wassersilo_T%C3%BCbingen&oldid=183895956

WaterWorld. (2004). Largest Steel Water Tank In U.S. Gets New Coat Of Paint. Retrieved from https://www.waterworld.com/articles/print/volume-20/issue-10/epa-action/largest-steel-water-tank-in-us-gets-new-coat-of-paint.html

Wecker, K. (2019). Germany's atomic phaseout: How to dismantle a nuclear power plant. Retrieved from https://p.dw.com/p/3Ef94

Wernet, G., Bauer, C., Steubing, B., Reinhard, J., Moreno-Ruiz, E., & Weidema, B. (2016). The ecoinvent database version 3 (part I): overview and methodology. *The International Journal of Life Cycle Assessment, 21*(9), 1218-1230. doi:10.1007/s11367-016-1087-8

What's On. (2019). A Visit to Perlan - Wonders of Iceland. In perlan-utanfr-res.jpg (Ed.). https://www.whatson.is/perlan-wonders-of-iceland/.

Wight, J. K., Richart, F. E., & MacGregor, J. G. (2012). *Reinforced concrete : mechanics and design* (6th ed.). Upper Saddle River, N.J.: PEARSON PRENTICE HALL.

Appendix

Appendix I Operation principle of lithium-ion batteries

Lithium-ion liquid electrolyte batteries are electrochemical storage systems that utilize the electrochemical potential difference between two electrodes. The liquid electrolyte can freely pass through a separator between the positive and negative electrode and thereby exchanges positively charged lithium-ions (Li+). While the lithium-ions pass through the separator, the electrons break lose and are channeled through a cable connection providing useful electrical current for appliances. The positive electrode – or cathode – usually consists of a lithium metal oxide, whereas the negative electrode – or anode – is usually made of graphite (IRENA, 2017). Figure 48 depicts the operation principle for a liquid electrolyte lithium-ion battery as just described.

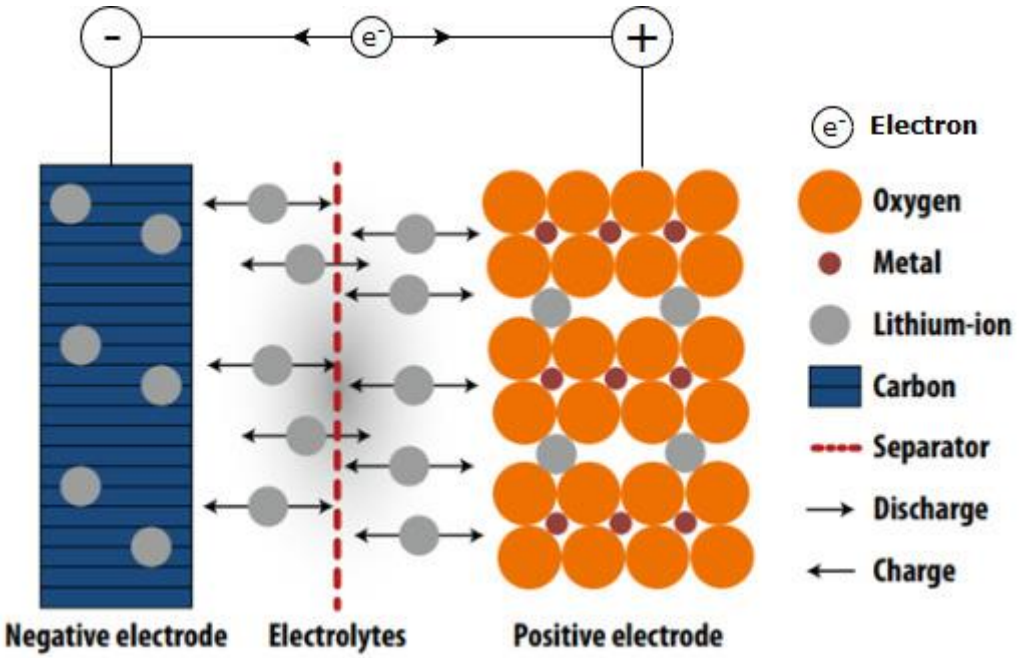

Figure 48 Schematic operation principle and main components of a lithium-ion cell with lithium metal oxide cathode and graphite anode. Adapted from IRENA (2017, p. 64).

Many different cell chemistries are available for the lithium-ion battery technology, providing different properties and advantages. The current study focuses on the Nickel-manganese-cobalt (NMC) chemistry in combination with the lithium manganese oxide (LMO) chemistry. According to IRENA (2017), "a blend of NMC and LMO cells [is often applied in combined systems, and] provides a balance between performance and cost" (p. 66). The NMC/LMO cell chemistry blend is expected to make good progress within the next decade.

The transformation process can be viewed in Figure 8.

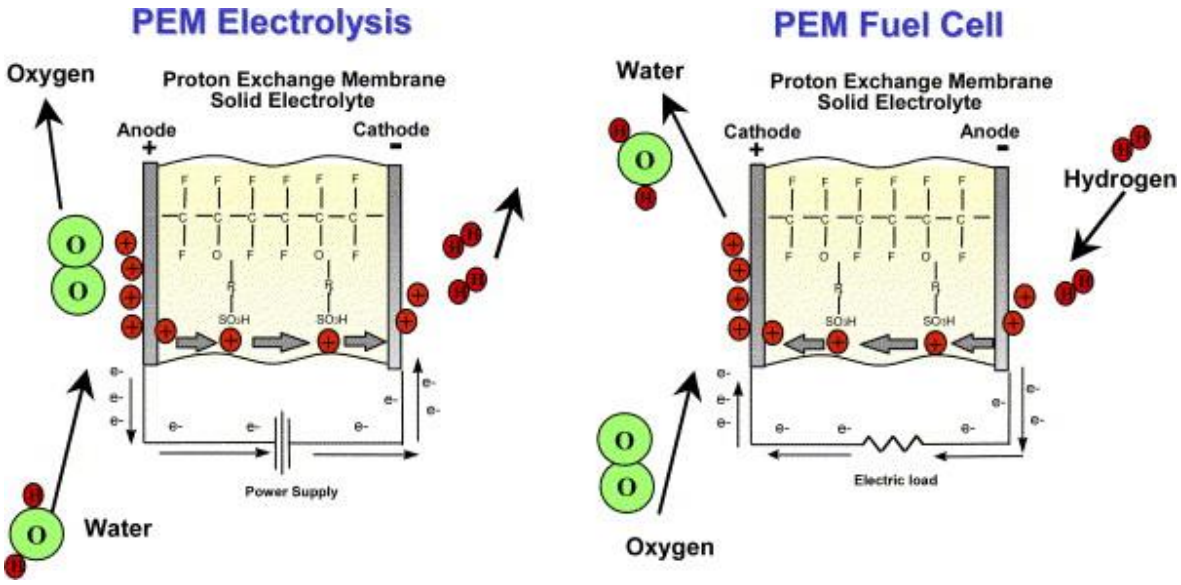

Figure 49 Schematic operation principle of PEM electrolysis and fuel cell processes. Reprinted from Barbir (2005, p. 662).

The electrolysis and fuel cell processes in the current study are based on the polymer electrolyte membrane technology described by Barbir (2005). The schematic operation principle of both processes can be viewed in Figure 49. The electrolysis process requires water and a DC voltage. After applying a high enough voltage, water is split into its components: oxygen, protons and electrons on the anode. While the oxygen is released into the environment, the protons pass through the polymer electrolyte membrane and the electrons flow through the cable connection to form hydrogen with the protons on the cathode on the other side of the membrane. The fuel cell applies the reverse principle: hydrogen is split up into protons and electrons on the anode. The electrons flow through the current connection and provide useful power while the protons flow through the polymer electrolyte membrane to connect with oxygen on the cathode. Water is a by-product of the fuel cell process.

Appendix III Detailed requirements list

Háskóli Íslands – University of Iceland Faculty of Industrial Engineering, Mechanical Engineering and Computer Science	**Requirements list** **for** ***- Pumped Hydro Energy Storage in Urban Built Environment -***	Master's thesis in Environment and Natural Resources Advisors: Halldór Pálsson, Hafþór Ægir Sigurjónsson, Bjarni Bessason, Daði Sverrisson **Semester** Spring 2019

Organizational Data		Process Data		Value – Data			
Number	Date of change	Type	**Requirements**	Minimum Demand	Target Demand	Ideal Demand	Unit
			Motor-generator				
R01	14.04.19	D	Power output		4		MW
R02	14.04.19	D	Efficiency	95	96	100	%
			Lower reservoir				
R03	14.04.19	D	Low cost	20	15	10	% of CAPEX
R04	14.04.19	D	Water intake area assessable and easy to maintain				
R05	14.04.19	D	Protection against intake of foreign objects (size)	0.5	0.2	0.2	mm
			Tailrace				
R06	14.04.19	D	Corrosion prevention measures for permanent exposure to water				
			Pump-turbine				
R07	14.04.19	D	Corrosion prevention measures for permanent exposure to water				
R08	14.04.19	D	Cavitation prevention measures				
R09	14.04.19	W	Efficiency (major importance)	80	85	93	%
			Penstock				
R10	14.04.19	D	Corrosion prevention measures for permanent exposure to water				
			Upper reservoir				
R11	14.04.19	D	Water intake area assessable and easy to maintain				
R12	14.04.19	D	Protection against intake of foreign objects (size)	0.5	0.2	0.2	mm
R13	14.04.19	D	Overpumping protection				
R14	14.04.19	D	Energy stored	8	12	16	MWh

Type of demand: D-demand to be met under all circumstances; W-wish that should be taken into consideration

Replaces edition from -		**Version: 2 15.04.2019**
Editor: Stuart James		**Page 1 of 2**

Háskóli Íslands – University of Iceland Faculty of Industrial Engineering, Mechanical Engineering and Computer Science Stuart Daniel James	**Requirements list** **for** ***- Pumped Hydro Energy Storage in Urban Built Environment -***	Master's thesis in Environment and Natural Resources Advisors: Halldór Pálsson, Hafþór Ægir Sigurjónsson, Bjarni Bessason, Daði Sverrisson **Semester** Spring 2019

Organizational Data		Process Data		Value – Data			
Number	Date of change	Type	**Requirements**	Minimum Demand	Target Demand	Ideal Demand	Unit
			Surge tank				
R15	14.04.19	D	Only if required				
R16	14.04.19	D	Corrosion prevention measures for permanent exposure to water				
			Overall requirements				
R17	14.04.19	D	Suitable design for implementation in the urban built environment				
R18	14.04.19	D	System roundtrip efficiency	35	60	80	%
R19	14.04.19	D	Levelized cost of electricity storage	130	115	40	€/MWh
R20	14.04.19	D	Duration of one cycle at maximum power output	4	4	4	h
R21	14.04.19	W	Availability factor (medium importance)	80	90	95	%
R22	15.04.19	W	Area requirement for storage system (major importance)	2500	2000	1000	m^2
R23	15.04.19	W	Find synergies with other systems (major importance)				
R24	15.04.19	W	Total capital expenses (major importance)		9 million		€
R25	15.04.19	D	Maintainability				
R26	15.04.19	D	System lifetime	40	50	100	years
R27	15.04.19	D	Compliance with water regulations				
R28	15.04.19	D	Appealing architectural design				

Type of demand: D-demand to be met under all circumstances; W-wish that should be taken into consideration

Replaces edition from -		**Version: 2 15.04.2019** **Page 2 of 2**
Editor: SJ		

Appendix IV Quality Function Deployment – "House of Quality"

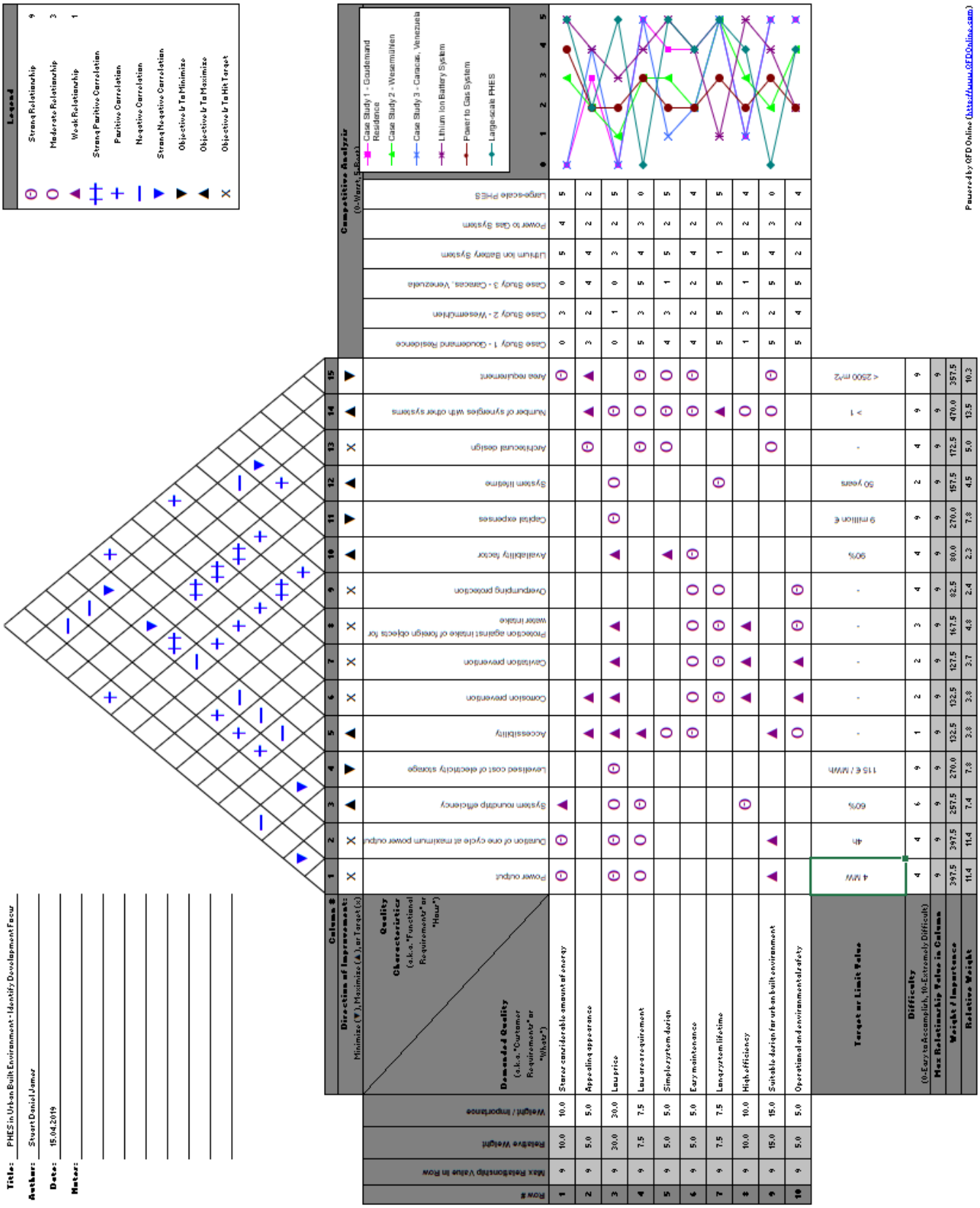

Appendix V Size of the upper reservoir tank for one single tank

Tank height z [m]	Effective hydrostatic head h_{eff} [m]	Required volume V [m^3]	Tank radius r [m]
10	10	794,528	159.0
20	15	529,685	91.8
30	20	397,264	64.9
40	25	317,811	50.3
50	30	264,843	41.1
60	35	227,008	34.7
70	40	198,632	30.1
80	45	176,562	26.5
90	50	158,906	23.7
100	55	144,460	21.4
110	60	132,421	19.6
120	65	122,235	18.0
130	70	113,504	16.7

Appendix VI Size of a single upper reservoir tank for two tanks in total

Tank height z [m]	Effective hydrostatic head h_{eff} [m]	Required volume V [m^3]	Tank radius r [m]
10	10	397,264	112.5
20	15	264,843	64.9
30	20	198,632	45.9
40	25	158,906	35.6
50	30	132,421	29.0
60	35	113,504	24.5
70	40	99,316	21.3
80	45	88,281	18.7
90	50	79,453	16.8
100	55	72,230	15.2
110	60	66,211	13.8
120	65	61,118	12.7
130	70	56,752	11.8

Appendix VII Size of a single upper reservoir tank for four tanks in total

Tank height z [m]	Effective hydrostatic head h_{eff} [m]	Required volume V [m^3]	Tank radius r [m]
10	10	198,632	79.5
20	15	132,421	45.9
30	20	99,316	32.5
40	25	79,453	25.1
50	30	66,211	20.5
60	35	56,752	17.4
70	40	49,658	15.0
80	45	44,140	13.3
90	50	39,726	11.9
100	55	36,115	10.7
110	60	33,105	9.8
120	65	30,559	9.0
130	70	28,376	8.3

Appendix VIII Size of a single upper reservoir tank for eight tanks in total

Tank height z [m]	Effective hydrostatic head h_{eff} [m]	Required volume V [m^3]	Tank radius r [m]
10	10	99,316	56.2
20	15	66,211	32.5
30	20	49,658	23.0
40	25	39,726	17.8
50	30	33,105	14.5
60	35	28,376	12.3
70	40	24,829	10.6
80	45	22,070	9.4
90	50	19,863	8.4
100	55	18,057	7.6
110	60	16,553	6.9
120	65	15,279	6.4
130	70	14,188	5.9

Appendix IX Simulated costs for electromechanical equipment

Tank height z [m]	Simulated cost Kaplan EM equipment [€2018]	Simulated cost Dériaz EM equipment [€2018]	Simulated cost PaT EM equipment [€2018]
10	784,943	847,904	1,481,791
20	545,483	824,311	1,379,210
30	444,046	808,779	1,322,528
40	390,202	797,692	1,283,730
50	357,665	789,443	1,254,422
60	336,267	783,173	1,230,973
70	321,330	778,372	1,211,489
80	310,430	774,708	1,194,861
90	302,199	771,954	1,180,383
100	295,813	769,948	1,167,581
110	290,745	768,570	1,156,120
120	286,650	767,728	1,145,755
130	283,290	767,350	1,136,302
150	278,144	767,769	1,119,597
200	270,546	773,984	1,086,752
250	266,594	785,418	1,061,941
300	264,301	800,536	1,042,089
350	262,877	818,467	1,025,595
400	261,954	838,658	1,011,519
450	261,338	860,734	999,262
500	260,922	884,427	988,425

Appendix X Total CAPEX for single core over the tank height variation

Tank height z [m]	Tank radius r [m]	CAPEX Kaplan, single core [€2018]	CAPEX Dériaz, single core [€2018]
10	159.0	47,950,028	50,934,273
20	91.8	21,967,517	24,111,780
30	64.9	15,728,420	17,479,733
40	50.3	13,298,699	14,822,042
50	41.1	12,211,674	13,585,901
60	34.7	11,586,583	12,855,579
70	30.1	11,247,740	12,438,515
80	26.5	11,040,106	12,170,527
90	23.7	10,908,386	11,990,927
100	21.4	10,836,686	11,880,428
110	19.6	10,779,984	11,791,767
120	18.0	10,760,671	11,745,787
130	16.7	10,735,874	11,698,517
150	14.5	10,718,883	11,646,128
200	11.0	10,765,173	11,639,400
250	8.8	10,842,896	11,692,855
300	7.4	10,925,718	11,767,490
350	6.3	11,018,390	11,862,208
400	5.6	11,099,384	11,952,351
450	4.9	11,179,537	12,046,907
500	4.5	11,272,545	12,158,391

Appendix XI Total CAPEX for two cores over the tank height variation

Tank height z [m]	Tank radius r [m]	CAPEX Kaplan, two cores [€2018]	CAPEX Dériaz, two cores [€2018]
10	112.5	49,805,202	52,789,447
20	64.9	22,749,475	24,893,739
30	45.9	16,143,100	17,894,413
40	35.6	13,527,159	15,050,501
50	29.0	12,404,823	13,779,050
60	24.5	11,705,386	12,974,381
70	21.3	11,345,019	12,535,793
80	18.7	11,124,427	12,254,848
90	16.8	10,975,683	12,058,224
100	15.2	10,905,341	11,949,084
110	13.8	10,832,192	11,843,975
120	12.7	10,809,770	11,794,886
130	11.8	10,773,136	11,735,778
150	10.3	10,745,559	11,672,804
200	7.8	10,762,451	11,636,678

250	6.2	10,817,558	11,667,517
300	5.2	10,866,964	11,708,736
350	4.5	10,940,286	11,784,104
400	3.9	10,991,481	11,844,449
450	3.5	11,050,841	11,918,211
500	3.1	11,118,159	12,004,005

Appendix XII Total CAPEX for four cores over the tank height variation

Tank height z [m]	Tank radius r [m]	CAPEX Kaplan, four cores [€2018]	CAPEX Dériaz, four cores [€2018]
10	79.5	51,759,128	54,743,372
20	45.9	23,815,398	25,959,662
30	32.5	16,770,736	18,522,048
40	25.1	13,889,817	15,413,159
50	20.5	12,629,937	14,004,164
60	17.4	11,827,062	13,096,057
70	15.0	11,400,780	12,591,555
80	13.3	11,152,860	12,283,281
90	11.9	10,996,519	12,079,060
100	10.7	10,925,737	11,969,480
110	9.8	10,846,375	11,858,158
120	9.0	10,824,063	11,809,180
130	8.3	10,778,359	11,741,002
150	7.3	10,741,714	11,668,959
200	5.5	10,736,682	11,610,908
250	4.4	10,770,232	11,620,191
300	3.7	10,805,177	11,646,950
350	3.2	10,861,981	11,705,799
400	2.8	10,894,809	11,747,777
450	2.5	10,934,108	11,801,478
500	2.2	10,988,933	11,874,778

Appendix XIII Total CAPEX for eight cores over the tank height variation

Tank height z [m]	Tank radius r [m]	CAPEX Kaplan, eight cores [€2018]	CAPEX Dériaz, eight cores [€2018]
10	56.2	54,547,246	57,531,491
20	32.5	26,125,529	28,269,793
30	23.0	19,043,038	20,794,351
40	17.8	16,188,896	17,712,238
50	14.5	14,963,694	16,337,921
60	12.3	14,156,412	15,425,407
70	10.6	13,745,246	14,936,020

80	9.4	13,490,444	14,620,865
90	8.4	13,293,532	14,376,073
100	7.6	13,214,051	14,257,794
110	6.9	13,115,522	14,127,305
120	6.4	13,073,259	14,058,376
130	5.9	13,025,931	13,988,574
150	5.1	12,966,286	13,893,531
200	3.9	12,939,614	13,813,841
250	3.1	12,967,161	13,817,120
300	2.6	12,987,578	13,829,351
350	2.2	13,041,679	13,885,497
400	2.0	13,077,205	13,930,173
450	1.7	13,119,740	13,987,110
500	1.6	13,175,095	14,060,941

Appendix XIV Numerical results from the environmental assessment of the energy storage options, charged by the German electricity mix, and the SCCT baseline scenario

Impact Category [Unit]	SCCT Baseline	Proposed PHES	Lithium-Ion	P2G2P	Large PHES
Climate change impact [kg CO2-eq/kWh]	0.74093	0.99396	0.69224	2.04664	0.91585
Non-renewable exergy resources, fossil [MJ-eq/kWh]	13.63288	11.19756	7.89524	23.16188	10.3100
Non-renewable exergy resources, fossil [MJ-eq/kWh]	0.0091	0.05129	0.09783	0.18721	0.03089
Non-renewable exergy resources, fossil [MJ-eq/kWh]	0.00312	0.05288	0.03775	0.11192	0.04859

Appendix XV Numerical results from the environmental assessment of the energy storage options, charged by electricity from onshore wind turbines

Impact Category [Unit]	SCCT Baseline	Proposed PHES	Lithium -Ion	P2G2P	Large PHES
Climate change impact [kg CO2-eq/kWh]	0.74093	0.04347	0.04473	0.11579	0.03651
Non-renewable exergy resources, fossil [MJ-eq/kWh]	13.63288	0.41762	0.57519	1.33381	0.36924
Non-renewable exergy resources, fossil [MJ-eq/kWh]	0.0091	0.05429	0.10797	0.21746	0.04466
Non-renewable exergy resources, fossil [MJ-eq/kWh]	0.00312	0.00818	0.0078	0.02262	0.00792